

Electronic Thesis and Dissertation Repository

---

8-22-2011 12:00 AM

## Exploring Bacterial Nanowires: From Properties to Functions and Implications

Kar Man Leung, *The University of Western Ontario*

Supervisor: Jun Yang, *The University of Western Ontario*

A thesis submitted in partial fulfillment of the requirements for the Doctor of Philosophy degree in Mechanical and Materials Engineering

© Kar Man Leung 2011

Follow this and additional works at: <https://ir.lib.uwo.ca/etd>



Part of the [Biological and Chemical Physics Commons](#), [Microbial Physiology Commons](#), and the [Nanoscience and Nanotechnology Commons](#)

---

### Recommended Citation

Leung, Kar Man, "Exploring Bacterial Nanowires: From Properties to Functions and Implications" (2011). *Electronic Thesis and Dissertation Repository*. 235.  
<https://ir.lib.uwo.ca/etd/235>

This Dissertation/Thesis is brought to you for free and open access by Scholarship@Western. It has been accepted for inclusion in Electronic Thesis and Dissertation Repository by an authorized administrator of Scholarship@Western. For more information, please contact [wlsadmin@uwo.ca](mailto:wlsadmin@uwo.ca).

EXPLORING BACTERIAL NANOWIRES: FROM PROPERTIES TO FUNCTIONS  
AND IMPLICATIONS

(Spine Title: Exploring the Properties and Functions of Bacterial Nanowires)

(Thesis format: Monograph)

by

Kar Man Leung

Department of Mechanical and Materials Engineering  
Faculty of Engineering

A thesis submitted in partial fulfillment  
of the requirements for the degree of  
Doctor of Philosophy

The School of Graduate and Postdoctoral Studies  
The University of Western Ontario  
London, Ontario, Canada

© Kar Man Leung 2011

THE UNIVERSITY OF WESTERN ONTARIO  
School of Graduate and Postdoctoral Studies

**CERTIFICATE OF EXAMINATION**

Supervisor

Examiners

\_\_\_\_\_  
Dr. Jun Yang

\_\_\_\_\_  
Dr. Xueliang Sun

Co-Supervisor

\_\_\_\_\_  
Dr. Liying Jiang

\_\_\_\_\_  
Dr. Leo W. M. Lau

\_\_\_\_\_  
Dr. Jayshri Sabarinathan

\_\_\_\_\_  
Dr. P. Ravi Selvaganapathy

The thesis by

**Kar Man Leung**

entitled:

**Exploring Bacterial Nanowires: From Properties to Functions and  
Implications**

is accepted in partial fulfillment of the  
requirements for the degree of  
Doctor of Philosophy

\_\_\_\_\_  
Date

\_\_\_\_\_  
Chair of the Thesis Examination Board

## Abstract

The discovery of electrically conductive bacterial nanowires from a broad range of microbes provides completely new insights into microbial physiology such as extracellular electron transfer, energy distribution, and cell-to-cell communication. There have been a variety of hypothesized functions of bacterial nanowires that raise a number of fundamental questions on these biological nanostructures. This thesis work is carried out to provide answers to these fundamental, but important, questions by employing advanced nanofabrication techniques and nanoscopic characterization tools.

By limiting the availability of electron acceptors, *Shewanella oneidensis* strain MR-1, a dissimilatory metal-reducing bacterium, produces extracellular bacterial nanowires connecting neighboring cells. Characterized by a variety of microscopy techniques, *Shewanella* nanowires are found to be up to tens of micrometers long, with a lateral dimension of  $\sim 10$  nm for single, non-bundled nanowires. Fluorescence microscopy reveals that the nature of bacterial nanowires is protein. In addition, CP-AFM and STM images suggest that bacterial nanowires are efficient electrical conductors.

Direct electrical transport measurements along *Shewanella* nanowires using nanofabricated electrodes and CP-AFM consistently reveal a measured nanowire resistivity on the order of  $1 \Omega \cdot \text{cm}$  along micro-meter length scales. With electron transport rates up to  $10^9/\text{s}$  at 100 mV, bacterial nanowires can serve as a viable microbial strategy for extracellular electron transport. By modulating the nanowire conductance in NW-FET configurations and CP-AFM measurements on nanowires supported on different electrode materials, it has been found that *Shewanella* nanowires behave as a gateable p-type semiconductor with a Fermi level close to

5.3 eV. This finding further suggests that *Shewanella* nanowires may serve as electronic cables for efficient energy distribution and electronic signal exchange within microbial communities.

Two separate AFM experiments, which are real-time elastic modulus mapping using torsional harmonic cantilevers and conventional AFM nanoindentation, mutually confirm that the elastic modulus of *Shewanella* nanowires is on the order of 1 GPa, with no significant variations in local elasticity along individual nanowires. With electrical properties comparable to those of moderately doped inorganic semiconductors and elasticity close to polymeric materials, bacterial nanowires may represent a new class of functional bionanomaterials that will potentially be building blocks for bionanoelectronics and flexible nanoelectronics.

## Keywords

Nanowires, Bacteria, Extracellular Electron Transfer, Microbiology, Bio-energy, Bioelectronics, Nanotechnology, Atomic Force Microscopy, Elasticity.

## Acknowledgments

This thesis is the result of not only my efforts but also many others who have supported me in different ways throughout my Ph.D. study.

First of all, I would like to express my deepest gratitude to my supervisors, Prof. Jun Yang and Prof. Leo Lau. Prof. Yang has always been friendly, supportive, and motivating me to think outside the box to get new insights into each research topic. His valuable comments and suggestions have led to significant achievements in this thesis work. Prof. Lau's guidance, deep knowledge, and brilliant advice gave me the confidence to carry out this research work and face all its challenges. Also, I enjoyed the parties in his house very much every Christmas and on other important days.

I would like to thank Prof. Gordon Southam, who taught me a lot about microbiology. Taking his Geomicrobiology course and working in his lab are very enjoyable experiences. I must also thank my collaborator, Dr. Greg Wanger, who is also my microbiology teacher. From them, I learned the subject of microbiology, from knowledge to hand-on skills, with a lot of fun. Moreover, I am so grateful to Prof. Yuri Gorby and Prof. Mohamed Y. El-Naggar for their helpful comments and suggestions. Our collaboration has been very productive and successful.

Technical support from the staff at the Western Nanofabrication Facility, including Dr. Todd Simpson, Dr. Rick Glew, and Mr. Tim Goldhawk, are highly appreciated. I would also like to appreciate assistance from the following colleagues: Dr. Yu Liu, Mr. Tomas Trebicky, Dr. Frank Zhao, Mr. Qiuquan Guo, Dr. Thomas Lei, Mr. Tingjie Li, and Dr. Mei Liu. Special thanks to all staff members of Surface Science Western, especially Ms. Sue Brown and Ms.

Suzanne Hicks for assistance in purchasing and logistics, and Mr. Ross Davidson, Mr. Brad Kobe and Mr. Gary Good for their technical assistance.

Finally, I would like to express my highest gratefulness to my wife, Ka Po, for her patience and understanding, for going through all ups and downs with me, and for her faith in me. I am forever grateful to my parents, Richard and Betty, and my brother, Eric, for their unconditional love and endless support.

# Table of Contents

<b>CERTIFICATE OF EXAMINATION</b> .....	ii
Abstract .....	iii
Acknowledgments .....	v
Table of Contents .....	vii
List of Tables .....	x
List of Figures .....	xi
List of Abbreviations .....	xvi
Chapter 1 .....	1
1 Introduction .....	1
1.1 Brief Background .....	1
1.2 Research Aim and Outline of this Thesis .....	2
Chapter 2 .....	5
2 Literature Review .....	5
2.1 Generation of Energy for Metabolism by Microbes .....	5
2.2 Bacterial Strategies for Extracellular Electron Transfer .....	8
2.3 Extracellular Electron Transfer Toward Practical Applications in Environmental Biotechnology and Bio-energy Generation .....	12
2.3.1 Bioremediation .....	12
2.3.2 Microbial Fuel Cells .....	15
2.4 Long-range Electron Transfer Facilitated by Extracellular Nanowires .....	17
2.4.1 Bacterial Nanowires from <i>Geobacter sulfurreducens</i> .....	17
2.4.2 Bacterial Nanowires Produced by <i>Shewanella oneidensis</i> Strain MR-1 ...	20
2.5 Summary .....	23



Chapter 3.....	24
3 Cultivation of <i>Shewanella oneidensis</i> MR-1 for Bacterial Nanowire Production and Characterization Techniques.....	24
3.1 Cultivation in Continuous Flow Chemostat Bioreactors .....	24
3.2 Sample Preparation and Characterizations of Bacterial Nanowires .....	29
3.2.1 Scanning Electron Microscopy .....	30
3.2.2 Transmission Electron Microscopy.....	35
3.2.3 Fluorescence Microscopy.....	39
3.2.4 Atomic Force Microscopy.....	41
3.2.5 Scanning Tunneling Microscopy .....	46
3.3 Concluding Remarks.....	49
Chapter 4.....	50
4 Electrical Transport Measurements along Bacterial Nanowires from <i>Shewanella oneidensis</i> MR-1 .....	50
4.1 Introduction.....	50
4.2 Experimental Methods.....	50
4.2.1 Cell Cultivation.....	51
4.2.2 Nanofabricated Devices for Electrical Measurements.....	52
4.2.3 Conducting-probe Atomic Force Microscopy Measurements .....	57
4.3 Direct Electrical Measurements Using Nanofabricated Electrodes.....	59
4.4 Measurements with Conducting Atomic Force Microscopy Probes .....	63
4.5 Discussion.....	68
4.6 Conclusions.....	69
Chapter 5.....	70
5 Semiconducting Behavior of <i>Shewanella</i> Bacterial Nanowires .....	70
5.1 Introduction.....	70
5.2 Experimental Methods.....	72

5.3 Electronic Transport Characteristics of <i>Shewanella</i> Nanowires Coupled to Electrodes.....	74
5.4 Modulating the Conductance of <i>Shewanella</i> Nanowires Configured in Nanowire Field-Effect Transistor Structures.....	78
5.5 Discussion.....	81
5.6 Concluding Remarks.....	82
Chapter 6.....	84
6 Mechanical Properties of <i>Shewanella</i> Nanowires Studied by Atomic Force Microscopic Techniques .....	84
6.1 Introduction.....	84
6.2 Experimental Methods.....	87
6.3 Quantitative Nanomechanical Property Mapping of <i>Shewanella</i> Nanowires by Torsional Harmonic AFM Probes.....	89
6.4 Conventional AFM Nanoindentation on <i>Shewanella</i> Nanowires.....	94
6.5 Discussions .....	96
6.6 Concluding Remarks.....	97
Chapter 7.....	99
7 Thesis Summary and Future Work .....	99
7.1 Summary.....	99
7.2 Thesis Contributions.....	102
7.3 Future Work.....	103
References.....	104
Curriculum Vitae .....	116

## List of Tables

Table 6.1: Measured elastic modulus of bacterial nanowires supported on different substrates.	96
---	----

## List of Figures

- Figure 2.1: Simplified diagram of aerobic respiration of bacteria by oxidizing glucose and reducing oxygen.. ..... 7
- Figure 2.2: Pathway of extracellular Fe(III) reduction in *S. oneidensis* with outer-membrane *c*-type cytochromes OmcA and MtrC. Black solid circles represent heme groups..... 10
- Figure 2.3: Two bacterial strategies for indirect extracellular electron transfer to iron oxide. (a) A chelator (yellow oval) brings soluble iron to the cell for reduction. (b) An electron shuttle (blue closed oval is in the oxidized state, open oval in the reduced state) catalyzes electron transfer from the cell to iron oxide at a distance from the cell..... 11
- Figure 2.4: A schematic drawing illustrating the basic structure of a microbial fuel cell... .. 16
- Figure 2.5: A conceptual bio-geobattery model describing generation of electric field by transferring electrons from the anode (reduced zone) to the cathode (oxidized zone) through bacterial nanowires..... 21
- Figure 3.1: (a) Continuous flow bioreactor employed for cultivation of *S. oneidensis* MR-1 (wild-type). The bioreactor is integrated with (b) a controlling unit for gas flow control, agitation control, pH and dissolved oxygen concentration monitoring, fresh medium supply, and old medium withdrawal... ..... 25
- Figure 3.2: Organic acid concentration (mM) and cell density (OD600) versus growth time (h) for *S. oneidensis* MR-1 (wild-type) cultivated in batch mode..... 27
- Figure 3.3: A screen view captured from the controller display showing the dissolved oxygen concentration of air and the percentage air versus nitrogen supplied to the bioreactor as a function of growth time..... 29
- Figure 3.4: An SEM image showing cells of *S. oneidensis* MR-1 cultivated in a continuous flow chemostat bioreactor under electron-acceptor-limited conditions. The cells

express a high amount of nanofilaments connecting neighboring cells. This sample was chemically fixed, dehydrated through a graduated series of ethanol, critical-point dried, and coated with Pt prior to SEM imaging..... 33

Figure 3.5: An SEM image showing cells of *S. oneidensis* MR-1 harvested in a continuous flow chemostat bioreactor operating under electron-acceptor-limited conditions. This sample was only chemically fixed and Pt coated prior to SEM imaging. Without going through ethanol dehydration processes and critical-point drying, the cell structures were severely deformed and collapsed, especially when subjected to high-vacuum environment in SEM, although nanofilamentous structures could still be observed..... 34

Figure 3.6: An SEM image showing cells of *S. oneidensis* MR-1 harvested in batch culture. In addition to nanofilaments, extracellular polymeric substances (EPS) are observed in the sample, which can challenge microscopic analysis and electrical measurements on bacterial nanowires..... 35

Figure 3.7: (a) TEM micrographs showing a negatively stained *S. oneidensis* MR-1 bacterium with nanofilaments (indicated by arrows in (b) and (c)) emanating from the cell body with a lateral dimension of ~10 nm measured from the TEM images..... 37

Figure 3.8: (a) TEM micrographs showing a negatively stained *S. oneidensis* MR-1 bacterium with a flagellum (indicated by the arrow in (b)) emanating from the pole of the cell and a branched nanofilament (indicated by the arrow in (c)) from the side of the cell..... 38

Figure 3.9: An optical micrograph showing cells of *S. oneidensis* MR-1. Nanofilaments such as nanowires and flagella cannot be observed owing to the limitation of resolution, which is typically 200 nm for visible light illumination.... 40

Figure 3.10: A fluorescence microscopic image of *S. oneidensis* MR-1 cells stained with non-specific protein-binding reagent in liquid media. The bacterial cells and nanofilaments (indicated by arrows) fluoresce under excitation at 470 nm..... 41

Figure 3.11:Tapping-mode (a) topography and (b) amplitude AFM images of <i>S. oneidensis</i> MR-1 cells. The scale bar is 2 $\mu\text{m}$ .....	43
Figure 3.12:(a) Topography image and (b) simultaneous conductivity map of a bacterial nanowire from <i>S. oneidensis</i> MR-1 collected in batch culture accompanied with some non-conducting substances, possibly EPS. (c) The height and (d) current profiles (indicated by black lines) across the nanowire reveal that the radial dimension of the nanowire is $\sim 10$ nm and the nanowire is electrically conductive.....	44
Figure 3.13:Simple model explaining the broadening effect due to AFM tip geometry. Comparing with the actual width of the object (upper), the apparent width in the topographic image (lower) is over estimated but the height can be measured very accurately.....	45
Figure 3.14:(a) STM image and (b) height profile confirm that bacterial nanowires from <i>S. oneidensis</i> MR-1 are highly conductive and can be composed of bundles of individual nanofilaments.....	48
Figure 4.1: Optical micrograph of a microfabricated structure on a $\text{SiO}_2/\text{Si}$ substrate with Au microelectrodes and contact pads for electrical measurements.....	53
Figure 4.2: Schematics of microfabrication procedures of devices used as platforms for electrical measurements of bacterial nanowires.....	54
Figure 4.3: SEM images of (a) close-circuit and (b) open-circuit controls. (c) I-V curves of (a) and (b) are indicated by squares and circles, respectively.....	56
Figure 4.4: AFM topography image of prefabricated Au microgrids on a $\text{SiO}_2/\text{Si}$ substrate.....	58
Figure 4.5: SEM image showing the gas injection system (GIS) used to introduce Pt precursor close to the substrate surface for EBID of Pt contacts on bacterial nanowires.....	60

Figure 4.6: (a) SEM image showing a single bacterial nanowire emanating from a wild-type <i>S. oneidensis</i> MR-1 cell contacted with two nanofabricated Pt electrodes. (b) Current-voltage curve of the bacterial nanowire in (a). (c) SEM image of another bacterial nanowire with the measured I-V curve shown in (d).....	61
Figure 4.7: (a) SEM image showing a single bacterial nanowire from the <i>S. oneidensis</i> flagellin-deficient mutant contacted with two nanofabricated Pt electrodes. (b) Current-voltage curve of the bacterial nanowire.....	62
Figure 4.8: (a and b) SEM images showing two individual extracellular appendages from the $\Delta$ mtrC/omcA mutants that are morphologically consistent with wild-type nanowires but are electrically non-conductive as confirmed by electrical measurements.....	63
Figure 4.9: Topographic AFM image showing air-dried <i>S. oneidensis</i> MR-1 cells and extracellular appendages deposited randomly on a SiO <sub>2</sub> /Si substrate patterned with Au microgrids.....	64
Figure 4.10: Schematic diagram illustrating electronic transport along a single bacterial nanowire in contact with Au microgrids measured by a Pt-coated AFM tip.....	65
Figure 4.11: (a) Contact mode AFM image showing a bacterial nanowire reaching out from a <i>S. oneidensis</i> MR-1 cell to the Au electrode. (b) An I-V curve obtained by probing the nanowire at a length of 600 nm away from the Au electrode (at the position marked by the black dot in (a)). (Inset) The I-V curves obtained on bare Au and SiO <sub>2</sub> , respectively.....	66
Figure 4.12: A plot of total resistance as a function of distance between AFM tip and Au electrode. The contact resistance is estimated by extrapolating the linear curve to zero length.....	67
Figure 5.1: (a and b) Current-voltage curves collected on two individual <i>Shewanella</i> bacterial nanowires when sandwiched between a Pt-coated AFM tip and Au-coated substrate.....	75

Figure 5.2: (a and b) Current-voltage curves collected on two individual <i>Shewanella</i> bacterial nanowires when sandwiched between a Pt-coated AFM tip and HOPG substrate.....	76
Figure 5.3: Structure of a NW-FET device with a single bacterial nanowire contacted by source (S) and drain (D) electrodes. The topography shown is an amplitude AFM image of the device.....	79
Figure 5.4: (a) $I_{DS}$ - $V_{DS}$ characteristics of a <i>Shewanella</i> nanowire at different gate voltages. (b) Transfer characteristic of the NW-FET at $V_{DS} = -1$ V.....	80
Figure 6.1: SEM image of a torsional harmonic cantilever with a T-shaped geometry and an off-axis tip.....	87
Figure 6.2: A tip-sample force waveform captured when operating under HarmoniX mode AFM.....	89
Figure 6.3: (a) Topography of a bacterial nanowire supported on HOPG and (b) the corresponding elastic modulus map simultaneously generated. Numerical values across the sections indicated by the white lines are plotted below the images....	91
Figure 6.4: Topographic (a and b) and corresponding elastic modulus (c and d) micrographs of bacterial nanowires supported on PMMA and borosilicate glass substrates, respectively. Numerical values across the sections indicated by the white lines are plotted below the images.....	92
Figure 6.5: (a) Tapping-mode topography image of a bacterial nanowire supported on HOPG. Inset of (a) shows the height profile across the section indicated by the black line. (b) Force-separation curves collected by indentation on three different points (indicated by asterisks; 1–square, 2–circle, and 3–triangle) on the nanowire. Inset of (b) shows an example of a force curve obtained by indentation on the edge of the nanowire.....	95



## List of Abbreviations

ADP	Adenosine diphosphate
AFM	Atomic force microscopy
ATP	Adenosine triphosphate
CP-AFM	Conducting-probe atomic force microscopy
D	Drain
DMRB	Dissimilatory metal-reducing bacteria
DOS	Density of states
EBID	Electron-beam induced deposition
EPS	Extracellular polymeric substances
FET	Field-effect transistor
GIS	Gas injection system
HOPG	Highly oriented pyrolytic graphite
I-V	Current-voltage
MFC	Microbial fuel cell
MOSFET	Metal-oxide-semiconductor field-effect transistor
NTA	Nitro-triacetic acid
NW	Nanowire
PBS	Phosphate buffered saline
PEM	Proton exchange membrane
PMMA	Polymethylmethacrylate
S	Source
SEM	Scanning electron microscopy
STM	Scanning tunneling microscopy
TEM	Transmission electron microscopy
THC	Torsional harmonic cantilever
UHV	Ultrahigh vacuum

# Chapter 1

## 1 Introduction

The background of this thesis work is briefly introduced here in the first chapter. In addition, the research aim and outline of this thesis are presented.

### 1.1 Brief Background

In microbial world, microbes can generate energy using diverse strategies for cell growth and/or maintenance. Such energy generating processes can be simplified as a chain of electron-transfer reactions, from extracting electrons from an electron donor (organic foodstuffs) to dumping electrons to a terminal electron acceptor, involving a series of redox reactions within the whole process (more details are discussed in Chapter 2). Although most bacteria use soluble electron acceptors such as oxygen or carbon dioxide, some bacteria are capable of extracellular electron transfer in harsh environments where the only available electron acceptors are insoluble or poorly soluble, for instance, metal-oxide minerals. In recent years, increasing attention has been paid to microbial metabolisms that involve electron transfer between cells and extracellular substrates. The recent discovery of electrically conductive bacterial nanowires produced by a variety of microbes suggests that electron transfer via nanowires may be widespread in nature, and inspires this thesis work in further exploring the properties of bacterial nanowires, testing a variety of hypothesized functions of bacterial nanowires related to energy distribution

and communication, and looking for their potential applications in nanobiotechnology and nanobioelectronics.

## 1.2 Research Aim and Outline of this Thesis

It is the aim of this thesis work to explore the functions and properties of bacterial nanowires from a dissimilatory metal-reducing bacterium, *Shewanella oneidensis* strain MR-1, which have immense implications in microbial physiology, ecology, electromicrobiology, biotechnology, and nanotechnology. To achieve this aim, the electrical, electronic and mechanical properties of *Shewanella* nanowires are studied using techniques including microfabricated chips, nanofabricated devices, and AFM-based electrical and mechanical measurements.

Chapter 2 presents a review of the currently known microbial strategies for electron transfer to extracellular electron acceptors and related applications in environmental biotechnology as well as in bio-energy production. It is also discussed that bacterial nanowires may be a more general, but previously unknown, microbial strategy for effective electron transfer to distantly located electron acceptors, including solid-phase metal-oxide minerals, electrodes and possibly neighboring cells.

In Chapter 3, detailed cultivation procedures and the optimal growth conditions to induce bacterial nanowire production by *Shewanella oneidensis* MR-1 are described. Characterizations of bacterial nanowires by a variety of microscopy techniques including optical microscopy, SEM, TEM, AFM and STM are presented. In addition, electrical

characterizations of bacterial nanowires using scanning probe microscopy (CP-AFM and STM) are demonstrated.

Chapter 4 demonstrates direct electrical transport measurements along bacterial nanowires from *S. oneidensis* MR-1 by two independent techniques: (i) nanofabricated electrodes patterned on top of individual nanowires, and (ii) conducting AFM probing at various points along a single nanowire bridging a prefabricated metallic microelectrode and the conductive AFM tip. This is the first study to prove that bacterial nanowires are able to conduct electrons along micron length scales.

Chapter 5 presents electronic transport studies across junctions between bacterial nanowires and electrodes using CP-AFM, and modulation of bacterial nanowire conductance under NW-FET device structures. This work reveals the mechanism of electrical transport in these biological nanostructures, and suggests that *Shewanella* nanowires may not only serve as conduits to transfer electrons throughout the extracellular matrix, but also as cables for efficient energy distribution and electronic information exchange such as for cell-cell communication within microbial communities.

Chapter 6 presents studies on the mechanical properties of *Shewanella* bacterial nanowires using two separate AFM techniques: (i) real-time elastic modulus mapping using torsional harmonic cantilevers with a T-shaped geometry and an offset tip, and (ii) conventional AFM nanoindentation with subsequent curve fitting based on the classical Hertz model. This work inspires us with new applications of bacterial nanowires: with their electronic properties comparable to those of moderately doped inorganic

semiconductors and elasticity similar to polymeric materials, bacterial nanowires may function as building blocks for bionanoelectronics and flexible nanoelectronics.

Most of the work presented in this thesis has been published in peer-reviewed journals or submitted for publication.

## Chapter 2

### 2 Literature Review

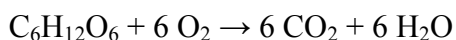
In this chapter, different reported strategies of how microbes generate energy are reviewed. The basic principle of biological energy generation is based on oxidation and reduction processes involving electron transfer within cells and/or outside of the cells to terminal electron acceptors. In the case of electron transfer outside of the cells known as extracellular respiration or extracellular electron transfer, a number of mechanisms have been proposed although not many of them are completely understood. Some of the mechanisms have been experimentally proved to be in good agreement with the proposed theories, but there are definitely still knowledge gaps in each model yet to be filled and perhaps unknown mechanisms to be explored.

#### 2.1 Generation of Energy for Metabolism by Microbes

Microbes can generate energy using diverse strategies. The fundamental principle of energy generation for metabolism is based on transfer of electrons from electron donors with lower (or more negative) reduction potentials (also known as reduction/oxidation or redox potentials), through an electron transport chain, to terminal electron acceptors with higher (or more positive) reduction potentials. The electron transport chain couples the electron transfer to the transfer of protons across a cell membrane, producing an electrochemical proton gradient as a result of a series of redox reactions, releasing chemical energy in the form of adenosine triphosphate (ATP), which is the common

currency used for intracellular energy transfer. ATP provides biological energy for a variety of cellular functions such as motility, synthesis of macromolecules (DNA, proteins, etc), and cell division.

Organic substances are the most common electron donors, whereas some prokaryotes (bacteria and archaea) can use inorganic substances as their energy sources. As mentioned earlier, the electron transport chain consists of a series of redox reactions in which electrons are transferred from a donor to an acceptor. The driving force of such reactions is based on the Gibbs free energy of the reactants and products. Whether a reaction can proceed depends on whether the reaction can decrease the Gibbs free energy of the system. In general when the electron acceptor is a freely diffusible gas (e.g. oxygen) in the liquid environment, electrons are extracted from oxidization of organic nutrients and transferred through multiple redox reactions, carried out by a series of protein complexes in the cell membranes, to oxygen, which is reduced to water. This process, which drives the production of ATP, is called oxidative phosphorylation. A simplified diagram of aerobic respiration of bacteria using glucose as the electron donor and oxygen as the electron acceptor is illustrated in Figure 2.1. An equation for the overall reaction is shown below:



In this respiration process, electrons are transported from enzymes to enzymes, which are embedded in the cell membrane, while protons ( $\text{H}^+$ ) are transferred across the membrane, creating a proton gradient. Powered by this transmembrane gradient, one of the most important enzymes called ATP synthase, which is a large protein complex, synthesizes

ATP by coupling adenosine diphosphate (ADP) and inorganic phosphate ( $P_i$ ) when the protons are transferring back through the channel in ATP synthase. The overall reaction is:

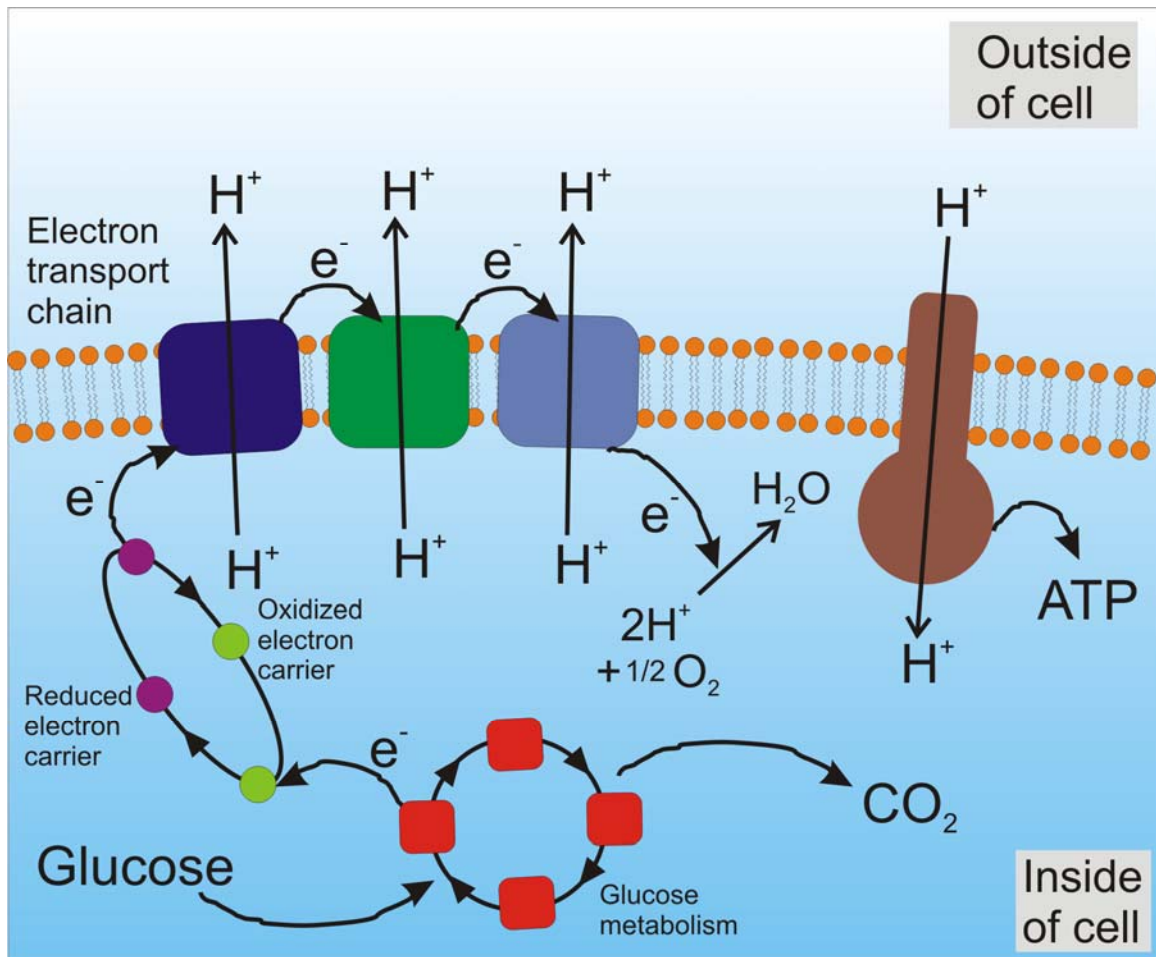


**Figure 2.1: Simplified diagram of aerobic respiration of bacteria by oxidizing glucose and reducing oxygen.**



Oxygen generates the highest Gibbs free energy change on hydrolysis than any other electron acceptors in the electron transport chain. Facultative anaerobic bacteria use oxygen as the terminal electron acceptor, but they can also survive by “breathing” other electron acceptors if oxygen is not present. Some bacteria such as strict anaerobes even die in presence of oxygen. Therefore, these types of bacteria use alternative electron acceptors for cellular respiration. Some of these acceptors are soluble such as nitrate, sulfate, and carbonate, while some are insoluble minerals, such as iron and manganese oxides. The latter case involves electron transfer outside of cells to solid interfaces. This process is called extracellular electron transfer or extracellular respiration.

## 2.2 Bacterial Strategies for Extracellular Electron Transfer

When electron acceptors are not freely soluble or readily dissolved, bacteria seek other strategies to facilitate interactions between the cellular electron transport chain and the extracellular substrates. Extracellular electron transfer is a promising research field including but not limited to cell biology, genetics, and biochemistry [1]. Although our understanding on how bacteria transfer electrons outside of cells is incomplete, a variety of mechanisms have been proposed and observed. The mechanism of bacterial extracellular electron transfer can be mainly divided into two categories: direct and indirect interactions.

For direct interactions, bacteria express proteins on the cell surfaces that are able to transfer electrons to the solid-phase electron acceptors when the proteins and the acceptors are in direct contact. Microbial reduction of insoluble Fe(III) oxides, which are

the most abundant form of Fe(III) in sedimentary environments, has been observed in dissimilatory metal-reducing bacteria (DMRB) for genera such as *Shewanella* [2, 3], *Geobacter* [3, 4], *Pelobacter* [5], *Geovibrio* [6], *Ferrimonas* [7], *Desulfuromusa* [8], and *Desulfuromonas* [9]. Commonly, the proteins that are involved in electron transfer to minerals such as iron/manganese (hydr)oxides are localized to the outer membrane of Gram-negative bacteria. In Gram-negative bacteria such as *Shewanella oneidensis* MR-1 and *Geobacter sulfurreducens*, it has been suggested that outer-membrane redox-active proteins called cytochromes play critical roles in dissimilatory reduction of solid metal (hydr)oxides by facilitating electron transport across the cell envelope [3]. Lower *et al.* showed that specific interaction forces are induced between *Shewanella oneidensis* and goethite ( $\alpha$ -FeOOH) under anaerobic conditions in which extracellular electron transfer is expected [10]. Xiong *et al.* observed high-affinity binding and direct electron transfer to hematite by the *Shewanella oneidensis* MR-1 outer-membrane *c*-type cytochrome OmcA [11]. Parikh and Chorover employed attenuated total reflection (ATR) Fourier transform infrared (FTIR) spectroscopy and revealed significant short-range bonding interactions during adhesion to iron oxide ( $\alpha$ -Fe<sub>2</sub>O<sub>3</sub>) by *Shewanella oneidensis* and other Gram-positive bacteria [12]. To date, the mechanism of how electrons are transported from these outer-membrane cytochromes is not fully understood, but studies shown above provided supporting evidences on bacterial extracellular electron transfer through direct contact. A model of Fe(III) reduction pathway by *S. oneidensis* is illustrated in Figure 2.2. In this model, electrons are extracted from lactate as an electron donor and transferred to a series of multi-heme cytochromes, which are located in the inner membrane (CymA), periplasm (MtrA), and outer membrane (OmcA and MtrC).

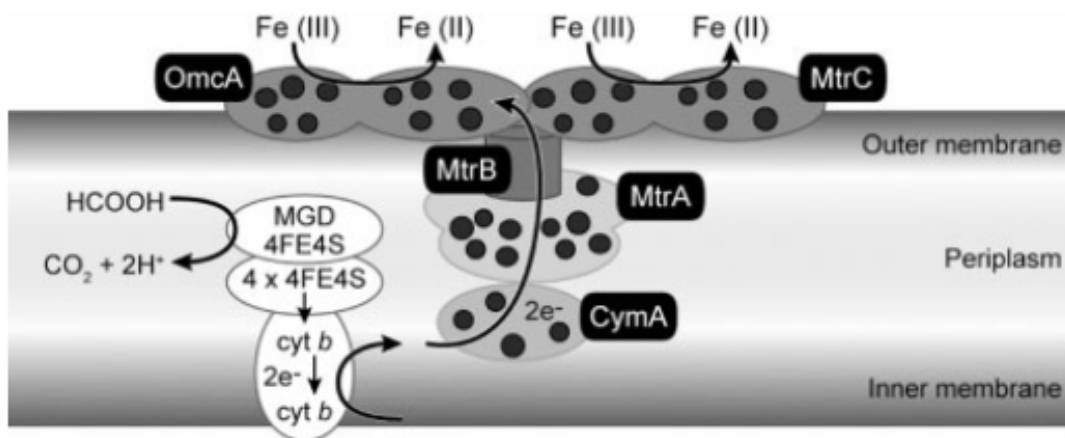


**Figure 2.2: Pathway of extracellular Fe(III) reduction in *S. oneidensis* with outer-membrane *c*-type cytochromes OmcA and MtrC. Black solid circles represent heme groups. Figure copied from Ref [13].**

For indirect extracellular electron transfer, bacteria are not or may not be able to be in direct contact with the terminal electron acceptors. They adopt another strategy by producing some small molecules that traverse the space between the cells and the extracellular substrates. In indirect electron transfer to poorly soluble minerals, these small molecules act either to chelate metals and deliver them to an intracellular metal oxidoreductase or by themselves serving as electron shuttles [1]. In the case of metal chelators, ligands such as citrate and nitro-triacetic acid (NTA) are capable of delivering soluble iron to the cell for reduction, either on the outside or on the inside [1]. An electron shuttle is a mobile molecule that serves as the terminal electron acceptor and is able to undergo redox cycling for thousands of times [14]. At its reduced state, the electron shuttle can transfer electrons to iron oxides whereupon it becomes re-oxidized and then reduced again when

serving as the terminal electron acceptor. Some organic molecules that can play this role are humic substances such as quinones, phenazines, and thiol-containing molecules like cysteine [14, 15]. A schematic diagram is presented in Figure 2.3 demonstrating how a bacterium uses a chelator or electron shuttle for extracellular respiration.

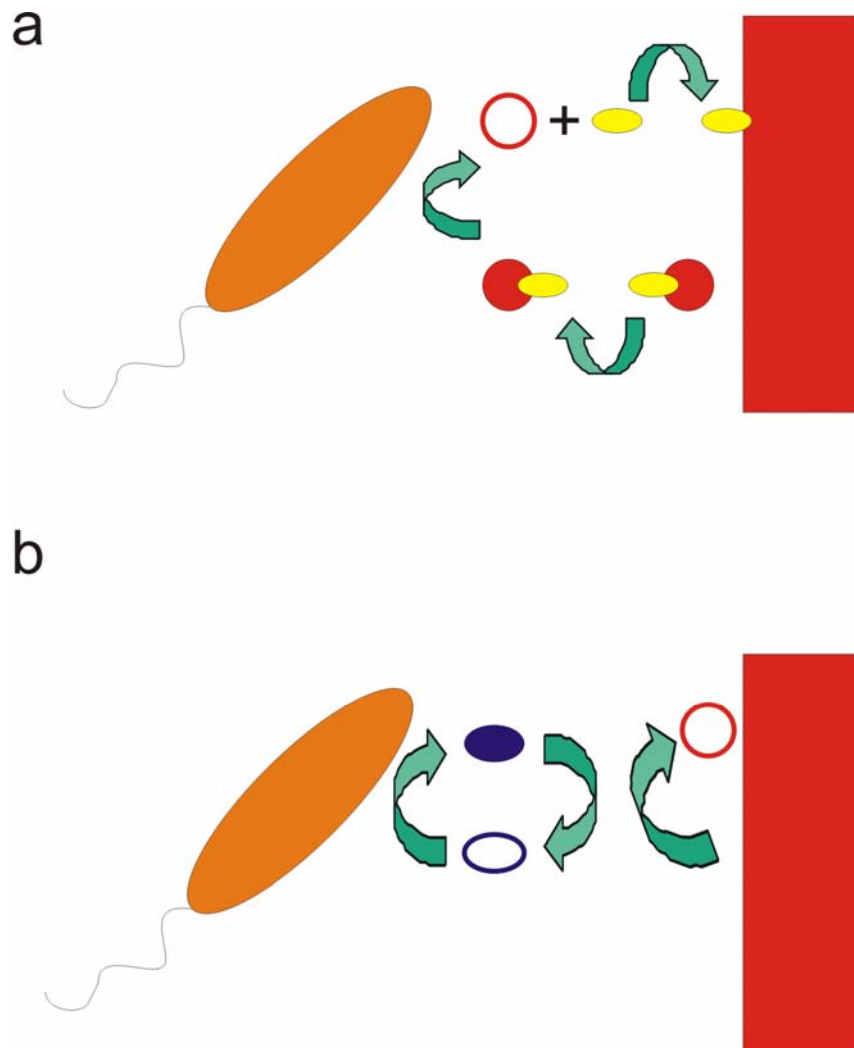


**Figure 2.3: Two bacterial strategies for indirect extracellular electron transfer to iron oxide. (a) A chelator (yellow oval) brings soluble iron to the cell for reduction. (b) An electron shuttle (blue closed oval is in the oxidized state, open oval in the reduced state) catalyzes electron transfer from the cell to iron oxide at a distance from the cell.**

## 2.3 Extracellular Electron Transfer Toward Practical Applications in Environmental Biotechnology and Bioenergy Generation

Microorganisms that are able to sustain metabolism in anoxic conditions by carry out extracellular electron transfer have been of great interest in biotechnological applications such as bioremediation and electricity generation. In order to realize practical applications in these areas, research is continuously ongoing to investigate the mechanism of extracellular electron transfer, how electrons are transferred to electron acceptors, and what factors control the rate and extent of the process [16]. In this subsection, the basic concepts of how extracellular electron transfer plays an important role in these applications will be outlined along with some examples.

### 2.3.1 Bioremediation

The goal of bioremediation is to restore contaminated environments by means of microbial metabolism in an inexpensive and environmentally friendly way. The restoration can be aided by utilizing proper microorganisms to oxidize, bind, immobilize, volatilize, or transform the contaminants [16]. Contaminants in these environments include organic pollutants (aromatic hydrocarbons and pesticides), chlorinated compounds, and metals. Aerobic degradation of toxic organic contaminants to non-toxic products can be achieved by utilizing aerobic microorganisms, for instance, *Pseudomonas* species, which are able to oxidize (extract electrons from) these contaminants and transfer electrons to oxygen as the terminal electron acceptor [17]. However, many contaminated sites such as aquifers, aquatic sediments, and submerged

soils, are anoxic, lack of accessibilities and on large scales. Therefore, bioremediation in these subsurface environments are of great research interest.

The respiratory flexibility of some bacteria makes them good agents for bioremediation in subsurface, anaerobic environments. For example, *Geobacter* species are capable of oxidizing organic (aromatic) contaminants coupled to reduction of Fe(III) oxides [18]. In addition to choosing proper bacterial species, the efficiency of bioremediation is also dependent on the availability of suitable electron acceptors for the chosen species in the contaminated areas. In subsurface environments, Fe(III) is usually the most abundant electron acceptors for the oxidation of organic compounds [19]. Thus, further enhancing the availability of Fe(III) in the sites can stimulate anaerobic degradation of organic contaminants, enriching the species and increasing the bioremediation efficiency [20]. The concentration of sulfate in seawater is high so sulfate is an important electron acceptor for biodegradation of organic contaminants in marine environments. In such environments, sulfate-reducing bacteria, such as *Desulfobacula* and *Desulfobacterium* species, are good candidates for the oxidization of hydrocarbons with sulfate as the electron acceptor [21]. Halogenated compounds are one of the most significant types of toxic pollutants. Dehalogenating microorganisms are able to use these pollutants as electron acceptors [22]. This process is called reductive dehalogenation, which is mainly known to occur under anaerobic conditions [23].

Bioremediation of metals and radionuclides such as chromium (Cr), technetium (Tc), and uranium (U), is an important process in controlling the fate and transport of these hazardous substances in anoxic subsurface environments [24]. Because toxic metals cannot be degraded, containment of these contaminants is a potential strategy to prevent

their spread and make the collection or removal processes possible. As the reduced forms of some metals and radionuclides are insoluble or have very low solubility, they can be precipitated as immobile forms stimulated by microbial reduction. For example, bioremediation of uranium-contaminated waters and soils has been suggested by reducing soluble uranyl ion ( $\text{UO}_2^{2+}$ ) to highly insoluble uraninite ( $\text{UO}_2$ ) [25, 26]. When uranium is reduced from the U(VI) oxidation state to U(IV), the solubility decreases resulting in immobilization. A variety of bacterial species are known to be capable of reducing U(VI) to U(IV) such as *Shewanella* [27, 28], *Geobacter* [29], *Desulfosporosinus* [30], *Desulfovibrio* [31, 32], and *Clostridium* [33]. The biomolecular mechanisms of uranium reduction are not well understood yet. However, it was reported for *Shewanella oneidensis* MR-1 that *c*-type cytochromes are essential for the reduction of U(VI) and formation of extracellular  $\text{UO}_2$  nanoparticles [34], implying a direct electron transfer mechanism from cytochromes located in the outer membrane to extracellular U(VI). Uraninite particles produced by microbial reduction are less than 3 nm in diameter [35]. Owing to the small size and high surface-to-volume ratio, it would be expected that the  $\text{UO}_2$  nanoparticles are still relatively mobile in liquid environments and can be re-oxidized easily. Further procedures after microbial reduction to uraninite, such as flocculation and adsorption onto colloidal particles, have been suggested in order to reduce the transport potential [35]. To realize practical uranium bioremediation, the following research direction should be on looking for an effective way to facilitate subsequent immobilization and promote long-term stability of reduced U(IV).

### 2.3.2 Microbial Fuel Cells

Other than metal oxide minerals that can serve as extracellular terminal electron acceptors, electrodes represent another possibly more convenient electron acceptor for some bacteria [36-38]. One of the most important potential applications utilizing microbial extracellular electron transfer to electrodes is electricity generation called microbial fuel cells (MFCs). In MFCs, the fuel source can be any microbially degradable organic matter. Although MFCs are not yet commercialized owing to challenges such as low power densities and high production costs [39], MFCs have a number of advantages over typical abiotic fuel cells that are powered by hydrogen and alcohol. These abiotic fuel cells require precious, expensive metal catalysts [40] to promote oxidation of the fuel source, in contrast to MFCs in which the catalysts are naturally occurring bacteria that are able to oxidize a variety of “costless” fuels such as organic waste and renewable biomass in soils and sediments. In addition, the catalysts used in some abiotic fuel cells can be poisoned by carbon monoxide. Some commercial fuel cells that are less susceptible to poisoning usually need to operate at high temperatures [41], whereas MFCs operates at room temperature or at temperatures that microbial metabolism can be sustained.

As shown in Figure 2.4, a MFC consists of an anode, which accepts electrons from the bacteria, and a cathode, which donates electrons to an electron acceptor. The anode compartment should be maintained under a condition that is free from available electron acceptors for the bacteria so that the only means for respiration is to transfer electrons to the anode. The cathode can be suspended in aerobic media or exposed to air [42]. Electrons flow from the anode to the cathode, as a result of electrochemical potential difference between the electrodes, through an external electrical circuit that can be a



resistor or other electrical components. The anode and cathode is typically separated by a proton exchange membrane (PEM), which restricts oxygen to diffuse from the cathode to the anode compartment and allows protons that are released from the oxidation of the organic fuel source to pass through the membrane from the anode to the cathode. The number of electrons that transfer from the anode to the cathode must be matched by an equal number of protons moving between the electrodes in order to preserve the electroneutrality. It has also been assumed that both anode and cathode can be biologically catalyzed by placing proper species of bacteria in each electrode compartment such that the cathode can serve as the electron donor to the bacteria [43].

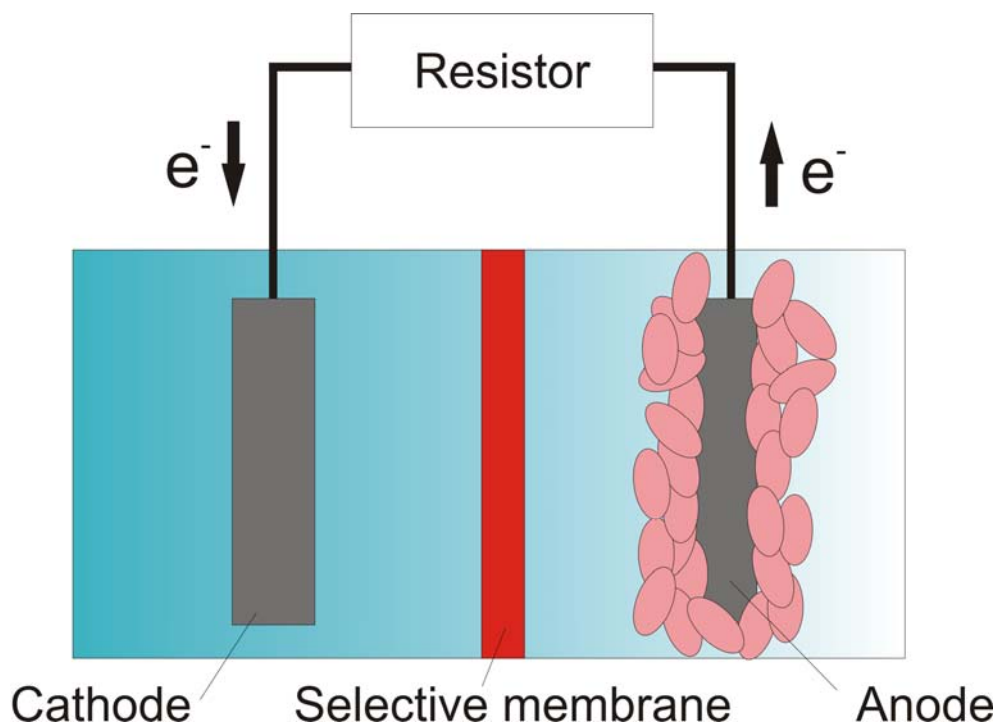


**Figure 2.4: A schematic drawing illustrating the basic structure of a microbial fuel cell.**

## 2.4 Long-range Electron Transfer Facilitated by Extracellular Nanowires

A novel, previously unrecognized, extracellular electron transfer pathway was reported in 2005 by Reguera *et al.* [44] that the DMRB *Geobacter sulfurreducens* can produce extracellular appendages termed as microbial nanowires, which are electrically conductive pili, to aid in establishing contacts with and transferring electrons to Fe(III) oxides. A similar phenomenon was discovered by Gorby *et al.* [45] in a variety of bacteria such as the DMRB *Shewanella oneidensis* MR-1, the oxygenic photosynthetic cyanobacterium *Synechocystis* PCC6803, and the thermophilic, fermentative bacterium *Pelotomaculum thermopropioncium* that can also produce electrically conductive appendages, namely bacterial nanowires, when grown under specific conditions. It should be noted that the terms “microbial nanowires” and “bacterial nanowires” are used interchangeably in the literature and are both referred to electrically conductive appendages with nanowire architectures produced by microbes. In this section, the discoveries and assessments of electrically conductive bacterial nanowires produced by *G. sulfurreducens* and *S. oneidensis* MR-1 are discussed.

### 2.4.1 Bacterial Nanowires from *Geobacter sulfurreducens*

*Geobacter sulfurreducens*, which are strictly anaerobic bacteria and the predominant Fe(III) reducers, must be in direct contact with Fe(III) oxides to reduce them. Reguera *et al.* [44] observed that *G. sulfurreducens* produced monolateral pili that were proposed to aid in establishing contact with Fe(III) oxides. Mutants with the gene, PilA, deleted did not produce pili and could not reduce insoluble electron acceptors such as poorly

crystalline Fe(III) and Mn(IV) oxides, suggesting that *G. sulfurreducens* required the assembly of functional pili in order to reduce insoluble electron acceptors. To evaluate the role of these pili in electron transfer to Fe(III) oxides, the authors measured the electrical conductivity through the pili with an atomic force microscope (AFM) equipped with a conductive tip. It was shown that there was a strong current response along the pilus filament when a voltage was applied to the tip, indicating that the pili were highly conductive and might function as the electrical connection between the cell and the surface of the Fe(III) oxides. However, it should be noted that the electrical measurements performed in such settings were “across-the-thickness” but not “along-the-length” measurements. Therefore, whether electrons can actually flow along *Geobacter* nanowires remains uncertain. In addition, another study showed that there are several proteins other than PilA can yield pilin-like filaments in *G. sulfurreducens* [46]. Whether any of these filaments are also conductive and which protein(s) is (are) the essential component(s) for electrical conduction require further investigations.

*G. sulfurreducens* are also electricigens that are capable of donating electrons to the anode of MFCs. In typical MFCs, the requirement for electricigens to establish contact with the fuel cell anode in order to produce electrical current can potentially be one of the limiting factors in power production. Therefore, it is generally thought that increasing the anode surface areas would be necessary to increase the power output of MFCs. Reguera *et al.* [47] developed MFCs employing *G. sulfurreducens* to convert acetate to electricity and observed a direct linear increase in the amount of biomass on the anodes as the current increased and biofilms developed. It was shown that the output current increased even though more cells were at distances significantly far away from the anode surface.

These findings suggested that the electrically conductive nanowires of *G. sulfurreducens* allowed increased stacking of cells on the anode surface and promoted long-range electron transfer across the multilayer biofilms on anodes. This study has important implications for the design of MFCs because it proves that it is possible to increase electricity production not only by increasing the surface area of the anode in contact with cells but also increasing the number of active cells donating electrons on a given surface.

For *G. sulfurreducens*, there are a number of c-type cytochromes that have been proposed to be on the outer cell surface and are essential for extracellular electron transfer [48]. For instance, OmcZ, primarily localized in the extracellular matrix, was shown to aid in electron conduction from *G. sulfurreducens* biofilms to the anodes of MFCs [49]. OmcS, another abundant outer-surface c-type cytochromes in *G. sulfurreducens* that is essential for the reduction of Fe(III) oxides, was revealed to be localized along *Geobacter* pili by immunogold labeling [50]. Although OmcS was associated with the pili, the large spacing (>2 nm) observed between individual OmcS molecules suggested that OmcS only facilitated electron transfer from pili to Fe(III) oxides *in vitro* rather than promoting electron conduction along the length of the pili. Therefore, it is more likely that electrons are conducted along *Geobacter* nanowires as a result of the intrinsic conductive properties of the pili, possibly due to the amino acid sequence of the type IV pilin subunit, PilA, and the tertiary structure of the assembled pilus.

## 2.4.2 Bacterial Nanowires Produced by *Shewanella oneidensis* Strain MR-1

*Shewanella oneidensis* is a facultative bacterium that is capable of surviving and proliferating in both aerobic and anaerobic environments. Similar to *G. sulfurreducens*, *S. oneidensis* is able to reduce Fe(III) and Mn(IV) mineral oxides as alternative terminal electron acceptors in anoxic environments. Bacterial nanowires produced by *Shewanella oneidensis* MR-1 were first discovered by Gorby et al. [45], also in 2005 while the report published in 2006, when the bacterial cells were grown under oxygen-limited conditions. Not only *Shewanella* nanowires, the authors also reported production of electrically conductive nanowires from the oxygenic phototrophic cyanobacterium *Synechocystis* PCC6803 and the thermophilic, fermentative bacterium *Pelotomaculum thermopropionicum*, suggesting that electrically conductive nanowires are not exclusive to DMRB and nanowires may represent a common bacterial strategy for efficient electron transfer and energy distribution. In this subsection, only characterizations of *Shewanella* nanowires are discussed.

To assess the ability of the discovered *Shewanella* appendages to conduct an electrical current, the authors employed a scanning tunneling microscope (STM) to image isolated appendages on conductive graphite surfaces under ambient conditions in air. Operating in constant-current mode, STM images revealed that the widths of the appendages ranged from 50 to 150 nm with the apparent heights of ~10 nm. The STM images also revealed a ridged structure of the appendages running along their lengths. The authors suggested that the ridges, with diameters of ~3 to 5 nm, appeared as individual electrically conductive nanowires. When a conductive material is imaged under STM, the apparent

height should be close to the actual height of the sample, whereas the apparent height of non-conductive samples should be zero. Therefore, the STM results indicated that the investigated *Shewanella* appendages (nanowires) were electrically conductive.

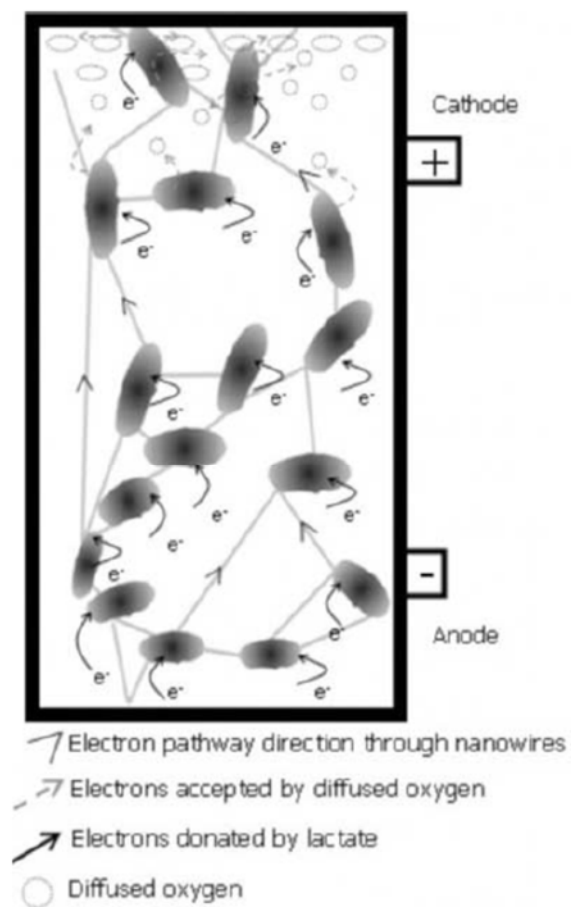


**Figure 2.5: A conceptual bio-geobattery model describing generation of electric field by transferring electrons from the anode (reduced zone) to the cathode (oxidized zone) through bacterial nanowires. Figure copied from Ref [51].**

Ntarlagiannis et al. [51] used quartzitic sand columns saturated with nutrient medium to show that electrically conductive nanowires of *Shewanella oneidensis* MR-1 are directly

associated with electrical potentials. The authors measured the self potentials (SP) at different locations along the columns relative to a reference electrode located at the bottom of the column. The SP measurements revealed that microbially induced charge transfer developed in the *Shewanella oneidensis* MR-1 column after a lag time of ~220 hours. In contrast, no significant voltages were recorded in the column using mutants lacking genes (OmcA and MtrC) that are suggested to be necessary to produce conductive nanowires. The authors associated the large SP gradients developed in the *Shewanella oneidensis* MR-1 column to the ability to transfer electrons through the nanowires, and proposed a conceptual bio-geobattery model (Figure 2.5) associated with the charge transfer mechanism in the column system performing similar to a MFC but without the use of direct electrical wiring between cathode and anode. In this model, electron donating (oxidation of lactate) and accepting (reduction of oxygen) processes serve as the anode and cathode reactions, respectively. The presence of nanowires serve as electrical connections linking the oxidizing and reducing zones, thus permitting electron transfer and producing an electric field.

El-Naggar et al. [52] reported quantitative electronic transport measurements across bacterial nanowires produced by *Shewanella oneidensis* MR-1 by resting a conductive AFM tip over individual bacterial nanowires supported on a conductive highly oriented pyrolytic graphite (HOPG) substrate, and measuring the current response as the voltage across each nanowire was swept. By converting the experimental data into normalized differential conductance spectra, which are  $(dI/dV)(I/V)^{-1}$ , the voltage dependence of the conductance revealed peaks indicating discrete energy levels with higher electronic density of states (DOS). The DOS features reflected the presence of certain electronic

structure of the molecules present on the bacterial nanowires that was suggested to mediate electron transport along *Shewanella* nanowires. Whether electrons are transported by hopping between localized states or through delocalized energy states across the nanowire remains unclear and requires further investigations.

## 2.5 Summary

A number of microbial strategies for electron transfer to extracellular electron acceptors have been reviewed. In addition to electron transfer through outer-membrane cytochromes and biosynthesized organic molecules, bacterial nanowires appear to be a common, but previously unrecognized, bacterial strategy for electron transfer to long-distance electron acceptors and possibly efficient energy distribution within microbial communities. Although the electrically conductive behavior of bacterial nanowires, particularly those of *G. sulfurreducens* and *S. oneidensis* MR-1, has been preliminarily confirmed, their specific conduction mechanisms as well as other physical properties are still unclear and await further investigations.



## Chapter 3

### 3 Cultivation of *Shewanella oneidensis* MR-1 for Bacterial Nanowire Production and Characterization Techniques

It has been remarked in the previous chapter that the DMRB *S. oneidensis* MR-1 produces electrically conductive bacterial nanowires under specific growth environments, which are electron-acceptor-limited conditions. In this chapter, experimental details of the bacterial cell cultivation method and growth parameters for inducing bacterial nanowire production by *S. oneidensis* MR-1 are presented. In addition, techniques employed in characterizing the *Shewanella* bacterial nanowires as well as procedures for preparing the biological samples for characterizations are discussed.

#### 3.1 Cultivation in Continuous Flow Chemostat Bioreactors

Cells of *S. oneidensis* strain MR-1 (wild-type) were cultured in continuous flow bioreactors (New Brunswick Scientific BioFlo 110, Figure 3.1) operating in chemostat mode with a dilution rate of  $0.05 \text{ h}^{-1}$  and an operating volume of 1 liter. Agitation was maintained at 50 rpm, to minimize mechanical shear forces, and pH was continuously monitored and maintained at 7.0 by using 2 M HCl. A chemically defined medium was used, containing the following: sodium lactate, 18 mmol/liter; PIPES buffer, 3 mmol/liter; ammonium chloride, 28 mmol/liter;  $\text{NaH}_2\text{PO}_4$ , 4.35 mmol/liter; ferric nitrilotriacetic acid (NTA), 0.1 mmol/liter; and sodium selenate, 0.001 mmol/liter. 10 ml of 10 $\times$  Wolfe's vitamin solution, and 10 ml of 10 $\times$  Wolfe's mineral solution were

supplied from stock solutions. The 10× Wolfe's vitamin solution (per liter of deionized water) contained 2.0 mg of biotin, 2.0 mg of folic acid, 10.0 mg of pyridoxine HCl, 5.0 mg of riboflavin, 5.0 mg of thiamine, 5.0 mg of nicotinic acid, 5.0 mg of pantothenic acid, 0.1 mg of cyanocobalamin, 5.0 mg of *p*-aminobenzoic acid, and 5.0 mg of thioctic acid. The 10× Wolfe's mineral solution (per liter of deionized water) contained 2.14 g of NTA, 0.1 g of  $\text{MnCl}_2 \cdot 4\text{H}_2\text{O}$ , 0.3 g of  $\text{FeSO}_4 \cdot 7\text{H}_2\text{O}$ , 0.17 g of  $\text{CoCl}_2 \cdot \text{H}_2\text{O}$ , 0.2 g of  $\text{ZnSO}_4 \cdot 7\text{H}_2\text{O}$ , 0.03 g of  $\text{CuCl}_2 \cdot 2\text{H}_2\text{O}$ , 5 mg of  $\text{KAl}(\text{SO}_4)_2 \cdot 12\text{H}_2\text{O}$ , 5 mg of  $\text{H}_3\text{BO}_4$ , 0.09 g of  $\text{Na}_2\text{MoO}_4$ , 0.11 g of  $\text{NiSO}_4 \cdot 6\text{H}_2\text{O}$ , and 0.02 g of  $\text{Na}_2\text{WO}_4 \cdot 2\text{H}_2\text{O}$ .

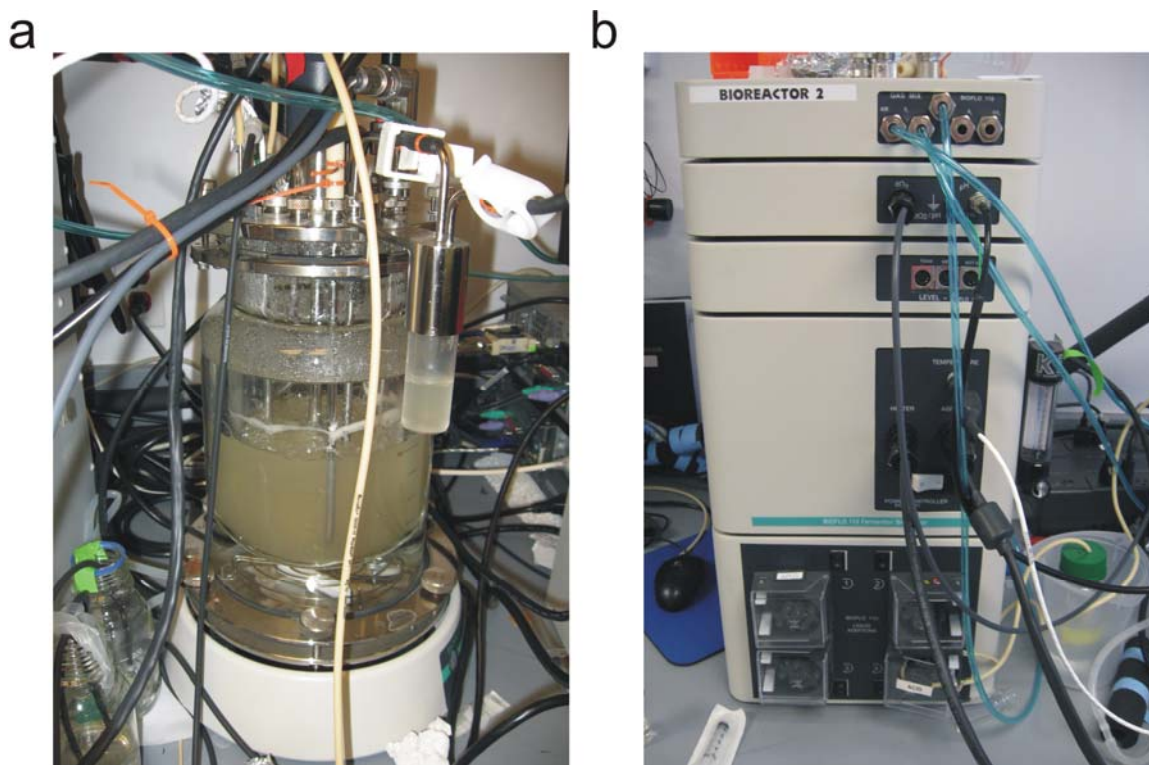


**Figure 3.1: (a) Continuous flow bioreactor employed for cultivation of *S. oneidensis* MR-1 (wild-type). The bioreactor is integrated with (b) a controlling unit for gas flow control, agitation control, pH and dissolved oxygen concentration monitoring, fresh medium supply, and old medium withdrawal.**

The bioreactor was first operated in batch mode, which is a closed loop system. In batch culture, the growth conditions undergo continual changes as no additional nutrients are added to supplement that depleted. Cell growth in batch culture can be divided into four distinct phases: lag, exponential or logarithmic phase, stationary phase, and dead phase. Figure 3.2 displays the organic acid concentration profile and cell density versus time for *S. oneidensis* MR-1 grown in batch culture. The organic acid concentrations were measured using high-performance liquid chromatography (HPLC), whereas the cell densities were obtained at 600 nm on a UV/Vis spectrophotometer. Lactate was the sole electron donor applied to the system at an initial concentration of 18 mM. As cells were grown aerobically, oxygen served as the sole terminal electron acceptor. In the first 12 h, cells were growing in their lag phase. In this phase, lactate was being consumed and the cell density started to increase moderately. Within this period, pyruvate and acetate were detected because lactate was not completely oxidized to carbon dioxide (CO<sub>2</sub>) but to pyruvate. Pyruvate could serve as electron donor for the cells and they were subsequently oxidized to acetate, which could also serve as electron donor. In the exponential or logarithmic phase (between 12 and 30 h of growth), the cell density increased rapidly with rapid consumption of lactate and production of pyruvate and acetate. Approaching the stationary phase (~30 h of growth), all lactate and pyruvate were consumed and only acetate was remaining to provide electrons to the cells. After 38 h of growth, all of the remaining acetate was depleted. In this phase, the cell density became stabilized as no nutrients (electron donors) were available in the system. This growth environment is called electron-donor-limited condition. At this stage, the bioreactor would be ready for switching to continuous mode.

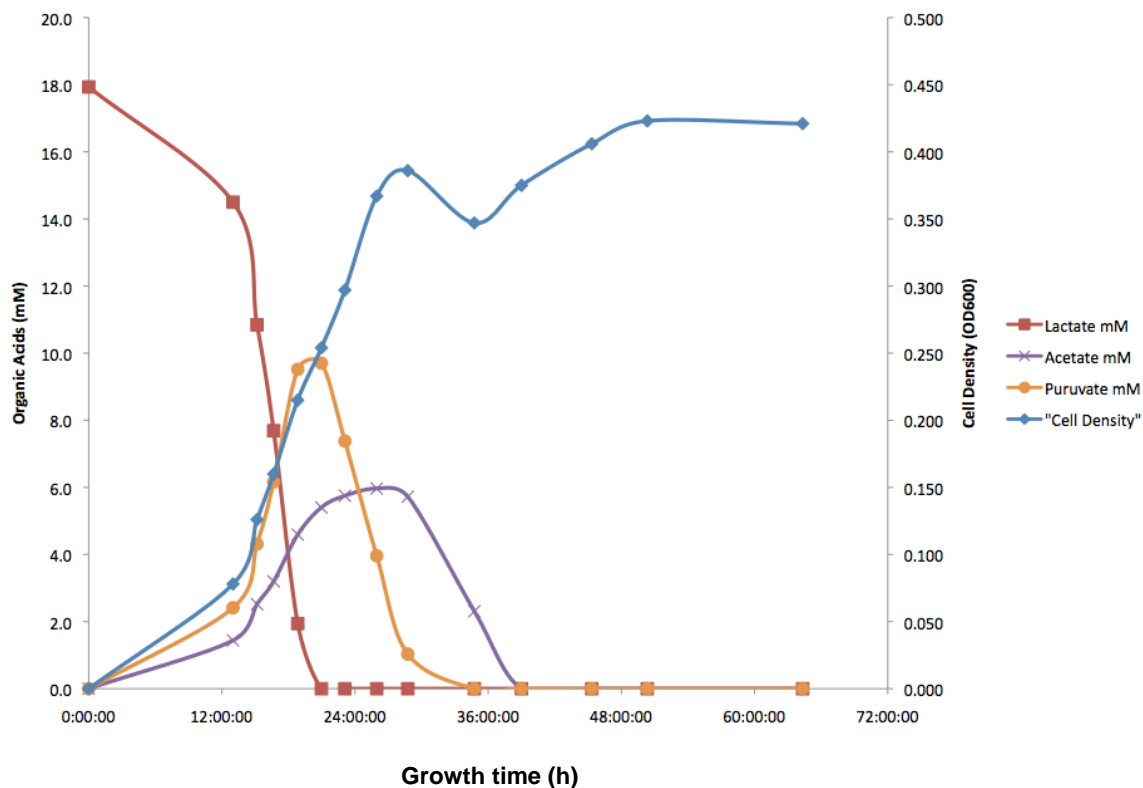


**Figure 3.2: Organic acid concentration (mM) and cell density (OD600) versus growth time (h) for *S. oneidensis* MR-1 (wild-type) cultivated in batch mode.**

Throughout cultivation in both batch and continuous modes, the dissolved oxygen ( $O_2$ ) tension (DOT) was monitored using a polarographic  $O_2$  probe and meter and was maintained at desired values by using a control loop and switching valves that automatically adjusted the air-nitrogen ( $N_2$ ) ratio of the influent gas stream. Figure 3.3 shows a captured screen view of the dissolved  $O_2$  concentration (blue line) and the amount of air (green line) supplied to the bioreactor versus growth time. The system was set up with two gas lines (air and pure  $N_2$ ). As the cells were growing and consuming the oxygen dissolved in the media, the controller had to put in a higher percentage of air versus  $N_2$  into the bioreactor, which was observed by the increase in the green line at the

initial growth stage. After certain time the cells were so active and their density was so high that the controller could not keep up, resulting in saturation at 100% (green line), meaning that 100% of the gas going into the bioreactor was air. At this point the active cell density was so high that all of the oxygen in the system was being consumed, therefore the dissolved O<sub>2</sub> concentration (blue line) dropped to the minimum level. A big spike in dissolved O<sub>2</sub> was suddenly observed at the point when the cells had consumed all of the electron donors (lactate, puruvate, and acetate) in the system. As the electron donors ran out, the cells stopped respiring. Since the controller was still supplying 100% air to the bioreactor, the dissolved O<sub>2</sub> began to rise as the cells had no more “food”. At this point, the bioreactor was switched to continuous mode and fresh media were fed at a slow rate. The dissolved O<sub>2</sub> was stepped down through the controller from 20% of air, to 10% and 5%. The cells were now poised to produce nanowires as the supply of electron acceptor was limited. By setting the dissolved O<sub>2</sub> to 0% (or below the detection of the polarographic O<sub>2</sub> electrode) (not shown in Figure 3.3), bacterial nanowires were produced in response to electron acceptor (O<sub>2</sub>) limitation. It should be noted here that the 0% dissolved O<sub>2</sub> was not equivalent to an anaerobic condition but it was a balance where a small amount of air was supplied that was consumed immediately by the cells. The bioreactor was allowed to run in this steady state for 24 h or more before nanowires were harvested.

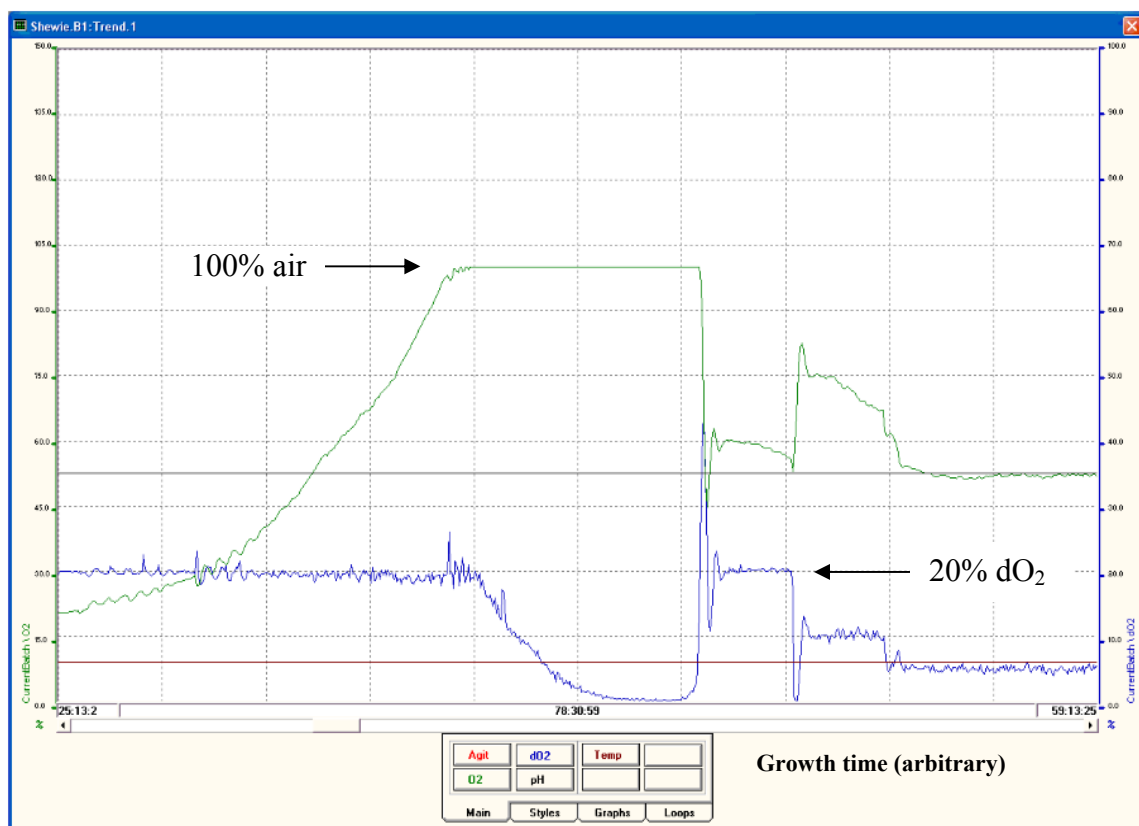


**Figure 3.3: A screen view captured from the controller display showing the dissolved oxygen concentration of air and the percentage air versus nitrogen supplied to the bioreactor as a function of growth time.**

## 3.2 Sample Preparation and Characterizations of Bacterial Nanowires

After the bacteria and nanowire samples were harvested from the bioreactor, they were examined by a variety of microscopic methods (electron, optical and scanning probe methods) and their electrical conductivity characterized by scanning probe techniques. For biological specimens, special preparation procedures and treatments are required for specific imaging methods in order to preserve the delicate samples, allow them to be imaged under certain working environments, and enhance the imaging quality. All Gram-

negative bacteria present pili, flagella or other extracellular appendages that play specific biological roles such as biofilm formation [53-56] or DNA transfer between cells [57-59]. Without recognizing the specific functions of these appendages, a more general term “nanofilament” can be used, considering their similarity in size, to describe appendages attached to the bacteria [60]. Instead, the term “nanowire” is used to describe a specific function of the nanofilament, i.e. transport of electrons, but not a particular structure. In the following subsection, different techniques employed in this thesis work for characterizing bacterial nanofilaments and nanowires are discussed, and details of the sample preparation procedures are presented.

### 3.2.1 Scanning Electron Microscopy

For many years, scanning electron microscopy (SEM) has been used to image bacterial cells as well as their ultrafine structures such as bacterial nanofilaments [61-63]. SEM is one type of electron microscopy technique that images a specimen by scanning it with a beam of high-energy electrons (on the order of keV) in a raster scan pattern. The electrons interact with the surface atoms of the specimen, generating a variety of signals that contain information about the specimen’s topography, composition, and other properties. Conventional SEM imaging requires specimens to be electrically conductive and electrically grounded to prevent the accumulation of electrostatic charge at the surface. Non-conductive specimens can be coated with a thin layer of conductive material such as gold, platinum, osmium, carbon, etc, on the surface to prevent the charging effect. Since the working chamber of typical SEM is at high vacuum (on the order of  $10^{-5}$  to  $10^{-7}$  Torr), specimens are normally required to be completely dry. Therefore, biological

samples usually require chemical fixation and dehydration treatment to preserve and stabilize their structures.

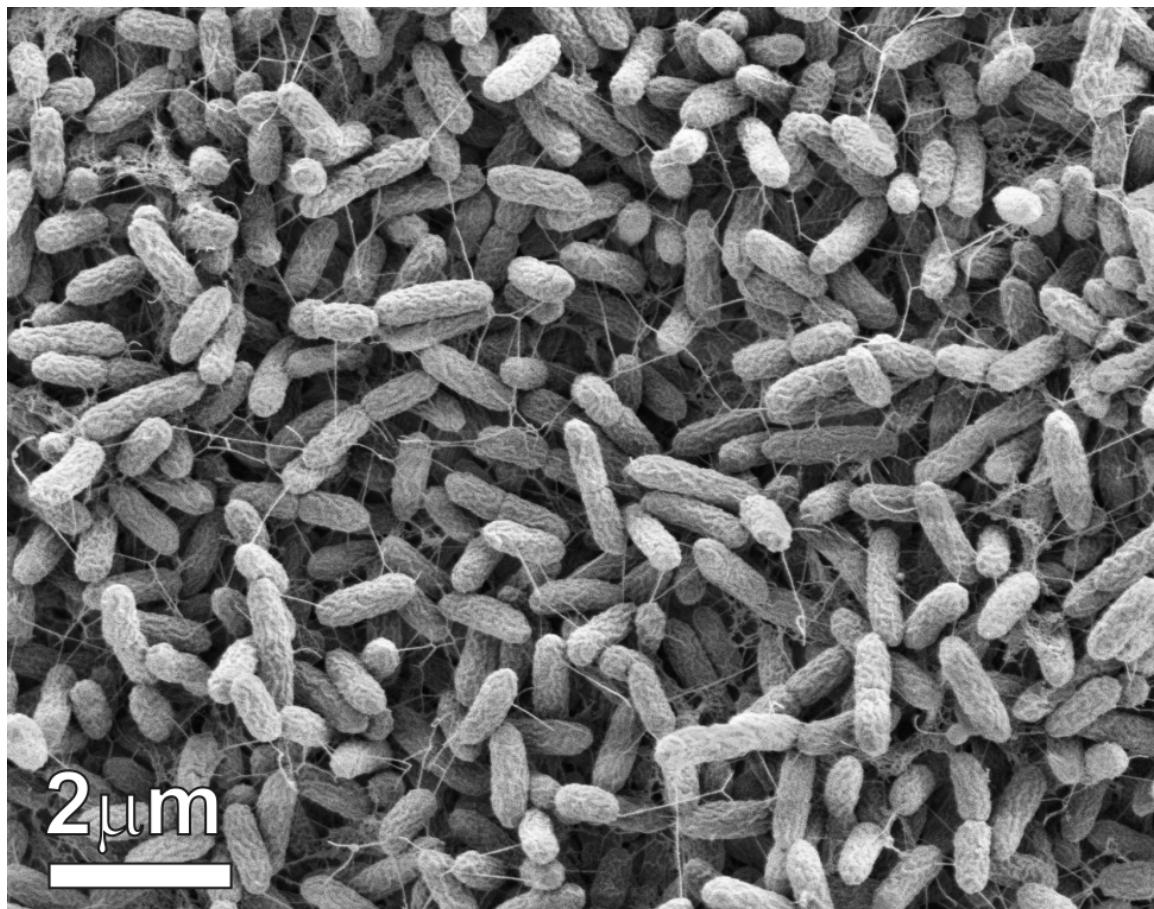
After samples were harvested from the bioreactor, SEM was one of the first characterization tools used for assessing whether bacterial nanowires were produced by the cells. Harvested cells (with potential nanowires) were first chemically fixed with 2% glutaraldehyde. Fixation is usually the first step to preserve biological samples (tissue and cells) as close to their natural states as possible for electron microscopy or other analysis. Chemical fixatives such as aldehydes are commonly used for preserving bacterial cells by killing the cells and thus preventing post-mortem decay that can cause autolysis and putrefaction. After chemical fixation, the bacterial samples were pushed through a membrane filter with pore size of 0.2  $\mu\text{m}$  using a syringe setting such that only the liquid media were removed while the cells remained on the filter as they could not pass through the pores. The filter with bacterial samples on it was then gently washed successively with pH 7 phosphate buffer solution (PBS), diluted PBS (1:1 with distilled water) and deionized water. The samples were then dehydrated through a graduated series of ethanol with increasing concentrations (25, 50, 75, 90, and 100%). After three final changes in 100% ethanol, the samples were subjected to critical-point drying. Air (evaporative) drying of specimens can cause severe deformation and collapse of structure. Such sample damage is primarily caused by the effects of surface tension as the common specimen medium is water which has a high surface tension to air. Critical-point drying is a drying technique that achieves a phase change of  $\text{CO}_2$  from liquid to dry gas without the effects of surface tension and is therefore widely used for delicate biological samples. Following



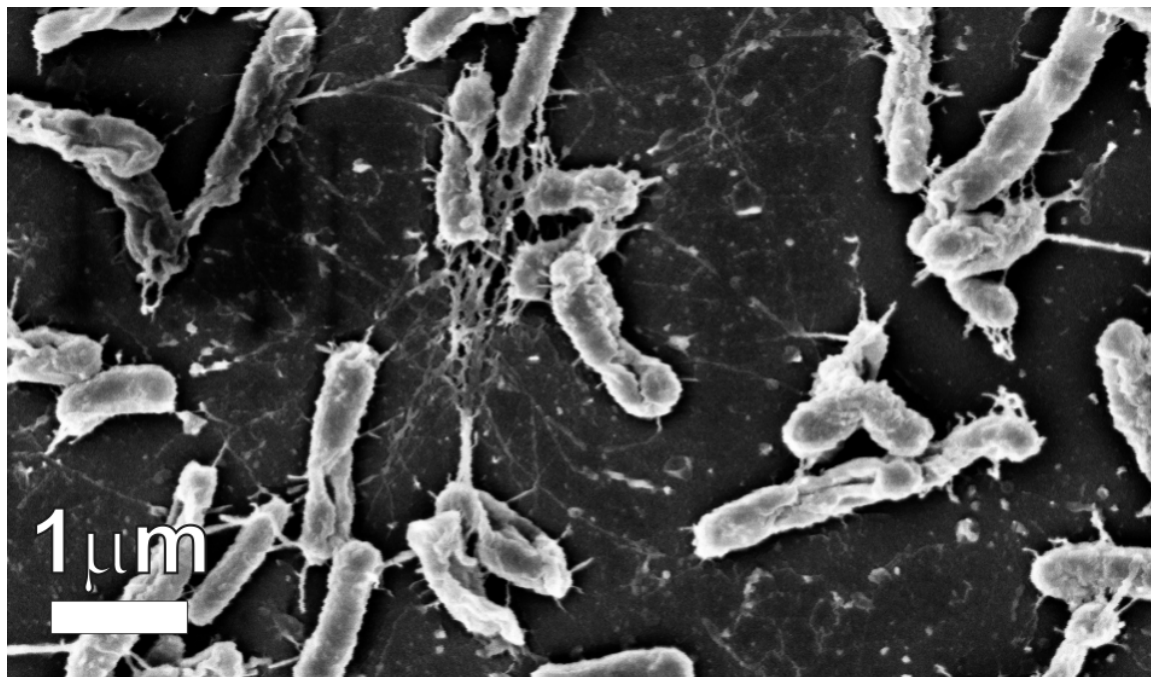
critical-point drying, samples were coated with a thin layer of Pt in a sputter-coater and examined on a LEO 1540XB field emission SEM.

Figure 3.4 shows an SEM image of cells of *S. oneidensis* MR-1 cultivated in a continuous flow chemostat bioreactor under electron-acceptor-limited conditions. It can be seen that a high amount of nanofilaments connecting neighboring cells are present in the bacterial colony. The observed length of the nanofilaments ranges from tens of nanometers to tens of micrometers, however the diameter of the nanofilaments cannot be accurately estimated from the SEM images. As the sample had gone through standard biological sample preparation procedures for SEM, i.e. chemical fixation, ethanol dehydration followed by critical-point drying, the cells structures were preserved and remained intact throughout the analysis. In contrast, if the bacterial cells were not dehydrated and critical-point dried prior to imaging, the cell structures appeared to be deflated, severely deformed and even collapsed as shown in Figure 3.5.

Bacteria produce extracellular polymeric substances (EPS) to facilitate cell attachment on surfaces, aggregation, flocculation and biofilm formation. EPS are composed of polysaccharides, proteins, lipids, nucleic acids and other biological macromolecules. As EPS would challenge microscopic analysis of the physical character of bacterial nanowires and electrical/electronic measurements, cultivating *S. oneidensis* MR-1 in continuous culture is referred over batch culture to eliminate EPS in the samples. Figure 3.6 shows cells collected in batch culture, which express EPS in addition to nanofilaments, contrasting the sample shown in Figure 3.4 which are free of EPS.



**Figure 3.4: An SEM image showing cells of *S. oneidensis* MR-1 cultivated in a continuous flow chemostat bioreactor under electron-acceptor-limited conditions. The cells express a high amount of nanofilaments connecting neighboring cells. This sample was chemically fixed, dehydrated through a graduated series of ethanol, critical-point dried, and coated with Pt prior to SEM imaging.**



**Figure 3.5: An SEM image showing cells of *S. oneidensis* MR-1 harvested in a continuous flow chemostat bioreactor operating under electron-acceptor-limited conditions. This sample was only chemically fixed and Pt coated prior to SEM imaging. Without going through ethanol dehydration processes and critical-point drying, the cell structures were severely deformed and collapsed, especially when subjected to high-vacuum environment in SEM, although nanofilamentous structures could still be observed.**

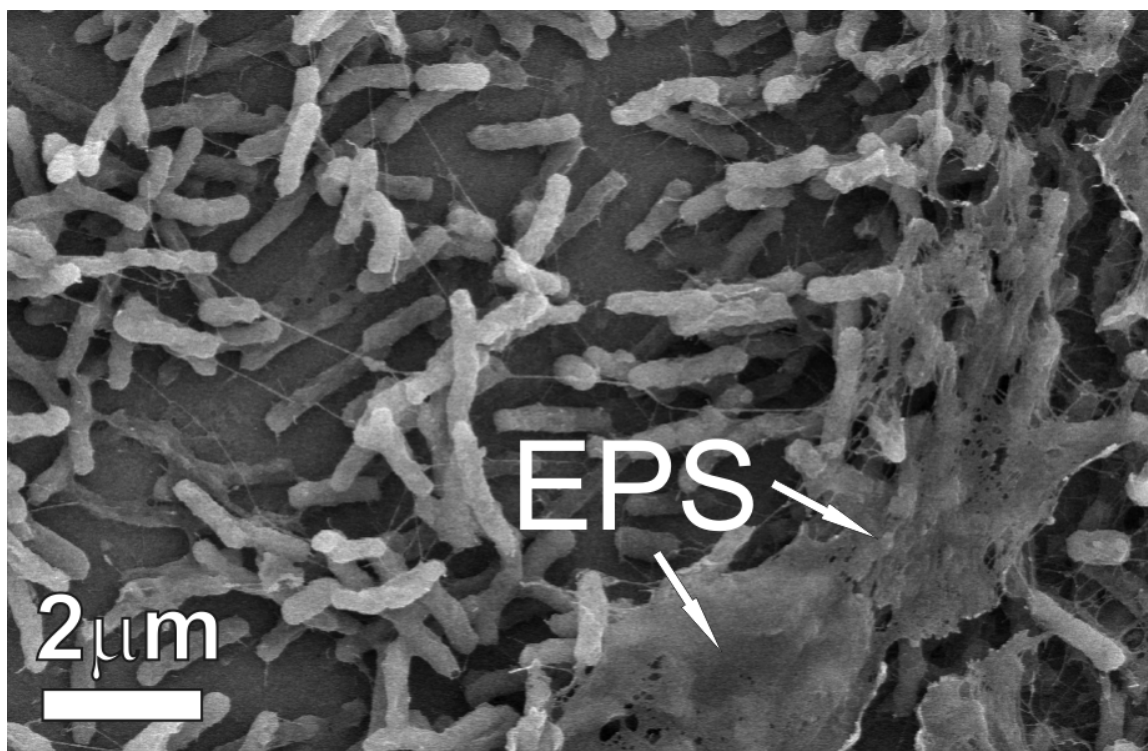


**Figure 3.6: An SEM image showing cells of *S. oneidensis* MR-1 harvested in batch culture. In addition to nanofilaments, extracellular polymeric substances (EPS) are observed in the sample, which can challenge microscopic analysis and electrical measurements on bacterial nanowires.**

### 3.2.2 Transmission Electron Microscopy

Transmission electron microscopy (TEM) has been used since two decades ago to image bacteria as well as their pili and flagella [64-67]. The high-magnification and high-resolution imaging capability of TEM allows it to provide much more accurate estimation, particularly on the lateral dimensions of nanofilaments which are usually less than 15 nm, when compared with SEM. Typically, TEM uses an electron beam with relatively high energy (~100 keV or higher) that is transmitted through the specimen where electrons can be scattered or directly pass through depending on the material

property of the specimen. Therefore, the electrons emerging from the specimen carry the structural information of the specimen. Because most biological samples are nearly “transparent” to the high-energy electrons, staining the samples with heavy metals such as lead, uranium or tungsten can scatter the imaging electrons and thus enhance contrast between different structures.

TEM analysis of nanofilaments of *S. oneidensis* MR-1 was carried out in a Philips CM-10 TEM system. Filtered uranyl acetate (2% solution dissolved in distilled water) was used as the negative-staining reagent. Negative staining is an easy and rapid method for examining biological structures (organelles, macromolecules and viruses) at the EM level because it requires no specialized equipment. The negative stain does not react with the specimen in a “positive staining” manner. However, uranyl ions will bind to proteins and sialic acid carboxyl groups and to lipid and nucleic acid phosphate groups, providing scattering sites for incoming electrons and thus enhancing contrast of the biological structure(s). The harvested samples were applied as droplet on a TEM grid, stained with 2% uranyl acetate, and dried in air after removing excess media on the grid using absorbent paper. The TEM micrographs presented in Figure 3.7 show a chemically fixed and negatively stained cell of *S. oneidensis* MR-1. The bacterium expresses a number of nanofilaments emanating from the cell body. The apparent lateral dimension of these nanofilaments is ~10 nm. The TEM micrographs (Figure 3.8) show another *Shewanella* bacterium with a flagellum emanating from the pole of the cell and a branched nanofilament from the side of the cell. Such branched structures are consistent with those displayed in the SEM image (Figure 3.4).

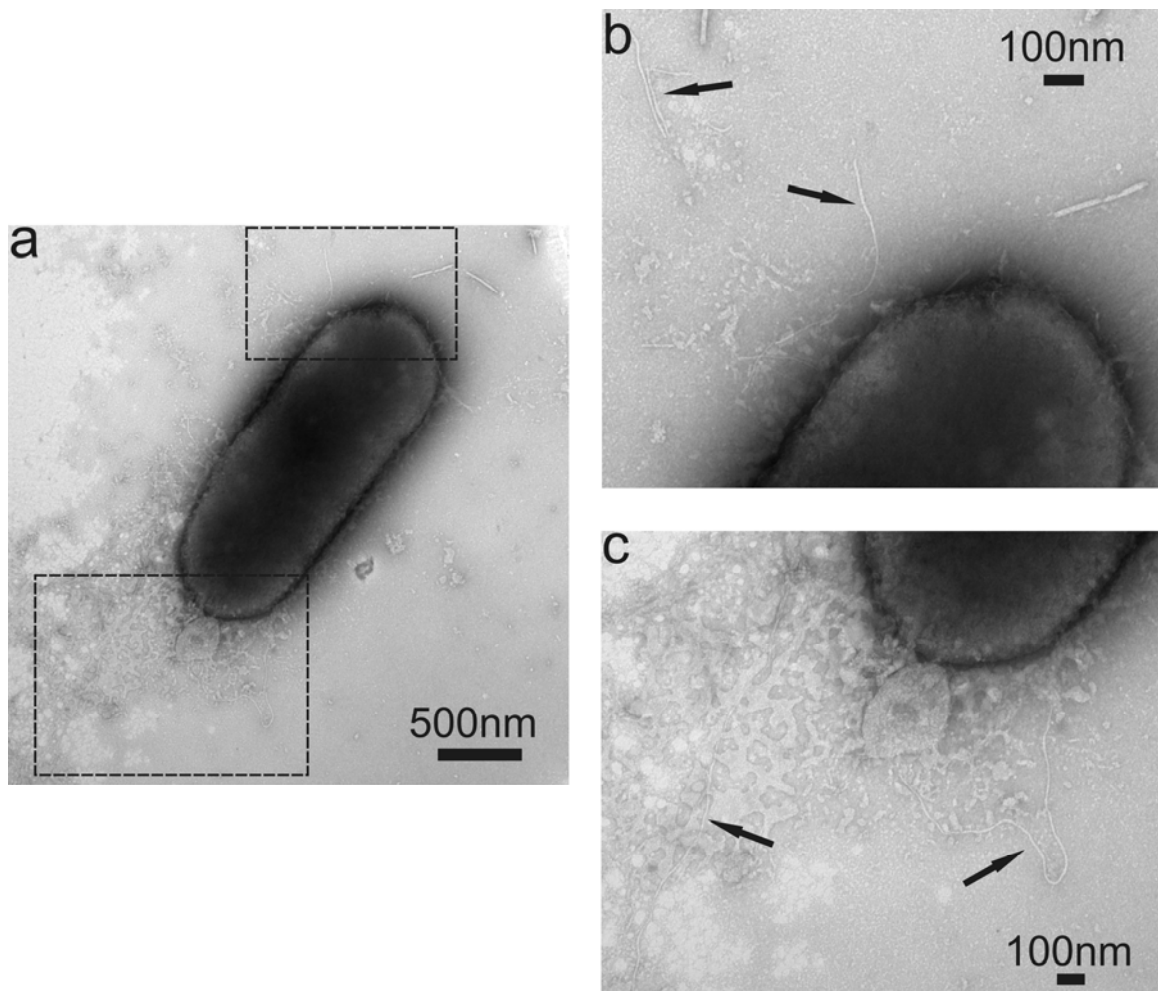


**Figure 3.7: (a) TEM micrographs showing a negatively stained *S. oneidensis* MR-1 bacterium with nanofilaments (indicated by arrows in (b) and (c)) emanating from the cell body with a lateral dimension of  $\sim 10$  nm measured from the TEM images.**

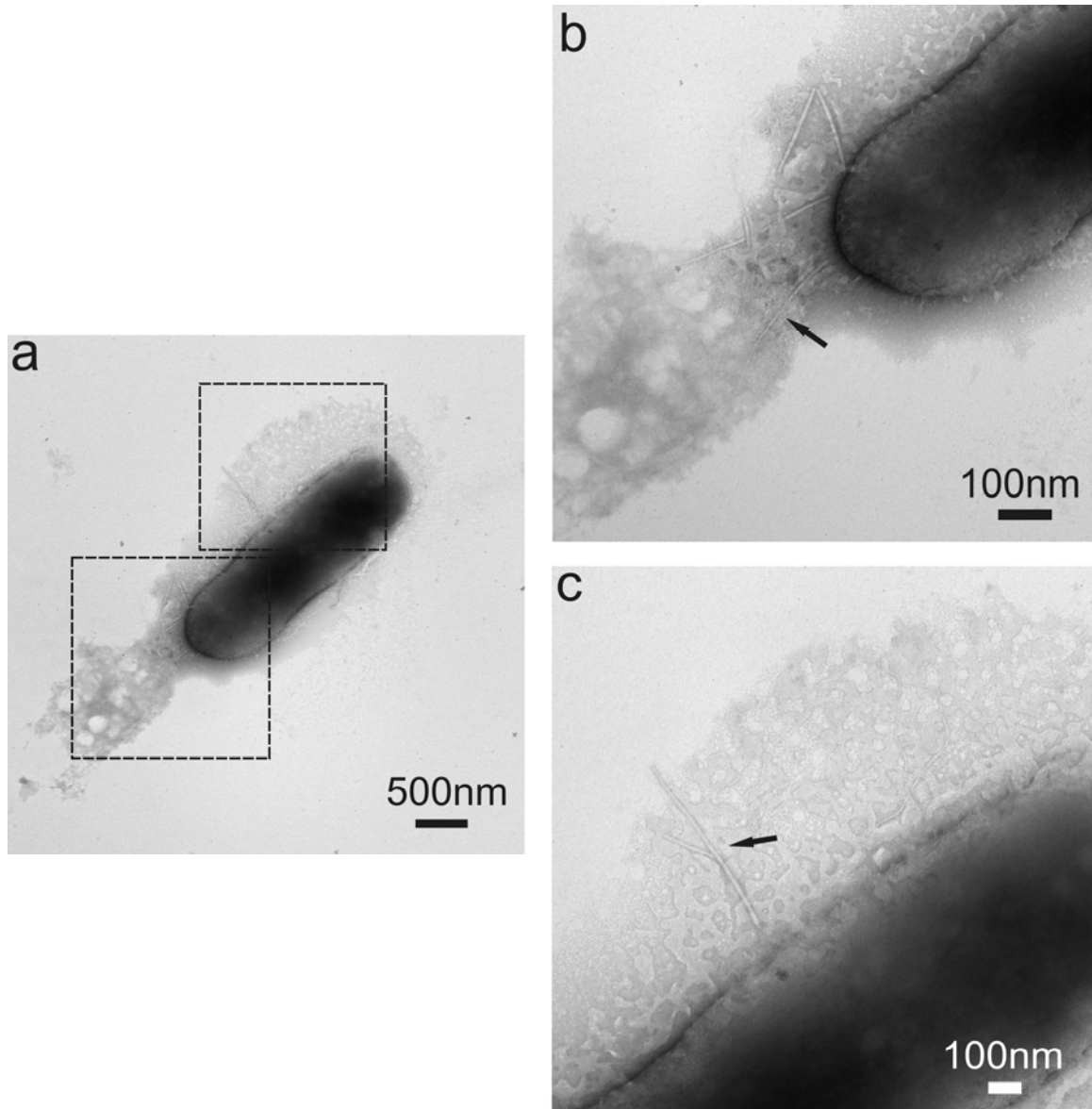


**Figure 3.8: (a) TEM micrographs showing a negatively stained *S. oneidensis* MR-1 bacterium with a flagellum (indicated by an arrow in (b)) emanating from the pole of the cell and a branched nanofilament (indicated by an arrow in (c)) from the side of the cell.**

### 3.2.3 Fluorescence Microscopy

Light (optical) microscopy is one of the most commonly and easily used tools in observing biological cells. The resolving power of a light microscope is the ability of the microscope to distinguish between two adjacent objects as distinct and separate. In general, the resolving power (or resolution) of light microscopy is mainly limited by the wavelength of light source ( $\lambda$ ) and the numerical aperture ( $NA$ ) of the objective lens, with the following relationship:

$$d = \frac{\lambda}{2NA} \quad (1)$$

In practice, the lowest value of  $d$  obtainable using visible light source is about 200 nm, which is much larger than the lateral dimension of bacterial nanofilaments. An optical micrograph of cells of *S. oneidensis* MR-1 is shown in Figure 3.9. Only cells but not nanofilaments can be seen using this imaging technique.

Fluorescence microscopy is one type of light microscopy technique using the phenomena of fluorescence and phosphorescence in addition to reflection and absorption in conventional light microscopy. A specimen is irradiated with light at a specific wavelength, causing fluorescence in the specimen. The light emitted by the effect of fluorescence from the specimen, which is at a different and longer wavelength, is then detected. In order to observe the nanofilaments and their nature, harvested *S. oneidensis* MR-1 samples were reacted with a non-specific protein staining reagent NanoOrange (Invitrogen) and examined using a fluorescence microscope (Zeiss Axio Imager Z1) with



an excitation  $\lambda$  of 470 nm. The fluorescence image is shown in Figure 3.10. By this method, it has been confirmed that the nature of the bacterial nanofilaments is protein.

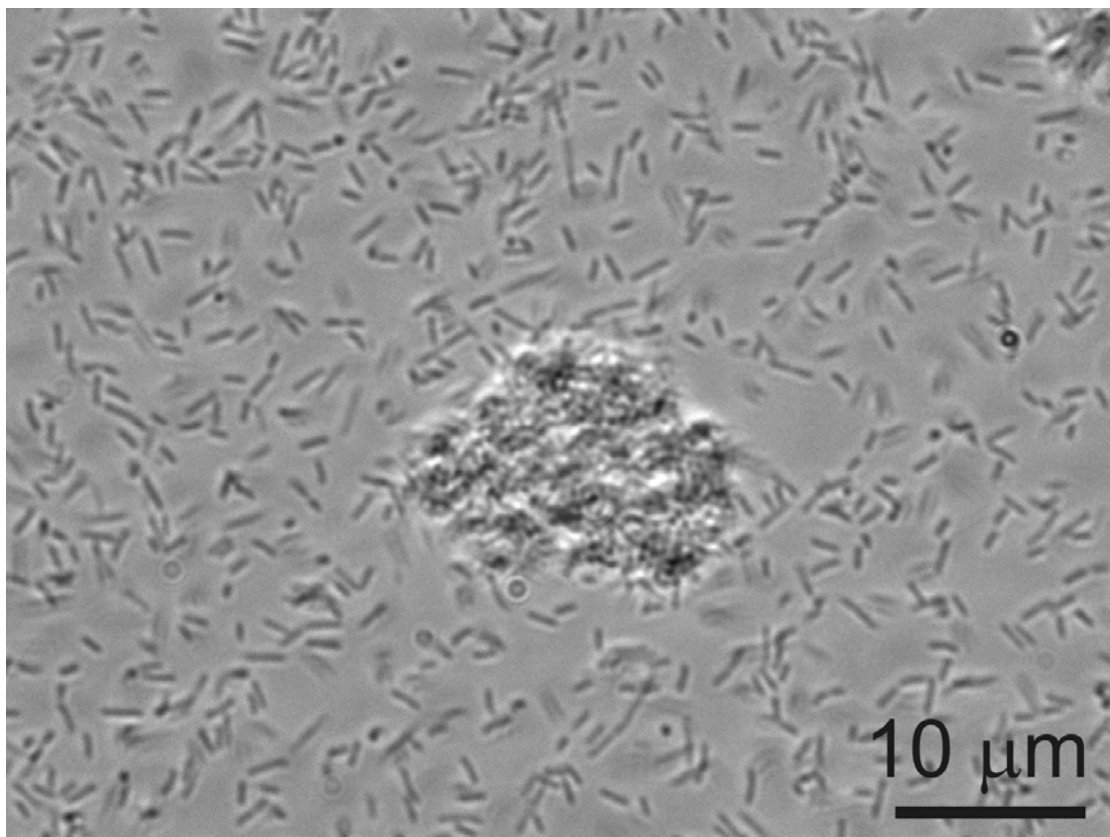


**Figure 3.9: An optical micrograph showing cells of *S. oneidensis* MR-1. Nanofilaments such as nanowires and flagella cannot be observed owing to the limitation of resolution, which is typically 200 nm for visible light illumination.**

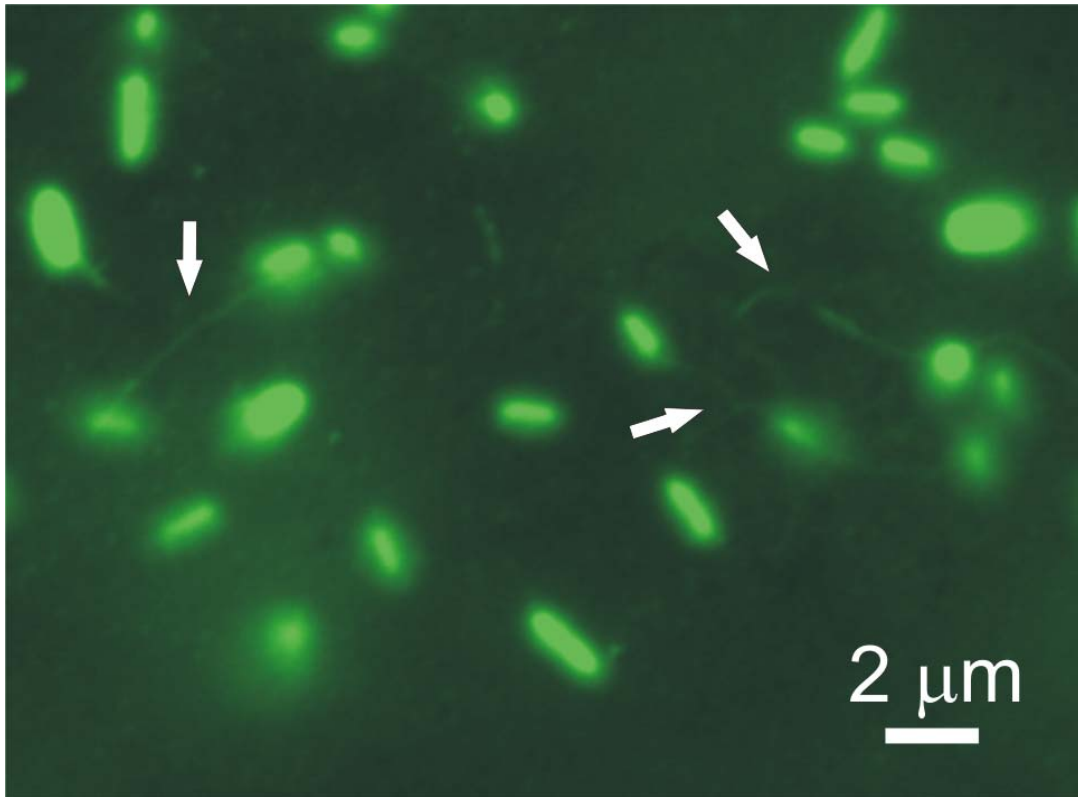


**Figure 3.10: A fluorescence microscopic image of *S. oneidensis* MR-1 cells stained with non-specific protein-binding reagent in liquid media. The bacterial cells and nanofilaments (indicated by arrows) fluoresce under excitation at 470 nm.**

### 3.2.4 Atomic Force Microscopy

Atomic force microscopy (AFM) belongs to the family of scanning probe microscopy that uses a laser beam deflection system where a laser is reflected from the back of an AFM cantilever with a sharp tip (probe) on the other side that is used to scan the specimen surface. The reflected beam is collected by a photodetector, which measures the beam position that contains information about the surface topography of the specimen. The typical radius of AFM tips ranges from a few to tens of nanometers, enabling the use of AFM to observe very fine structures down to sub-nanometer scale. The working

principle of AFM and its different modes of operation (contact, non-contact and tapping) as well as applications to biological sciences have been reviewed by Jalili and Laxminarayana [68]. Tapping-mode AFM allows high resolution imaging of soft samples that are difficult to examine using contact mode, so it is widely used for imaging biological samples. Exemplary tapping-mode topography and amplitude AFM images of *S. oneidensis* MR-1 cells are presented in Figure 3.11. The sample was chemically fixed and applied on a highly oriented pyrolytic graphite (HOPG) substrate. After rinsing with PBS and deionized water, the sample was dried in air prior to imaging using a Veeco Dimension V AFM system. As the sample did not go through critical-point drying, the cell shapes still appear to be intact but flattened. The helical nanofilaments can be distinguished as the flagella of the cells.

Another important AFM technique employed in this thesis work is conducting-probe atomic force microscopy (CP-AFM). For CP-AFM, it is basically operating as contact-mode AFM in which a bias voltage is applied between the tip and the sample. Therefore, CP-AFM is able to image both the topography and the conductivity of the sample at the same time. Usually, the AFM probes can be coated with a conductive layer of metallic material such as gold (Au) and platinum (Pt). In addition to conductivity mapping, the current-voltage (I-V) spectroscopy mode in CP-AFM supports the acquisition of I-V curves to investigate electrical properties of the sample. More details of this operation mode employed in studying bacterial nanowires will be discussed in Chapter 4.

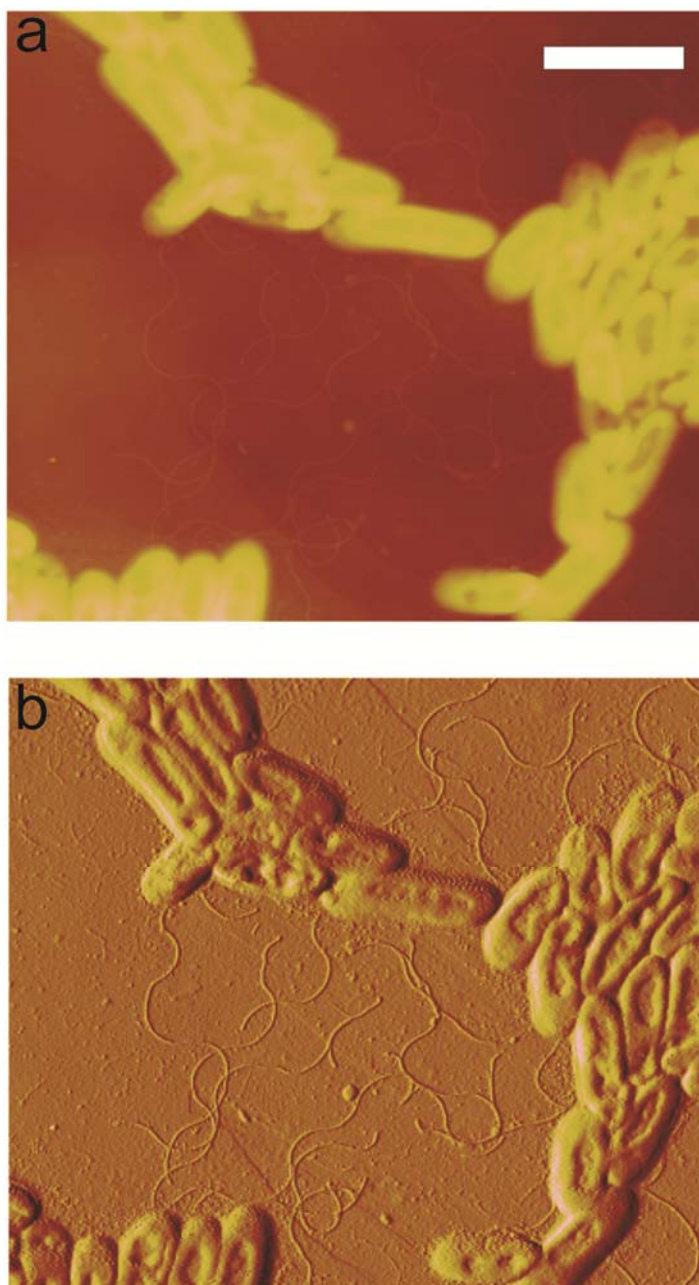


**Figure 3.11: Tapping-mode (a) topography and (b) amplitude AFM images of *S. oneidensis* MR-1 cells. The scale bar is 2 μm.**

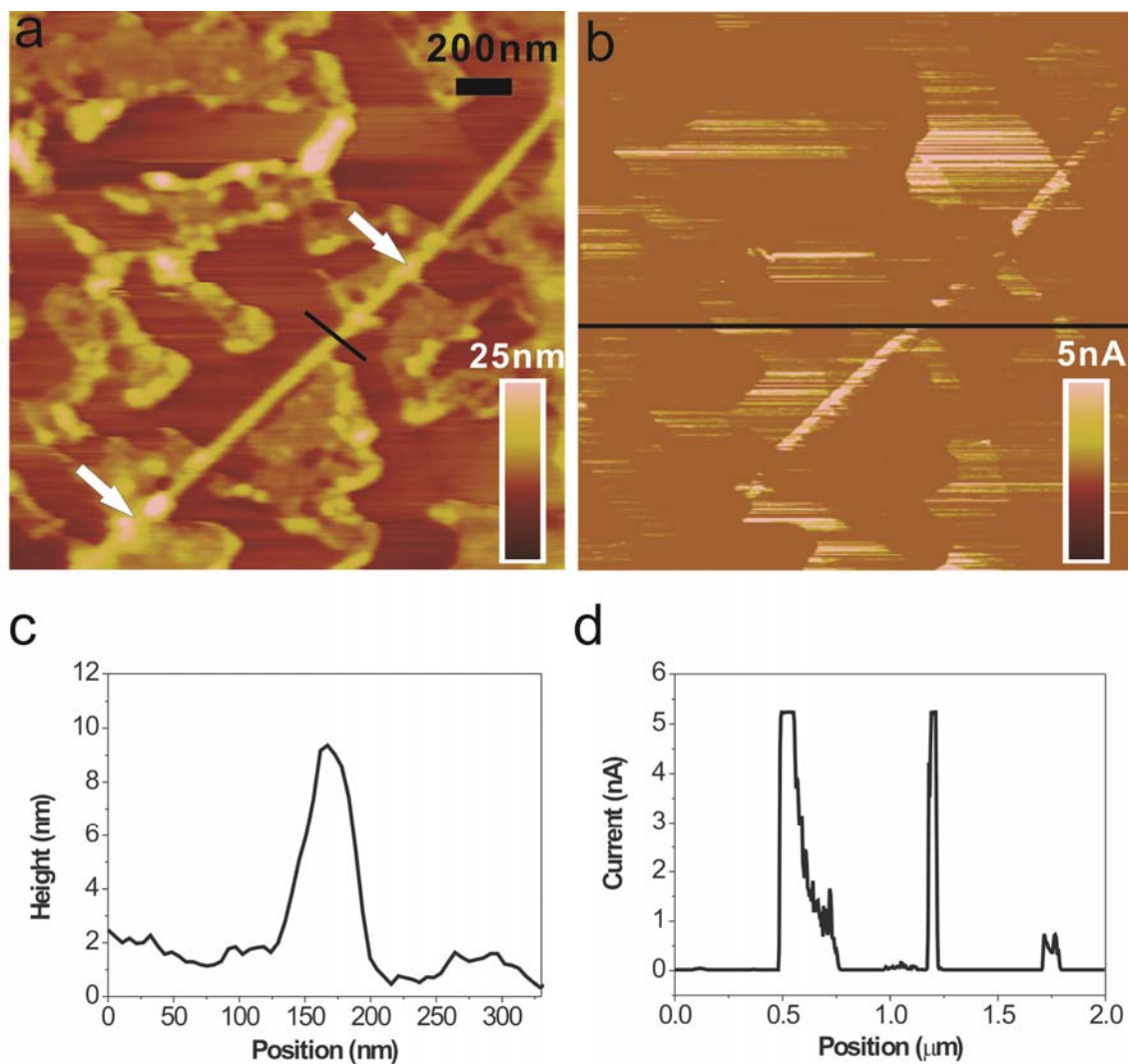


**Figure 3.12: (a) Topography image and (b) simultaneous conductivity map of a bacterial nanowire from *S. oneidensis* MR-1 collected in batch culture accompanied with some non-conducting substances, possibly EPS. (c) The height and (d) current profiles (indicated by black lines) across the nanowire reveal that the radial dimension of the nanowire is  $\sim 10$  nm and the nanowire is electrically conductive.**

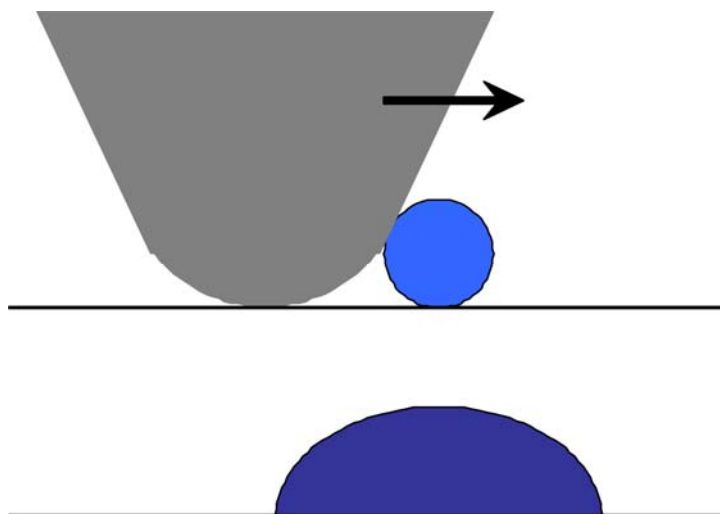


**Figure 3.13: Simple model explaining the broadening effect due to AFM tip geometry. Comparing with the actual width of the object (upper), the apparent width in the topographic image (lower) is over estimated but the height can be measured very accurately.**

In order to study the conductivity of bacterial nanowires, Pt-coated AFM probes (BudgetSensors) with a nominal spring constant of 0.2 N/m were used for contact-mode imaging and electrical measurements. The actual spring constants and sensitivities of individual conducting probes were determined by performing force-distance measurements on a sapphire substrate and using the thermal tune method. Topography imaging of the bacterial nanowire (Figure 3.12 (a)) was performed at a loading force of 4 nN. The measured height of the bacterial nanowire is  $\sim 10$  nm according to the profile (Figure 3.12(c)) across the nanowire (black line in Figure 3.12(a)), consistent with measurements by TEM. However, the apparent lateral dimension of the nanowire is much

larger than 10 nm (>50 nm) due to the effect of tip geometry resulting in profile broadening (an example shown in Figure 3.13), which is a known issue of AFM imaging. Bias voltage of 3 V was simultaneously applied to the substrate (HOPG) during imaging for obtaining the current map in Figure 3.12 (b). Except areas that are blanketed by insulating substances (indicated by white arrows), possibly EPS secreted by the cells as this sample was harvested in batch culture, the whole nanowire structure is assessed to be electrically conductive. Therefore, CP-AFM data suggest that bacterial nanowires from *S. oneidensis* MR-1 may be composed of closely-packed conductive proteins along the length to facilitate long-range electrical transport.

### 3.2.5 Scanning Tunneling Microscopy

The principle of scanning tunneling microscopy (STM), another type of scanning probe microscopy with setting similar to AFM, is based on tunneling of electrons between a sharp, conductive STM probe and the sample. Unlike CP-AFM, the probe in STM does not make direct contact with the sample surface. When the probe and the sample are brought into close proximity to each other (e.g. 1 nm) and a voltage is applied between them, electrons will flow across the gap generating a tunneling current. Owing to this working principle, samples for STM are required to be conductive or semiconductive. STM has extremely high depth resolution (on the order of 0.01 nm) because very small changes in the probe-sample separation induce large changes in the tunneling current as expressed by the relationship,  $I \sim Ve^{-cd}$ , where  $I$  is the tunneling current,  $V$  the voltage between probe and sample,  $c$  a constant, and  $d$  the probe-sample separation distance. Although STM works in air as well as under liquids, ultrahigh vacuum (UHV) is

preferred to avoid contamination of samples from the surroundings as sample cleanliness is one of the most critical requirements in STM imaging. Moreover, it is not a common practice to study biological samples using STM as most biological samples are highly insulating.

Samples from bioreactor cultures of *S. oneidensis* MR-1 were applied to a freshly cleaved surface of HOPG. Following cleaning and drying procedures identical to that for AFM, the samples were examined by an Omicon STM system under high vacuum conditions (on the order of  $10^{-8}$  Torr) by using electrochemically etched tungsten (W) tips. Topography images were collected under constant-current imaging conditions (0.2 V gap voltage and 13 nA feedback current). In many cases, STM imaging of bacterial nanowires was challenged by bacterial cells, which are non-conductive and relatively much high in height, and organic contaminants, which can mask the surface of the sample. These insulating objects could result in tip contamination and even crashing during constant-current mode of operation while the tip was trying to move toward the sample for obtaining a measurable tunneling current. The STM image shown in Figure 3.14 revealed that isolated nanowires from *S. oneidensis* MR-1 could possess a ridged or bundled structure running along their lengths. The ridges, with apparent diameters of 6-10 nm, appeared as individual electrically conductive nanowires. Similar structures of bacterial nanowires from different microorganisms were reported by Gorby et al [45]. For a conductive material imaged in STM, the apparent height should be close to the actual height, whereas the apparent height of a non-conducting sample should be zero. Therefore, the STM data suggest that the *Shewanella* nanowires are highly conductive.



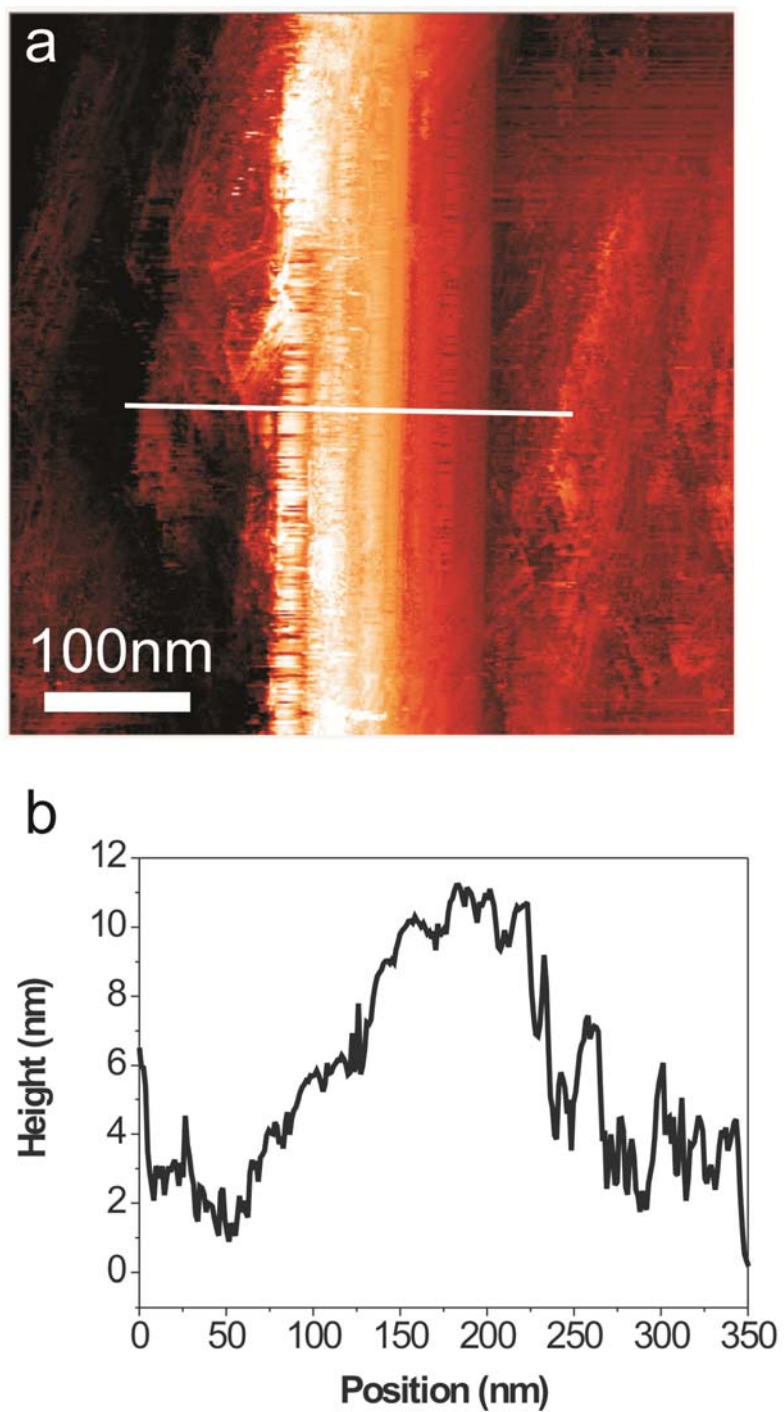


**Figure 3.14: (a) STM image and (b) height profile confirm that bacterial nanowires from *S. oneidensis* MR-1 are highly conductive and can be composed of bundles of individual nanofilaments.**

### 3.3 Concluding Remarks

*Shewanella oneidensis* strain MR-1 (wild-type) produce bacterial nanowires when grown under oxygen-limited conditions. Cultivation in continuous flow bioreactors is preferred because it can maximize the production of nanowires and minimize the amount of EPS in the media that will challenge microscopic analysis and electrical measurements of bacterial nanowires. Bacterial nanowires range from tens of nanometer to tens of micrometers long, with a lateral dimension of ~10 nm for single, non-bundled nanowires as measured by SEM, TEM, AFM and STM. Fluorescence microscopy with non-specific protein staining reveals that the nature of bacterial nanowires is protein. CP-AFM and STM confirms that bacterial nanowires are efficient electrical conductors. With multiple lines of evidence, it suggests that *Shewanella* nanowires are composed of closely packed conductive proteins that may facilitate long-range transport of electrons from cells to solid-phase electron acceptors located at significant distances from the cells.

## Chapter 4

### 4 Electrical Transport Measurements along Bacterial Nanowires from *Shewanella oneidensis* MR-1

#### 4.1 Introduction

Prokaryotes can use a wide variety of dissolved electron acceptors such as oxygen, nitrate, and sulfate that are accessible to their intracellular enzymes. However, DMRB are challenged by the low solubility of solid-phase Fe(III) and Mn(IV) minerals that serve as their terminal electron acceptors, and therefore use extracellular transfer to overcome this obstacle [69]. Recent reports have suggested that extracellular electron transport may be facilitated by conductive filamentous appendages (i.e. bacterial nanowires) [44, 45, 52]. So far, CP-AFM [44, 52] and STM [45] studies demonstrated transverse electrical conduction in nanowires from a DMRB (*Geobacter sulfurreducens*), another metal reducer (*Shewanella oneidensis* MR-1), an oxygenic photosynthetic cyanobacterium (*Synechocystis* PCC6803), and a thermophilic fermentative bacterium (*Pelotomaculum thermopropionicum*), when cultivated under electron-acceptor limitation. Several biological assays have demonstrated results consistent with electron transport along bacterial nanowires, including measurements of improved electricity generation in microbial fuel cells and enhanced microbial reduction of solid-phase iron oxides [44, 45, 47]. However, our direct knowledge of nanowire conductivity has been limited to local measurements of transport only across the thickness of the nanowires [44, 45, 52]. Thus

far, there has been no evidence presented to verify electron transport along the length of bacterial nanowires, which can extend many micrometers, well beyond a typical bacterial cell's length. In this chapter, electron transport measurements along individually addressed bacterial nanowires derived from electron-acceptor limited cultures of the DMRB *S. oneidensis* MR-1 are presented. Transport along *Shewanella* bacterial nanowires was independently evaluated by two techniques: (i) nanofabricated electrodes patterned on top of individual nanowires, and (ii) conducting AFM probing at various points along a single nanowire bridging a prefabricated metallic microelectrode and the conductive AFM tip.

## 4.2 Experimental Methods

### 4.2.1 Cell Cultivation

*S. oneidensis* strain MR-1 (wild-type), the flagellin-deficient mutant and the double-deletion mutant  $\Delta mtrC/omcA$  lacking two decaheme cytochromes were cultured in continuous flow chemostat bioreactors (BioFlo 110; New Brunswick Scientific) with a dilution rate of  $0.05 \text{ h}^{-1}$  and an operating liquid volume of 1 L. Chemical defined media were used with lactate serving as the sole electron donor. Detailed experimental setup and cultivation procedures can be found in Chapter 3. Appendages were produced in response to electron acceptor ( $\text{O}_2$ ) limitation, when the dissolved  $\text{O}_2$  tension was lowered below the detection of the polarographic  $\text{O}_2$  electrode.

An estimate of the specific cell respiration rate was calculated as follows: By starting with a wild-type *S. oneidensis* MR-1 bioreactor in steady state condition, cell density was determined using a Petroff-Hauser counting chamber to be  $7.72 \times 10^8$  cells/mL. The flow of growth medium to the bioreactor was then shut off. Shortly thereafter, all the remaining electron donor (i.e. lactate) was consumed, triggering a rapid increase in dissolved O<sub>2</sub> concentration. Next, lactate was added to the bioreactor to a final concentration of 50 mM. The oxidation of lactate immediately caused a rapid decrease in dissolved O<sub>2</sub> concentration. A subsequent rapid increase in dissolved O<sub>2</sub> concentration indicated that the lactate had been consumed. The time it took for the 50 mM lactate to be consumed was measured to be 180 s. Knowing the cell density and the number of electrons extracted per lactate molecule (12 electrons/lactate molecule), the rate of electron transfer per cell was calculated to be  $2.6 \times 10^6$  electrons per cell per second.

#### 4.2.2 Nanofabricated Devices for Electrical Measurements

Thermally oxidized Si substrates with an oxide thickness of 1 μm were spin-coated with positive photoresists (Shipley Microposit S1805) at 500 rpm for 5 s followed by 3000 rpm for 45 s, yielding a film thickness of ~500 nm. The substrates were soft-baked at 115 °C for 1 min prior to photolithography for microelectrodes and contact pads through a pre-patterned, glass photomask in a Karl Suss MA6 Mask Aligner. The substrates were immersed in developing solution (Microposit MF-319) with gentle agitation, selectively dissolving photoresists that were exposed to UV irradiation. Electrode materials (5 nm of Cr as adhesion layer and 35 nm of Au as conducting layer) were deposited on the developed substrates using an electron-beam evaporation system at a deposition rate of

0.1 nm/s. The sacrificial materials (i.e. undeveloped photoresists) with the Cr/Au layer on top were washed away by immersing the substrates in a solution of lift-off solvent (Microchem Remover PG) with sonication. An optical micrograph of a selected fabricated device is presented in Figure 4.1. The fabrication procedures are schematically illustrated in Figure 4.2.

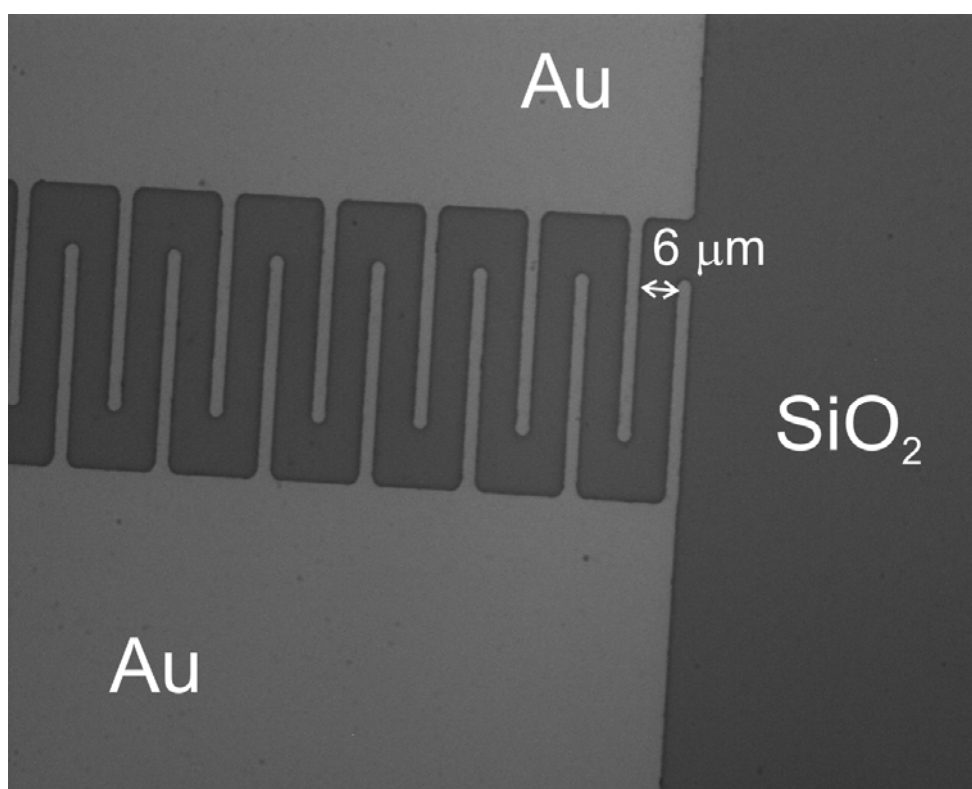


**Figure 4.1: Optical micrograph of a microfabricated structure on a SiO<sub>2</sub>/Si substrate with Au microelectrodes and contact pads for electrical measurements.**

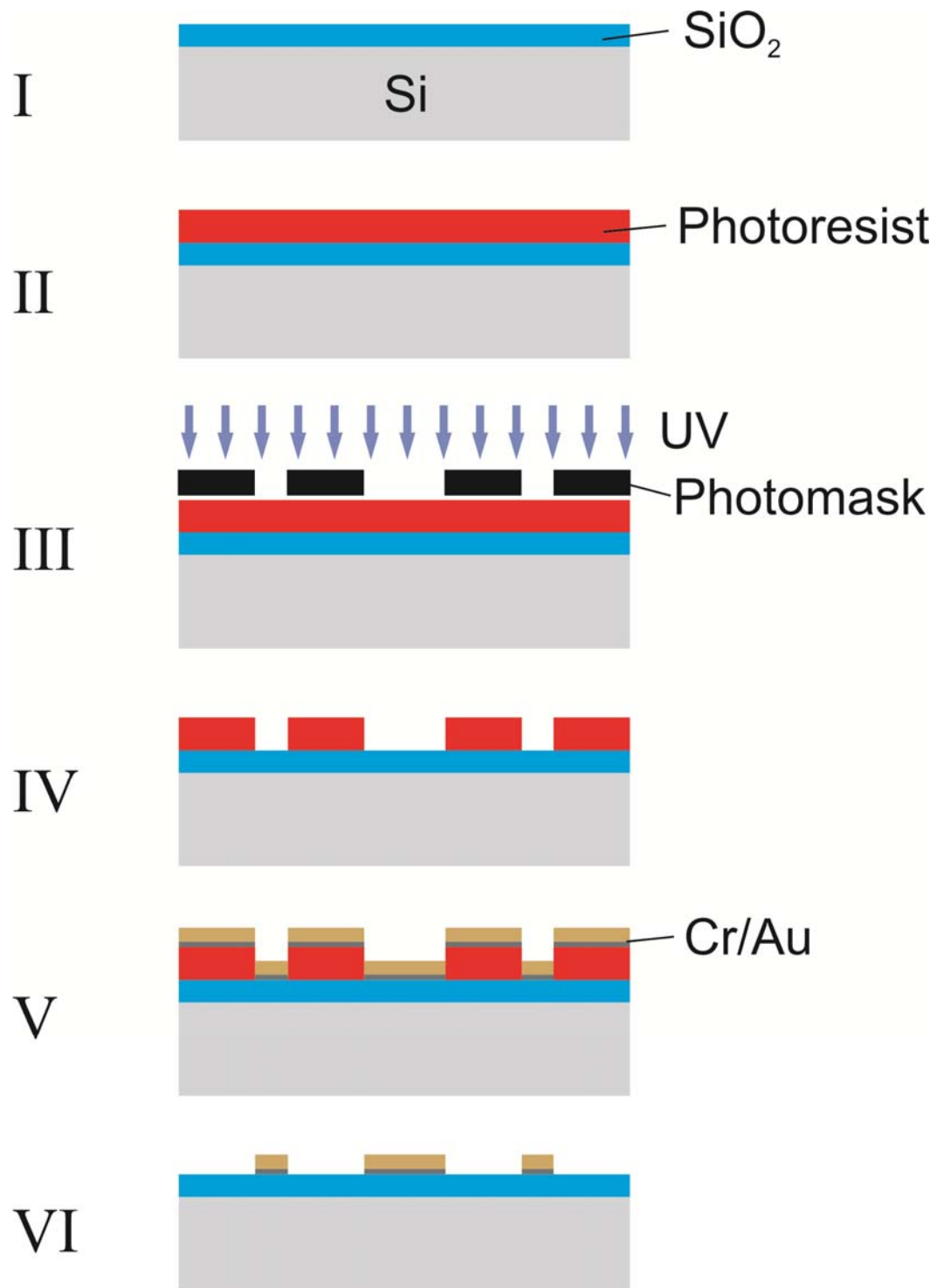


**Figure 4.2: Schematics of microfabrication procedures of devices used as platforms for electrical measurements of bacterial nanowires.**

Chemically fixed samples using glutaraldehyde (2.5% concentration) were applied to the oxidized Si chips with pre-patterned Au microelectrodes. Allowing sample adsorption on the surface for 5 minutes, the substrates were rinsed with filtered PBS followed by de-ionized water, and then dried in air. Imaging and electrode deposition were carried out in a LEO 1540XB FIB/SEM system. Cells with attached nanowires were located in the proximity of the prefabricated Au microelectrodes. A Pt gas precursor was introduced close to the sample surface using a gas injection system (GIS). By steering the electron beam over the area to be modified, the secondary electrons produced from the sample surface having a similar energy (<50 eV) to bond energies in molecules can cause bond breaking of the adsorbed precursor molecules, resulting in material deposition known as electron-beam induced deposition (EBID). Pt nanoelectrodes (20 – 30 nm thick) were directly deposited to contact the bacterial nanowires and the prefabricated microelectrodes using EBID at an acceleration voltage of 2 kV.

Current-voltage (I-V) measurements were performed on a Signatone probe station equipped with a Keithley 6517A electrometer, which applied the drain-to-source voltages and measured the drain-to-source currents, at room temperature and ambient pressure inside a Faraday cage. For each bacterial nanowire tested, resistance was calculated from the ohmic I-V trace. Knowing the resistance ( $R$ , in  $\Omega$ ), the resistivity ( $\rho$ , in  $\Omega\cdot\text{cm}$ ) was calculated by the equation:

$$\rho = \frac{RA}{L}, \quad (2)$$



where  $L$  is the length of the nanowire segment between the two probes and  $A$  is the cross-sectional nanowire area.

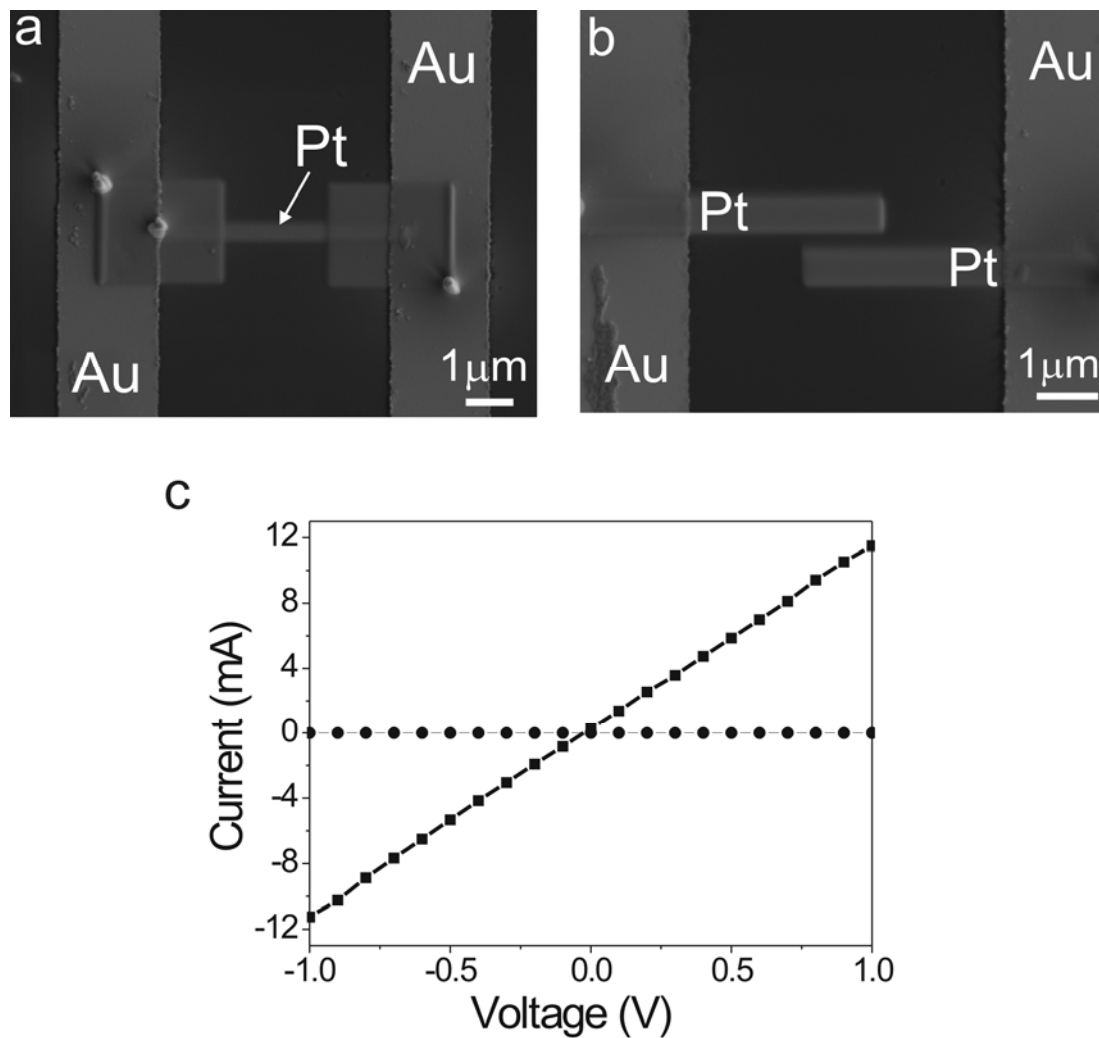


**Figure 4.3: SEM images of (a) close-circuit and (b) open-circuit controls. (c) I-V curves of (a) and (b) are indicated by squares and circles, respectively.**

The Pt electrodes deposited by EBID were separately characterized to assess their contribution to the measured conductance of the nanowires. A close-circuit control (Figure 4.3(a)) was performed by depositing a Pt line (30-nm thick, 2- $\mu$ m long, 400-nm wide) connecting the prefabricated Au microelectrodes. From a current of 11.5 mA at 1 V, the resistivity of the EBID deposited Pt is calculated to be  $5.22 \times 10^{-5} \Omega \cdot \text{cm}$ , which is on the same order of magnitude as the resistivity of bulk Pt. An open-circuit control (Figure 4.3(b)) was conducted by depositing two Pt probes very close together (<200 nm without a bridging nanowire) on a prefabricated chip. This sample showed no current response to applied voltage, ruling out any metallic contamination between the electrodes under the deposition conditions used in this study.

#### 4.2.3 Conducting-probe Atomic Force Microscopy Measurements

Au microgrids (3 nm of Cr and 20 nm of Au), as shown in Figure 4.4, were fabricated on a SiO<sub>2</sub>/Si substrate by standard photolithography. Fabrication procedures and sample preparation methods were identical to those mentioned in the previous section. The Au microgrids were electrically connected to the sample stage of a Veeco Dimension V AFM system using conductive silver paint. Pt/Cr coated Si AFM probes (BudgetSensors ContE) with a nominal spring constant of 0.2 N/m were used for both tapping and contact mode imaging. I-V curves were measured in point-spectroscopy mode with a typical gain setting of 1V/nA. The loading force applied for electrical measurements was 4 nN, which was found to be the minimum force required to establish a stable short-circuiting contact between the conductive AFM tip and the Au electrode. In many cases, an imaging force of 10 nN or greater began to dislocate and damage the biological structures. Under such

conditions, the apex of the conductive AFM tip could be coated with insulating debris. Therefore, the minimum force (4 nN) was chosen for the electrical measurements to maintain an intimate electrical contact and not to damage the delicate bacterial nanowires. The sample voltage was ramped between -1 and 1 V at 0.2 Hz, yielding consistent and repeatable data. The resistance at each position along the nanowire was calculated using the most linear part ( $\pm 0.4$  V) of the I-V curve.

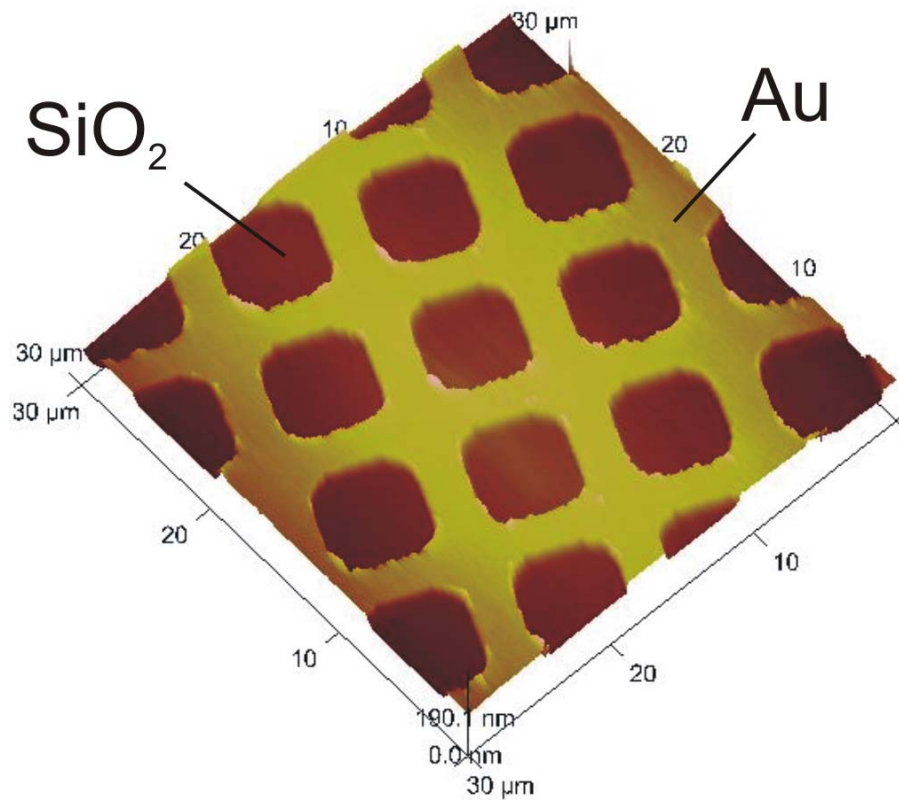


**Figure 4.4: AFM topography image of prefabricated Au microgrids on a SiO<sub>2</sub>/Si substrate.**

### 4.3 Direct Electrical Measurements Using Nanofabricated Electrodes

Individual bacterial nanowires were located using secondary electron imaging and were then contacted by EBID of Pt electrodes by introducing Pt precursor close to the substrate surface through a GIS (Figure 4.5). I-V sweeps were collected at ambient conditions. Figure 4.6 illustrates the results from a single bacterial nanowire extending from a wild-type *S. oneidensis* MR-1 cell. Following deposition of the Pt contacts (Figure 4.6(a)), a nearly ohmic current response to applied voltage was observed (Figure 4.6(b)) with resistance  $R = 529 \text{ M}\Omega$ , yielding a corresponding electron transport rate, at 100 mV, of about  $10^9$  electrons per second. The resistivity of the nanowire from this measurement is estimated to be  $2 \text{ }\Omega\cdot\text{cm}$ , which is comparable in magnitude to that of moderately doped silicon nanowires [70]. Another bacterial nanowire (Figure 4.6(c)), which was sampled from a different bioreactor, was investigated for electrical transport, resulting in a measured resistivity of  $9 \text{ }\Omega\cdot\text{cm}$  ( $R = 2.2 \text{ G}\Omega$ ).

In addition to wild-type *S. oneidensis* MR-1, nanowires were also observed in cells of the flagellin-deficient mutant of *S. oneidensis* that lack the ability to produce flagella. Figure 4.7 illustrates the I-V measurement of a single nanowire from the *S. oneidensis* flagellin-deficient mutant. A linear I-V curve was observed, confirming the conductivity of the nanowire and its ohmic characteristic with the electrodes. The calculated resistivity of this nanowire is  $147 \text{ }\Omega\cdot\text{cm}$ , which is higher compared with that of the nanowire from wild-type *S. oneidensis* MR-1. What factors (other than contact resistance) caused the difference in resistivity of the two *Shewanella* strains are unclear and deserve further investigations.

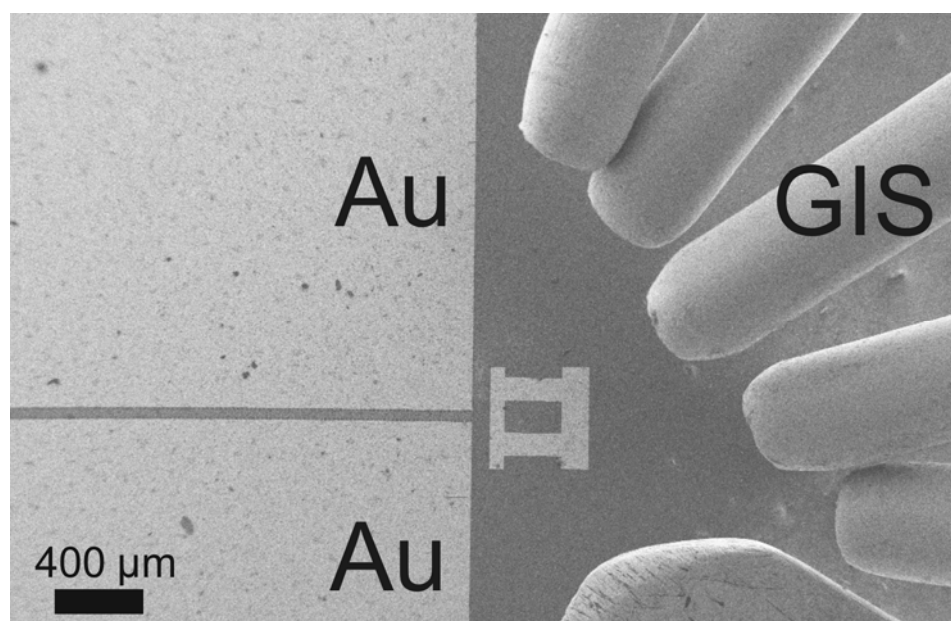


**Figure 4.5: SEM image showing the gas injection system (GIS) used to introduce Pt precursor close to the substrate surface for EBID of Pt contacts on bacterial nanowires.**

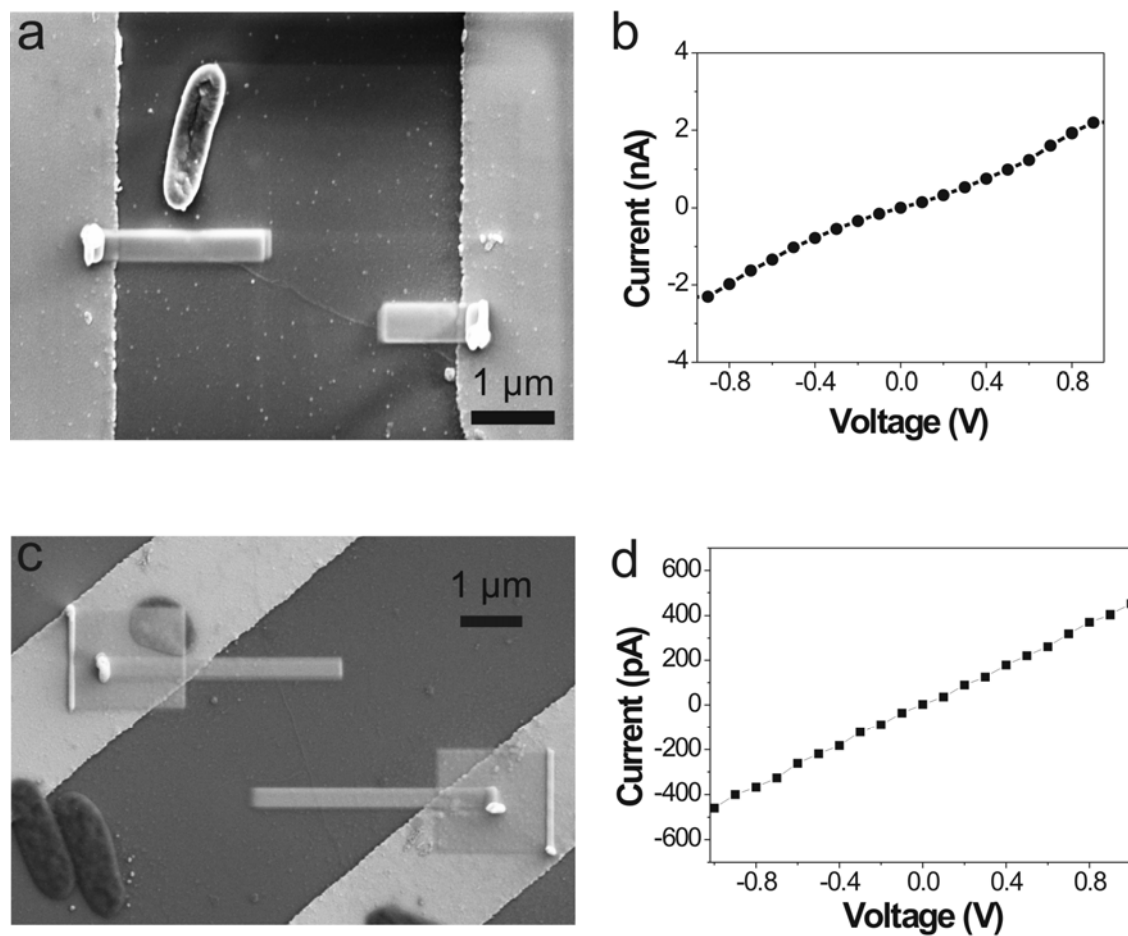


**Figure 4.6: (a)** SEM image showing a single bacterial nanowire emanating from a wild-type *S. oneidensis* MR-1 cell contacted with two nanofabricated Pt electrodes. **(b)** Current-voltage curve of the bacterial nanowire in (a). **(c)** SEM image of another bacterial nanowire with the measured I-V curve shown in (d).

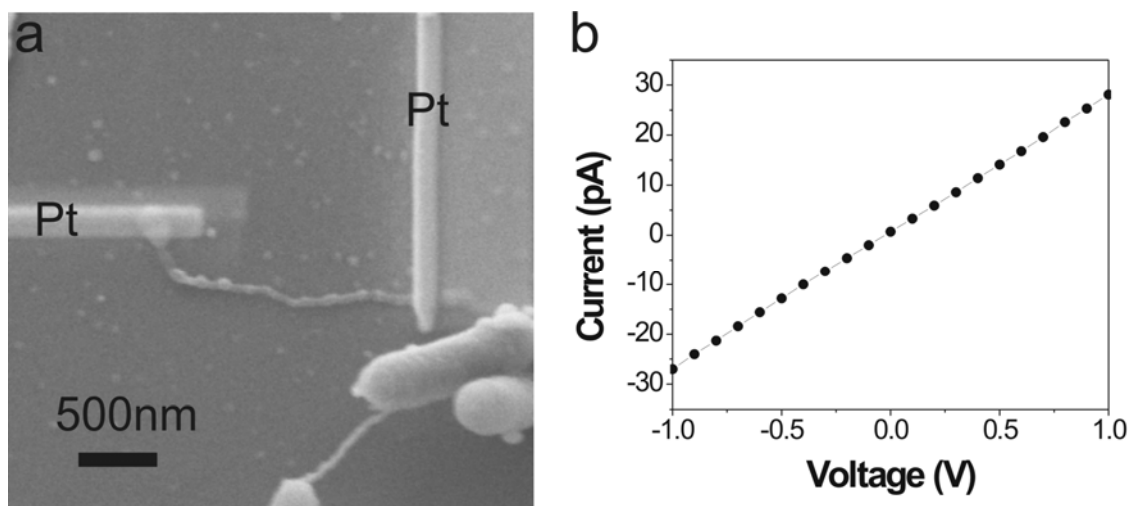


**Figure 4.7: (a) SEM image showing a single bacterial nanowire from the *S. oneidensis* flagellin-deficient mutant contacted with two nanofabricated Pt electrodes. (b) Current-voltage curve of the bacterial nanowire.**

Mutants ( $\Delta mtrC/omcA$ ) lacking genes for multiheme *c*-type cytochromes MtrC and OmcA were also studied. The  $\Delta mtrC/omcA$  mutants were cultivated under identical conditions as wild-type *S. oneidensis* MR-1. In response to electron acceptor limitation, the  $\Delta mtrC/omcA$  mutants produced appendages morphologically consistent with wild-type nanowires. The appendages were contacted by nanofabricated electrodes and tested for electrical conductivity (Figure 4.8). The  $\Delta mtrC/omcA$  appendages were found to be non-conductive, showing no measurable current response to applied voltage down to the noise floor. This finding is in good agreement with previous report [45] that STM imaging of appendages from the  $\Delta mtrC/omcA$  mutants was unsuccessful, which was attributed to the lack of electrical conductivity of the appendages.

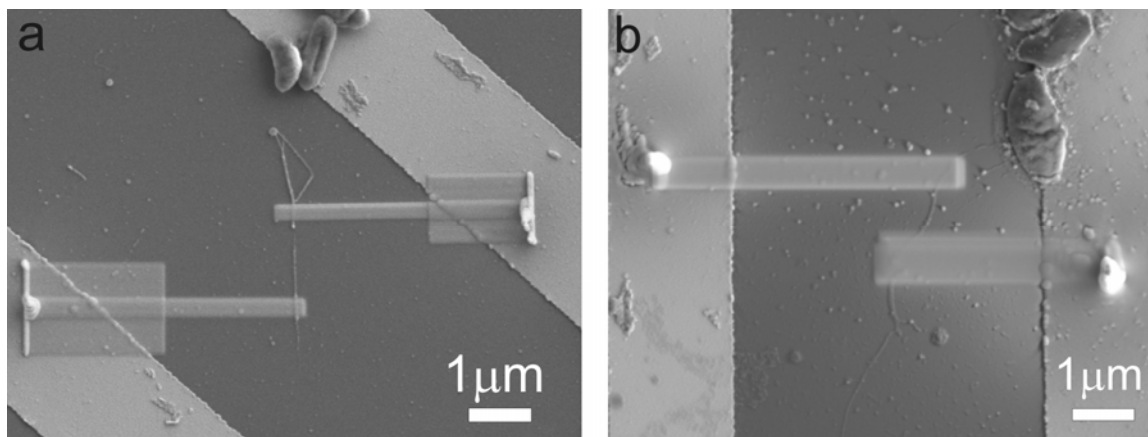


**Figure 4.8: (a and b) SEM images showing two individual extracellular appendages from the  $\Delta\text{mtrC}/\text{omcA}$  mutants that are morphologically consistent with wild-type nanowires but are electrically non-conductive as confirmed by electrical measurements.**

#### 4.4 Measurements with Conducting Atomic Force Microscopy Probes

In order to determine whether the resistivity values obtained from the two-contact devices include a significant contribution from contact resistance between electrodes and nanowires, CP-AFM was used to measure the resistance of a single nanowire as a function of its length. CP-AFM is a convenient tool for probing local electrical properties at the nanometer scale, and has been increasingly used for the electrical characterization of biological molecules [71-73]. CP-AFM was also previously employed to demonstrate transverse conduction through bacterial nanowires produced by *Geobacter sulfurreducens* [44] and *S. oneidensis* MR-1 [52]. In the previous experiments, however, the nanowires were supported on conductive surfaces of HOPG, precluding their



measurements of their longitudinal conduction. To verify longitudinal transport along bacterial nanowires using CP-AFM, *S. oneidensis* MR-1 nanowires from chemically fixed samples were immobilized on SiO<sub>2</sub>/Si substrates with lithographically patterned Au microgrids as electrodes (Figure 4.9). Electronic transport along a nanowire in contact with the Au microgrid was measured by using a Pt-coated AFM tip as a second electrode, as schematically illustrated in Figure 4.10.

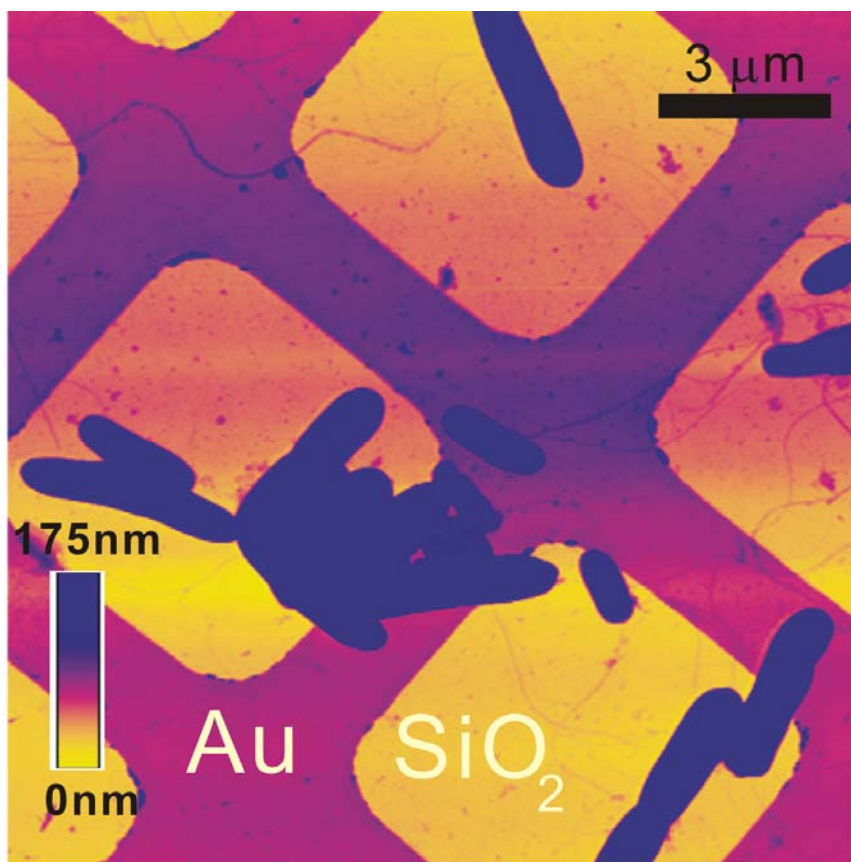


**Figure 4.9: Topographic AFM image showing air-dried *S. oneidensis* MR-1 cells and extracellular appendages deposited randomly on a SiO<sub>2</sub>/Si substrate patterned with Au microgrids.**

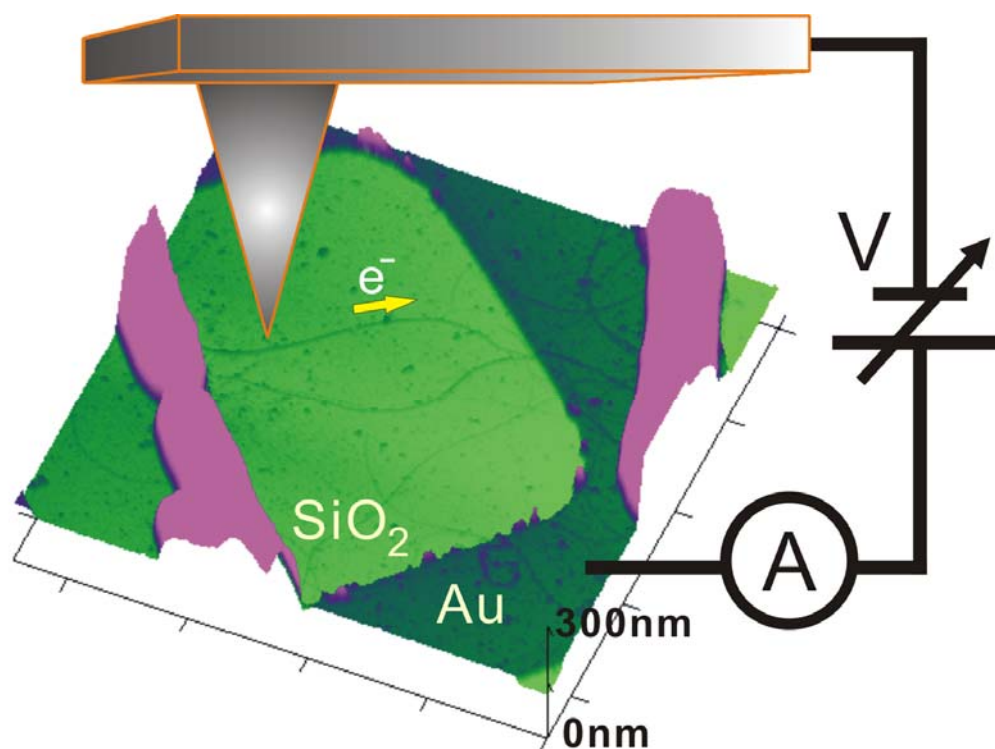


**Figure 4.10: Schematic diagram illustrating electronic transport along a single bacterial nanowire in contact with Au microgrids measured by a Pt-coated AFM tip.**

With the AFM tip at the position shown in Figure 4.11(a), ~600 nm away from the Au electrode and in contact with the nanowire, the I-V curve shown in Figure 4.11(b) was obtained. The current response to the applied voltage was found to be approximately linear and consistent with the results obtained using nanofabricated Pt electrodes. As a control, it was observed that whenever the AFM tip was placed directly on the insulating SiO<sub>2</sub> surface, a background current (<10 pA) was obtained, confirming that extraneous conduction through adsorbed water layers or other contaminants was negligible.

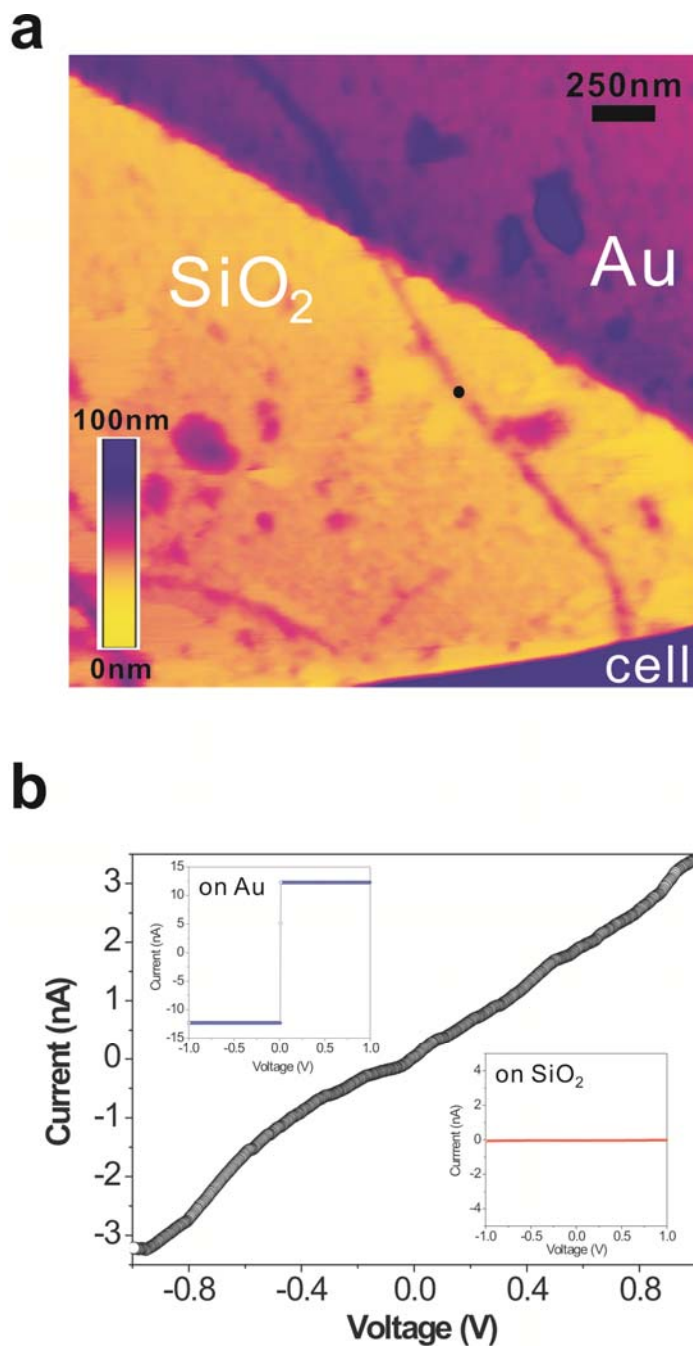


**Figure 4.11: (a) Contact mode AFM image showing a bacterial nanowire reaching out from a *S. oneidensis* MR-1 cell to the Au electrode. (b) An I-V curve obtained by probing the nanowire at a length of 600 nm away from the Au electrode (at the position marked by the black dot in (a)). (Inset) The I-V curves obtained on bare Au and SiO<sub>2</sub>, respectively.**

Figure 4.12 shows multiple measurements on the same nanowire at different points along its length. A linear relationship between measured resistance and length was observed. By extrapolating the curve to zero length, the overall contact resistance is estimated with a value of 58 M $\Omega$ . When subtracted from the total resistance, it yields a bulk resistivity for the nanowire on the order of 1  $\Omega\cdot\text{cm}$ , in good agreement with measurements using nanofabricated Pt electrodes (Figure 4.6).

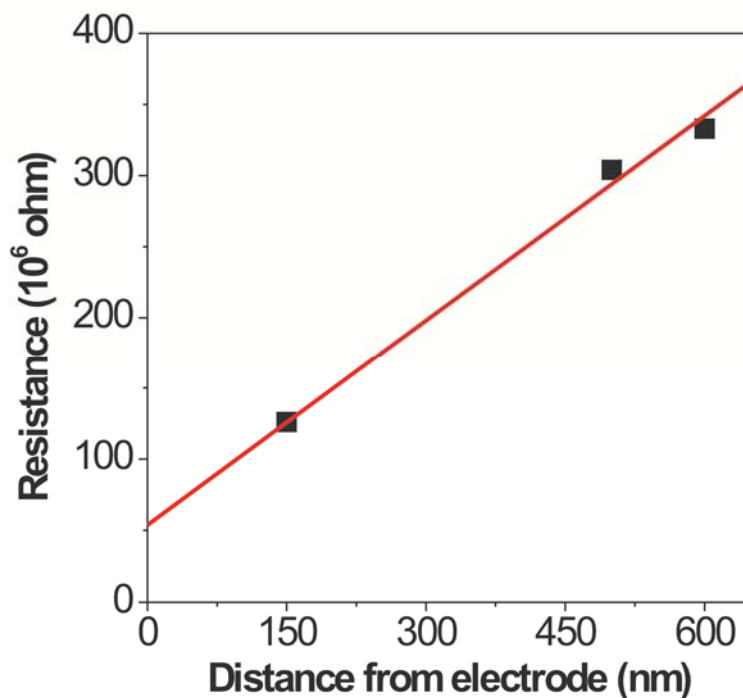


**Figure 4.12: A plot of total resistance as a function of distance between AFM tip and Au electrode. The contact resistance is estimated by extrapolating the linear curve to zero length.**

## 4.5 Discussion

The discovery of bacterial nanowires spawned a common question among microbiologists, biogeochemists, and physicists: Can bacterial nanowires transport electrons along their entire length, and with what resistivity? To answer this question, the electrical transport along bacterial nanowires was evaluated by two independent techniques: (1) nanofabricated electrodes patterned on top of individual nanowires, and (2) CP-AFM at various points along a single nanowire bridging a metallic electrode and the conductive AFM tip. The *S. oneidensis* nanowires were found to be electrically conductive along micrometer-length scales with electron transport rates up to  $10^9/s$  at 100 mV of applied bias and a measured resistivity on the order of  $1 \Omega \cdot \text{cm}$ .

Recent measurements by McLean et al. [74] of the rate of electron transfer per cell from *S. oneidensis* MR-1 to fuel cell anodes were on the order of  $10^6$  electrons per cell per second. These measurements are consistent with the specific respiration rate estimated under the cultivation conditions used in this study ( $2.6 \times 10^6$  electrons per cell per second). A comparison with our transport measurements demonstrates that a single bacterial nanowire could discharge this entire supply of respiratory electrons to a terminal electron acceptor.

A previous STM study [45] associated *c*-type cytochromes with the conductivity of bacterial nanowires from *S. oneidensis* MR-1. In order to identify the role of cytochromes in nanowires, mutants ( $\Delta\text{mtrC}/\text{omcA}$ ) lacking genes for multiheme *c*-type cytochromes MtrC and OmcA were studied. It was found that these mutants produce non-conductive nanofilaments, indicating that, in the case of *S. oneidensis* MR-1, cytochromes are necessary for conduction along bacterial nanowires. However, this finding does not

preclude other mechanisms for long-range electron transport along bacterial nanowires from other microorganisms. For instance, *Geobacter* nanowires are presumed to be conductive as a result of the amino acid sequence of the type IV pilin subunit, PilA, and possibly, the tertiary structure of the assembled pilus [44].

## 4.6 Conclusions

In conclusion, this study demonstrates direct electrical transport along bacterial nanowires from *S. oneidensis* MR-1, with a measured resistivity on the order of  $1 \Omega\cdot\text{cm}$  and transport rates that allow for bacterial nanowires to serve as a viable microbial strategy for extracellular electron transport. The measurements reported in this study motivate further investigations into the molecular composition and physical transport mechanism of bacterial nanowires, both to understand and realize the broad implications for natural microbial systems and biotechnological applications such as microbial fuel cells.

## Chapter 5

### 5 Semiconducting Behavior of *Shewanella* Bacterial Nanowires

The work presented in Chapter 4 confirming electrical transport along nanowires from *Shewanella oneidensis* MR-1 motivated a number of research interests such as in investigating their conductive nature, exploring potential applications, and testing a variety of hypotheses related to energy distribution and cell-cell communication within the microbial community. This chapter presents studies on the electronic transport coupling of *Shewanella* nanowires to metallic materials and the nature of current carriers in *Shewanella* nanowires using conductive probe AFM measurements and by constructing nanowire field-effect transistors (NW-FETs) with back gating to modulate the conductivity.

#### 5.1 Introduction

Electron (or charge) transfer is the most fundamental process in biology, and particularly important in transfer through and between biomolecules such as proteins that are necessary to fulfil physiological requirements. The nature of charge transfer and electronic conduction in proteins has been speculated for over 70 years. That biological electron flow as semiconductive and electrons travel within energy bands was first proposed by Szent-Györgyi in 1941 [75]. Several years later after this first proposition, theoretical work from Evans and Gergely indicated that dry proteins are electronic

semiconductors with a bandgap of a few eV [76]. A similar conclusion was drawn by Rosenberg in 1962, whose experimental data suggested that both dry and wet proteins are electronic and not ionic in nature, while for wet proteins the adsorbed water only decreases the semiconduction activation energy but does not affect the number of charge states available or the mobility of the charge carriers [77]. More recent analyses from Gray and Winkler in 1996 pointed out that long-range electron transfer in proteins is dependent on the electronic states of the intervening medium between redox sites [78]. In addition, they reported that charge transport in proteins can occur over a long distance well over 20 Å, facilitated by multi-step tunnelling or hopping of electrons or holes [79].

As proteins might represent a new type of electronic conductors [80] and serve as functional materials for biomolecular electronics as well as biosensing and photoactivable components in next-generation devices, charge transport studies on proteins and other biomolecules have been progressing and increasingly gaining attention from scientists not only from biology but also a wide range of fields such as chemistry, physics and engineering. With more advanced nanotechnology developed, transport properties of proteins and biomolecules have been studied using scanning probe (nanoscopic) techniques and nano-engineered platforms down to single molecular levels [81-85].

Previous study demonstrating electrical transport along *Shewanella* bacterial nanowires, which are proposed to be composed of closely-packed conductive protein molecules along the nanofilaments, motivated the research work presented in this chapter in learning the nature of conductivity of these biological nanowires, exploring their potential applications in bionanodevices, and investigating possible routes for energy distribution and perhaps communication within the nanowire-producing microbial community. In this



research work, the electronic transport properties of bacterial nanowires in contact with materials with dissimilar work functions were studied using CP-AFM settings. In addition, the transport carrier types of bacterial nanowires were investigated under nanowire field-effect transistor (NW-FET) configurations with back gating to modulate the conductivity along individual nanowires.

## 5.2 Experimental Methods

Chemically fixed samples from bioreactor cultures of *S. oneidensis* MR-1 were applied to HOPG substrates, Au-coated silicon substrates and oxidized Si substrates with prefabricated microelectrodes and contact pads. Details of cultivation conditions and procedures for sample preparation were described in Chapter 4. After allowing sample adsorption on the surface for 5 minutes, the substrates were rinsed with filtered phosphate buffered saline solution followed by de-ionized water, and then dried in air for subsequent electrical measurements.

HOPG and Au-coated substrates were used for CP-AFM measurements. The Au-coated substrates were prepared by depositing 5 nm of Ti (as an adhesion layer) followed by 150 nm of Au on Si substrates using electron-beam evaporation at a working pressure of  $2 \times 10^{-6}$  Torr and a deposition rate of 1 Å/s. The HOPG substrates were freshly cleaved before use. The HOPG and Au-coated substrates were electrically connected to the sample stage of the AFM system (Veeco Dimension V) using conductive silver paint. Pt-coated AFM probes (BudgetSensors) with a nominal spring constant of 0.2 N/m were used for contact-mode topography imaging and electrical measurements. The actual

spring constants and sensitivities of individual conducting AFM probes were determined by force-distance measurements on a sapphire substrate and thermal tuning.

For NW-FET device fabrication and measurements, heavily doped Si substrates were thermally oxidized to yield an oxide thickness of 100 nm. The SiO<sub>2</sub>/Si substrates were spin-coated with positive photoresists (Shipley S1805) and patterned by photolithography for microelectrodes and contact pads (details can be found in Chapter 4), followed by deposition of 5 nm of Cr and 35 nm of Au on top. Native oxides on the back side of the substrates were stripped off using buffered hydrofluoric acid prior to deposition of Au (100 nm) serving as the electrical contact for back gating. Imaging and deposition of Pt nanoelectrodes (i.e. source and drain) were carried out in a LEO 1540 XB FIB/SEM at an acceleration voltage of 2 kV. The nanoelectrodes (20-30 nm thick) were deposited by EBID to contact the bacterial nanowires and the prefabricated Au microelectrodes by introducing a Pt precursor to the chamber. Post-deposition imaging was avoided to eliminate possible chemical reactions on unwanted areas. Electrical measurements were performed inside a Faraday cage at room temperature and ambient pressure using a probe station (Signatone) equipped with a Keithley 6517A electrometer, which applied the drain-to-source voltages and measured the drain-to-source currents. A separate power source was used for back gating. Following electrical measurements, samples were inspected by tapping-mode AFM.

### 5.3 Electronic Transport Characteristics of *Shewanella* Nanowires Coupled to Electrodes

The electronic transport properties of bacterial nanowires from *S. oneidensis* MR-1 were investigated by CP-AFM measurements by sandwiching individual *Shewanella* nanowires between a Pt-coated AFM probe and a conductive substrate (Au or HOPG). Current-voltage curves were collected at ambient conditions employing Pt-coated conducting AFM probes serving as the top electrode and conducting substrates (Au and HOPG) as the bottom electrode. Figure 5.1 displays two typical I-V curves obtained on individual *Shewanella* nanowires when supported on Au (which can be considered as Pt/nanowire/Au systems), which appear to be linear within the swept voltage range. This finding implies formation of ohmic contacts at both the Pt/nanowire and nanowire/Au interfaces, considering that Pt and Au have very similar work functions ( $\sim 5.3$  eV).

In contrast, I-V curves collected on nanowires when supported on HOPG (i.e. Pt/nanowire/HOPG systems), as shown in Figure 5.2, reveal distinct electronic transport behaviour compared with that on Au. The I-V curves are featured with non-linear and asymmetric characteristics within a similar voltage range, which are consistent with the data shown by El-Naggar et al [52]. Since the Pt/nanowire junction is ohmic (or nearly ohmic), the non-ohmic behaviour observed in the Pt/nanowire/HOPG systems is attributed to the junction barrier at the nanowire/HOPG interface.

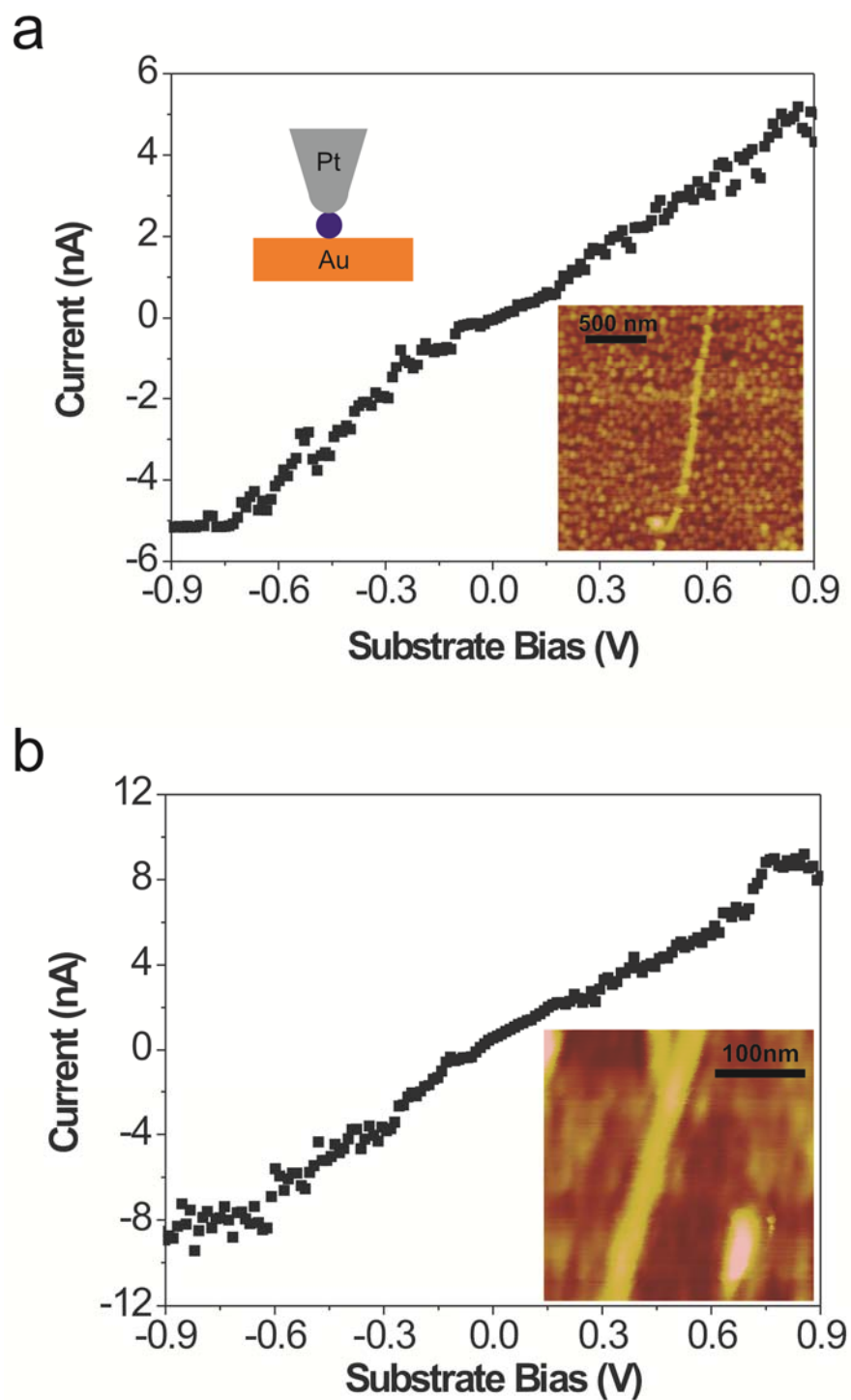


**Figure 5.1: (a and b) Current-voltage curves collected on two individual *Shewanella* bacterial nanowires when sandwiched between a Pt-coated AFM tip and Au-coated substrate.**

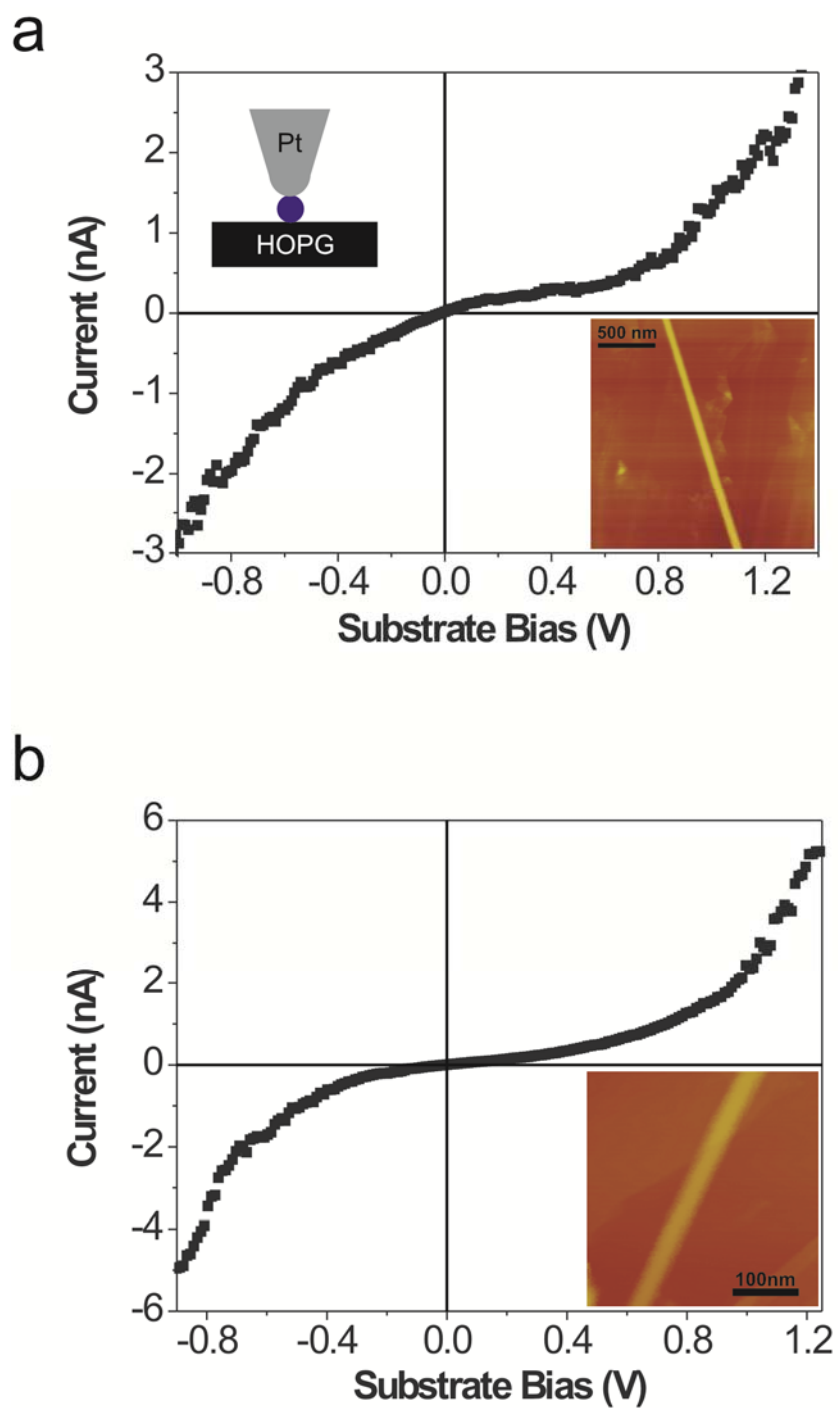


**Figure 5.2:** (a and b) Current-voltage curves collected on two individual *Shewanella* bacterial nanowires when sandwiched between a Pt-coated AFM tip and HOPG substrate.

According to theory of semiconductor physics, when there is difference in energy between the Fermi level of a semiconductor and that of a contacting metal, charges must overcome an energy barrier called Schottky barrier in order to pass across the interface. Correlating this theory with the findings in this work, it is postulated that bacterial nanowires behave as a semiconductor and therefore a Schottky barrier exists at the nanowire/HOPG junction owing to Fermi level mismatching. Based on the observed ohmic contact behaviour with Au and Pt, the Fermi level of *Shewanella* bacterial nanowires is very close to 5.3 eV. According to the I-V measurements shown in Figure 5.2, the nanowire/HOPG junction behaves as a rectifying diode (i.e. Schottky diode) and is operating in forward-bias mode when the HOPG is negatively biased. Unlike an ideal diode, the tested nanowire/HOPG junctions exhibit relatively high leakage currents in the reverse-bias regime (i.e. positive substrate bias) and poor breakdown characteristics, with an  $I_{\text{Forward}}/I_{\text{Reverse}}$  ratio of 3.2 and 3.7 at 0.8 V for the junction shown in Figure 5.2(a) and 5.2(b), respectively. Such non-ideal diode performance may be attributed to the small physical distance and thus a strong electric field between the electrodes (i.e. Pt-probe and HOPG) during measurements. The reverse-bias current rises rapidly when electrons from the highest occupied molecular orbital (HOMO) of the bacterial nanowire can tunnel to the empty states above the Fermi level of HOPG as a result of the strong electric field.

Schottky diodes fundamentally operate differently to p-n diodes. The reverse current of a p-n diode arises from diffusion of minority carriers through the depletion layer, and the forward current is due to minority carrier injection from n to p sides. On the other hand, the reverse current of the Schottky diode is due to carriers that overcome the energy barrier, while the forward current is due to majority carrier injection from the

semiconductor. Therefore, the electrical current in the Schottky diode is dominated by the majority carriers of the semiconductor. The experimental data in this work that forward biasing occurs at negative substrate (i.e. HOPG) bias and reverse biasing at positive substrate bias imply that *Shewanella* bacterial nanowires behave as a semiconductor with holes as the majority carriers, that is, a p-type semiconductor.

#### 5.4 Modulating the Conductance of *Shewanella* Nanowires Configured in Field-Effect Transistor Structures

The electronic transport characteristics of *Shewanella* bacterial nanowires were further investigated using back-gated NW-FET configurations under ambient conditions at room temperature. Figure 5.3 illustrates the device structure of one of the tested NW-FET devices. The drain-to-source current versus drain-to-source voltage ( $I_{DS}$ - $V_{DS}$ ) curves at a series of gate voltages ( $V_G$ ) are plotted in Figure 5.4(a). The  $I_{SD}$ - $V_{SD}$  curves are all linear, confirming that the Pt/nanowire/Pt system is ohmic, consistent with the CP-AFM measurements. Current saturation is not observed within the swept voltage range ( $\pm 1.5$  V).  $I_{SD}$  increases slightly with negative gate voltages, whereas  $I_{SD}$  decreases significantly with positive gate voltages. At  $V_G = 8$  V,  $I_{DS}$  becomes negligibly small since the electric field is high enough to deplete the charge carriers in the nanowire. The observed modulation of nanowire conductance supports our interpretation on CP-AFM data that the majority carriers in bacterial nanowires are holes. In fact, the NW-FET demonstrated here resembles a normal-on p-channel metal-oxide-semiconductor FET (MOSFET) operating in depletion mode. The carrier mobility ( $\mu$ ) can be derived from the transconductance ( $\partial I_{DS}/\partial V_G$ ) at a fixed drain-source voltage according to the equation:

$$\mu = \left( \frac{\partial I_{DS}}{\partial V_G} \right) \left( \frac{C}{L^2} V_{DS} \right)^{-1}, \quad (3)$$

where  $C = 2\pi\epsilon\epsilon_0 L / \ln(4h/d)$  for a nanowire geometry [86],  $L$  is the drain-source nanowire length,  $h$  is the oxide thickness, and  $d$  is the diameter of the nanowire. The mobility of the NW-FET shown in Figure 5.3 is estimated to be  $0.23 \text{ cm}^2/\text{Vs}$ , which is the highest among tested devices and is comparable to those of organic semiconducting nanowires [87].

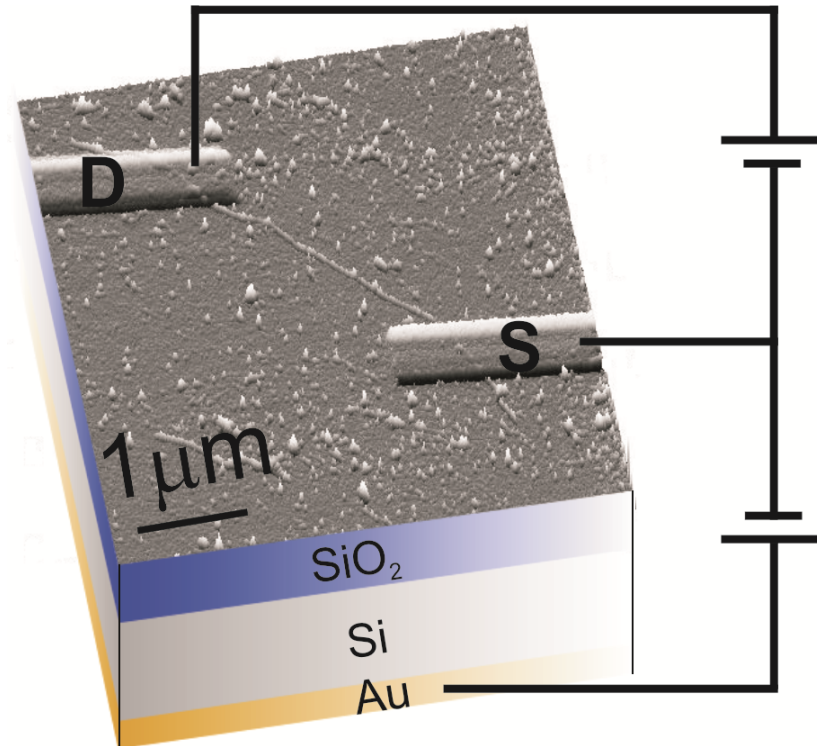


**Figure 5.3: Structure of a NW-FET device with a single bacterial nanowire contacted by source (S) and drain (D) electrodes. The topography shown is an amplitude AFM image of the device.**



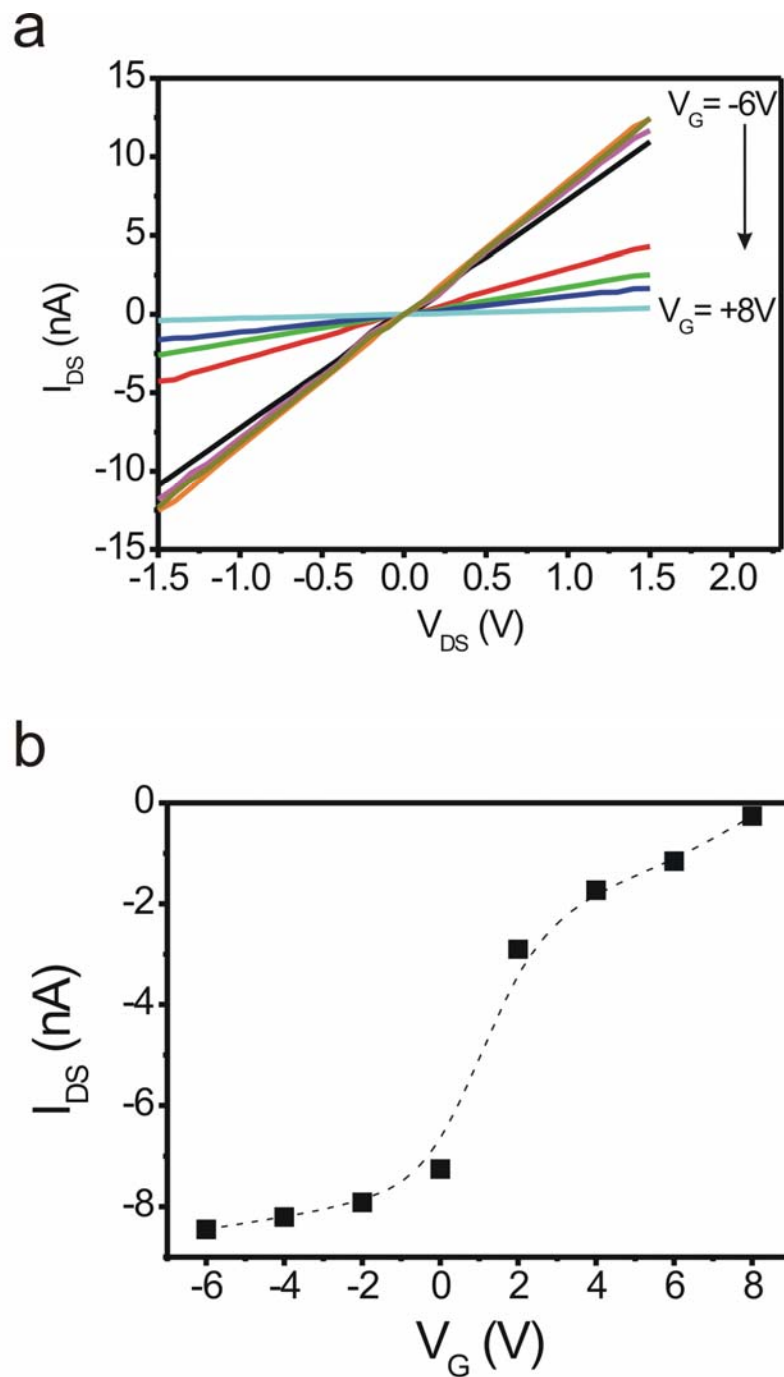


Figure 5.4: (a)  $I_{DS}$ - $V_{DS}$  characteristics of a *Shewanella* nanowire at different gate voltages. (b) Transfer characteristic of the NW-FET at  $V_{DS} = -1$  V.

## 5.5 Discussion

There have been a few mechanisms reported for modulating the conductance of biomolecular structures through an externally applied electric field. For example, it was reported that an external electric field can induce displacement of metal ions in M-DNA, in which the imino protons of every base pair are substituted by divalent metal ions such as  $Zn^{2+}$ ,  $Ni^{2+}$  or  $Co^{2+}$ , that can significantly alter the hopping rate along the helix axis [88]. However, the required electric field to cause such displacement is relatively high (2 MV/cm) compared with the electric field employed in this work. On the other hand, it was demonstrated in another report that the conduction state of Azurin (an electron-transfer protein) can be controlled by tuning the redox states of the protein through an external voltage source, realizing a switchable p- and n-channel FET by tuning the gate voltage within a specific range [89].

In the case of *Shewanella* nanowires, multiheme cytochromes (MtrC and/or OmcA) are proposed to be essential for electrical conduction along the nanowires. As the heme groups in these cytochromes are conjugated systems, the electrical conduction along bacterial nanowires might be facilitated by electronic coupling between the heme groups if they are in close proximity to each other and/or preferentially oriented to promote  $\pi$ - $\pi$  interaction. Shi et al. [90] demonstrated that MtrC and OmcA tend to interact to form a stable complex, which was found to have enhanced Fe(III)-NTA reductase activity. Whether these complexes are involved in *Shewanella* nanowires requires further investigations. The observed p-type conduction nature in *Shewanella* nanowires could be due to partial oxidation of the conjugated molecules, thereby pulling some electrons out from the valence band and creating holes. If an intervening bridge is involved in

mediating electronic coupling, oxidized bridge states may also contribute to the hole-transfer process [78]. Although *Shewanella* nanowires are possibly associated with or composed of redox proteins (e.g. cytochromes), the hole-transfer (p-type) nature of the nanowires may be a rather general phenomenon regardless of the redox properties of the biomolecules involved.

The semiconductive, gateable nature observed in *Shewanella* nanowires might also imply some previously unknown approaches adopted by nanowire-producing microbes in electronic information exchange and efficient energy distribution. With the fact that many *Shewanella* nanowires are present as “Y” junctions connecting a few cells, these findings together raise two interesting questions: (i) is gating from one of the branches (or cells) possible for modulating the flow of electrons or exchange of electronic signals within microbial communities, and (ii) how different are the electronic properties and thus the functions between nanowires from different nanowire-producing microbes? Answers to the above questions might reveal some new insights into microbial physiology.

## 5.6 Concluding Remarks

Bacterial nanowires produced by *Shewanella oneidensis* MR-1 behave as a gateable p-type semiconductor with a Fermi level close to 5.3 eV. This finding indicates that *Shewanella* nanowires may not only serve as conduits to transfer electrons throughout the extracellular matrix including solid-phase electron acceptors, but also as cables for efficient energy distribution and electronic information exchange within microbial communities. This study will inspire further investigations into the molecular and

electronic structures of nanowires from a variety of microbes, both to reveal their role(s) in diverse natural environments and for accelerating a wealth of potential applications, from enhanced power output from microbial fuel cells to the novel treatment of opportunistic pathogens. On the other hand, semiconducting bacterial nanowires might potentially be functional, one-dimensional bio-organic nanomaterials for applications such as nanoelectronics and nanosensors, which deserve further investigations.

## Chapter 6

### 6 Mechanical Properties of *Shewanella* Nanowires Studied by Atomic Force Microscopy Techniques

In Chapters 4 and 5, it has been revealed that bacterial nanowires produced by *S. oneidensis* MR-1 behave as a p-type semiconductor with a resistivity on the order of  $1 \Omega \cdot \text{cm}$ , which is comparable to that of lightly doped silicon nanowires [91]. These findings motivated the exploration of potential use of bacterial nanowires in biofuel cells, bionanoelectronics and other bionanodevices. In addition to electrical and electronic characterizations, it is also important to characterize the mechanical properties of bacterial nanowires considering the possible opportunities of integrating bacterial nanowires into functional devices. This chapter presents studies on the elasticity of bacterial nanowires, which was investigated using two independent atomic force microscopy techniques: (i) real-time elastic modulus mapping by HarmoniX AFM (developed by Veeco) using T-shaped cantilevers with an offset tip, and (ii) conventional AFM nanoindentation by force-distance curve fitting based on Hertz model.

#### 6.1 Introduction

Previous studies confirming long-range electrical transport along bacterial nanowires from *S. oneidensis* MR-1 have not only established the possible physiological functions of *S. oneidensis* nanowires, but also motivated research interests in exploring the potential for utilizing this new type of biological conductive nanomaterial in biofuel cells,

bionanoelectronics and other bionanodevices such as biosensors. While the basic electronic and electrical properties of nanowires from *S. oneidensis* MR-1 have been revealed [45, 52], their composition and molecular structure remain incompletely understood owing to technical difficulties in isolating and purifying bacterial nanowires for further characterizations. Thus, studying the elasticity of bacterial nanowires still attached to cells might indirectly provide useful information relating to their structural components and electron transport mechanisms. In view of future opportunities of integrating bacterial nanowires into micro/nanosystems to construct functional devices, it is essential to understand the mechanical properties of these conductive bio-nanowires when they are subjected to external forces or during manipulating and repositioning of the nanostructures into defined configurations.

Bacterial nanowires from *S. oneidensis* MR-1 range from tens of nanometers up to tens of micrometers long, with an average diameter of 10 nm for individual, non-bundled nanowires [92]. To study mechanical properties of materials in the nanometer scale, atomic force microscopy (AFM) has been most commonly employed owing to its high spatial resolution, force sensing capabilities, as well as the ability to measure electrical properties of materials [93, 94]. In this work, the elasticity of bacterial nanowires was studied under HarmoniX mode AFM using torsional harmonic cantilevers (THC), each with a T-shaped geometry and an offset tip (Figure 6.1). One of the main features of this AFM operation mode is the ability to provide quantitative nanomechanical mapping of material properties such as elastic modulus, adhesion, and dissipation, while simultaneously imaging sample topography [95]. This AFM technique, which enables real-time mapping of local elastic response of the material by detecting torsional motions

of the THC and generating high-speed force-distance curves from the time-varying forces at very shallow indentation depths, has been tested and proved to provide reliable measurements for materials with elastic moduli ranging from 1 MPa to 10 GPa [96]. The elastic modulus values obtained from HarmoniX mode AFM are estimated by fitting the force curves at each pixel with the Derjaguin–Muller–Toporov (DMT) model. The forces during indentation, according to this model, are described by the following equation:

$$F_{Interaction} = \frac{4}{3}E^* \sqrt{R}(d - d_0)^{3/2} + F_{Adh}. \quad (4)$$

In the equation,  $F_{Interaction}$  is the tip-sample force,  $E^*$  is the reduced elastic modulus of the tip and the sample,  $R$  is the tip radius,  $d_0$  is the surface rest position,  $d - d_0$  is the depth of indentation, and  $F_{Adh}$  is the constant adhesion force during the contact. With the high-resolution mapping capability, local mechanical properties of bacterial nanowires can be probed and the distribution of soft and rigid substructures (if any) along individual nanowires can be revealed.

In order to verify whether the modulus values of bacterial nanowires measured under this AFM mode were susceptible to the stiffness of the underlying substrate, bacterial nanowires were tested under identical imaging (feedback) conditions but supported on various substrates including highly oriented pyrolytic graphite (HOPG), polymethylmethacrylate (PMMA) and borosilicate glass. In addition, conventional nanoindentation on bacterial nanowires was also performed using typical force-measuring AFM probes and calculated the elastic modulus of bacterial nanowires according to the classical Hertz theory. The modulus values obtained by these two different AFM techniques were compared.

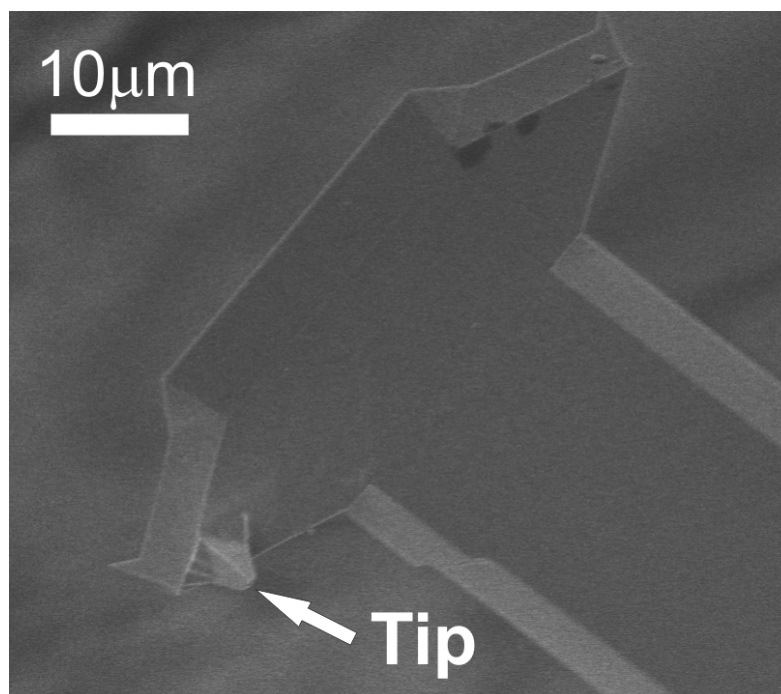


**Figure 6.1: SEM image of a torsional harmonic cantilever with a T-shaped geometry and an off-axis tip.**

## 6.2 Experimental Methods

Samples of a continuous flow bioreactor culture from *S. oneidensis* MR-1 (cultivation conditions were identical to those described in Chapter 3) were applied to three separate substrates (HOPG, PMMA, and borosilicate glass). PMMA photoresist (MicroChem 950PMMA-A4) was spin-coated on silicon (Si) substrates at 500 rpm for 5 s followed by 2000 rpm for 45 s. The substrates were soft-baked at 180 °C for 1 min. The final PMMA film thickness was ~300 nm. HOPG substrates (MikroMasch ZYB) were freshly cleaved before use. The bacterial samples were applied to each substrate for 15 min and then



rinsed with filtered phosphate buffered saline (PBS) followed by deionized water to remove salts from the culture media. The rinsed substrates were finally air dried for 24 h before all AFM experiments.

A commercial AFM (Veeco Dimension V) was used for both the HarmoniX and nanoindentation experiments on bacterial nanowires in air. The THC (Veeco HMX) used in the experiments had torsional and flexural resonance frequencies at 1005 kHz and 58 kHz, respectively. The spring constant of the THC was measured to be 2.5 N/m using the thermal noise method [97]. The THC sensitivities (force, dissipation, and DMT Modulus) were calibrated using a Si reference substrate and a polystyrene–low-density polyethylene (PS–LDPE) composite sample with known elastic moduli (PS: 2 GPa; LDPE: 100 MPa). The tip radius was calculated to be 8.9 nm prior to experiments according to the LogDMT modulus offset method using the PS–LDPE standard sample. Tip calibration was repeated after each set of experiment and the tip radius increased to 11.2 nm after a few sets of experiments due to possible tip deformation (blunting).

Conventional AFM nanoindentation experiments were carried out using a Si probe (Veeco RFESP), which had a flexural resonance frequency at 80 kHz with a calibrated spring constant of 8.44 N/m. The tip radius was measured to be 10 nm under SEM prior to experiments. The deflection sensitivity of the cantilever was calibrated by indenting on a sapphire substrate. Force-separation (F–S) curves were collected from nanoindentations on different locations along individual bacterial nanowires. The elastic modulus of the nanowires was calculated by fitting the approaching F–S curves according to the classical Hertzian model using commercial software (SPIP Image Metrology).

### 6.3 Quantitative Nanomechanical Property Mapping of *Shewanella* Nanowires by Torsional Harmonic AFM Probes

In this study, the peak tapping forces operated under HarmoniX mode were maintained below 15 nN in order to minimize damage of the samples but indent “deep” enough to extract the material properties of the bacterial nanowires. Such indentation was evidenced by the findings that the apparent heights of all bacterial nanowires investigated under this AFM mode in this work were less than the typical value (~10 nm) measured by traditional tapping-mode AFM due to relatively higher loading forces adopted, resulting in compression of the nanowires in the radial direction during imaging. A captured view of a tip-sample force waveform is presented in Figure 6.2, showing a peak force of ~14 nN when operated under HarmoniX mode.

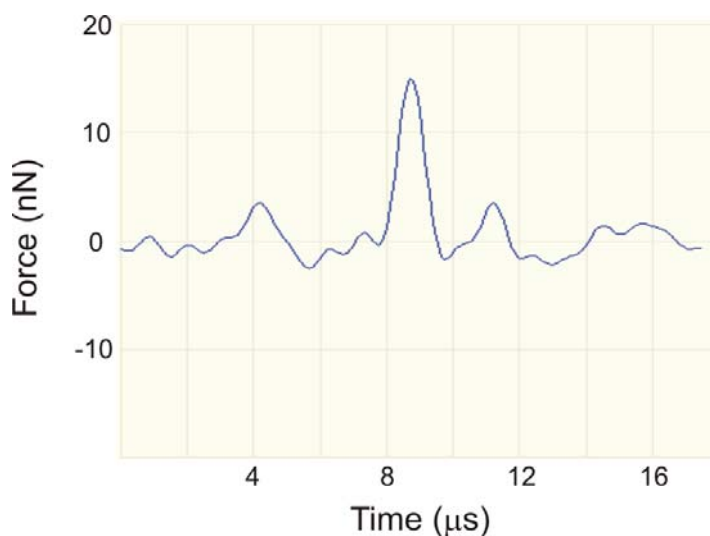


**Figure 6.2: A tip-sample force waveform captured when operating under HarmoniX mode AFM.**

The topography and section data of a bacterial nanowire supported on a HOPG substrate are shown in Figure 6.3(a), while Figure 6.3(b) is the corresponding elastic modulus map. The appeared height of the nanowire is 7 nm, which is  $\sim 3$  nm less than the typical measured value, reflecting an instantaneous compression of the nanowire by  $\sim 3$  nm by the HMX tip during imaging. The modulus profile across the section in Figure 6.3(b) exhibits distinctly a trough ( $\sim 1$  GPa) at the nanowire, revealing a lower elastic modulus of the nanowire compared to HOPG. The measured local modulus values of the HOPG substrate mostly fluctuate between 4.0 and 5.5 GPa, with a mean value of 4.8 GPa obtained over 180 data points. The fluctuation can be attributed to tapping on the substrate at spots covered by residues (organic compounds or salts from the culture media) remained after drying. Despite some variations, our measured elastic modulus for HOPG is, overall, in good agreement with values (5 GPa) reported by other groups measured using similar [96] or different techniques [98]. Considering the small radial dimension of bacterial nanowires, it is important to investigate whether the measured elastic modulus of the nanowires would be influenced by the stiffness of the underlying substrate material, known as the substrate effect. Therefore, additional measurements were carried out under identical feedback conditions on bacterial nanowires supported on substrates with lower (PMMA) and higher (borosilicate glass) elastic moduli compared to HOPG.

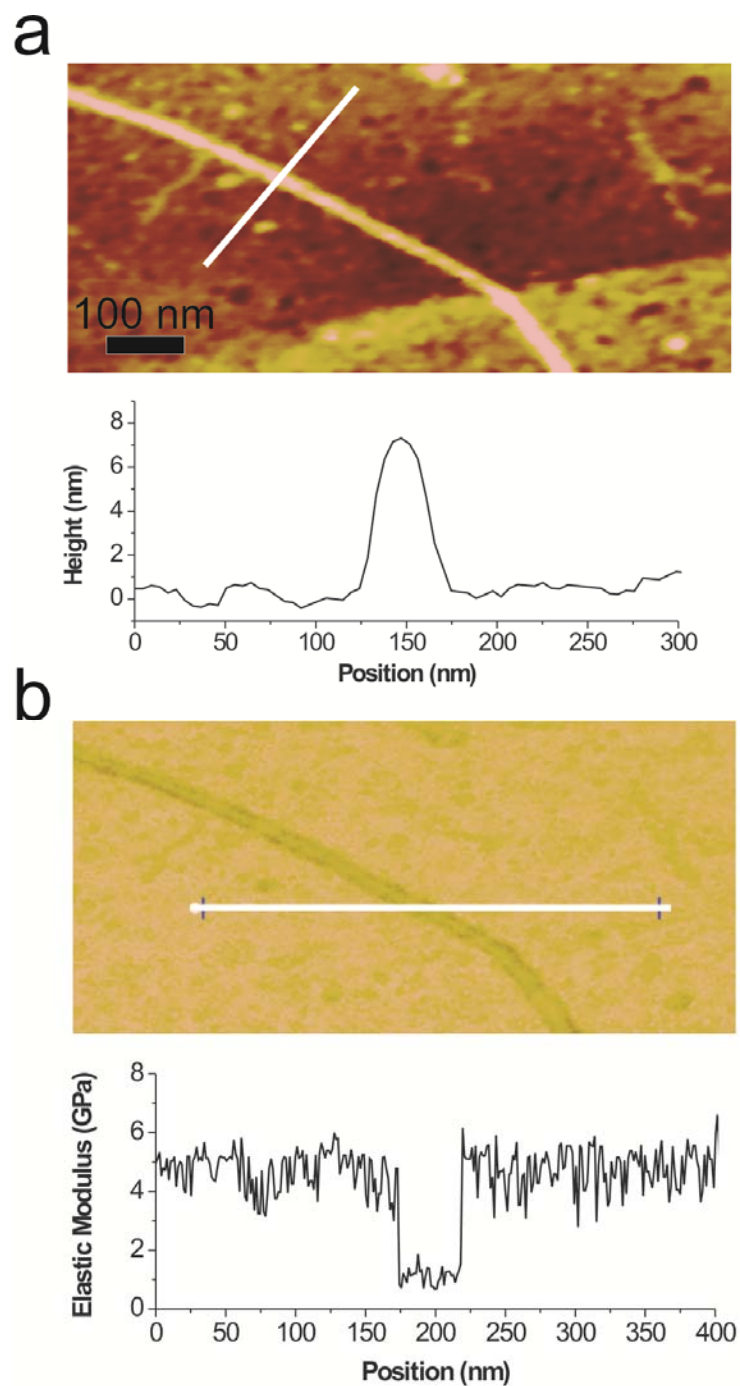


**Figure 6.3: (a) Topography of a bacterial nanowire supported on HOPG and (b) the corresponding elastic modulus map simultaneously generated. Numerical values across the sections indicated by the white lines are plotted below the images.**

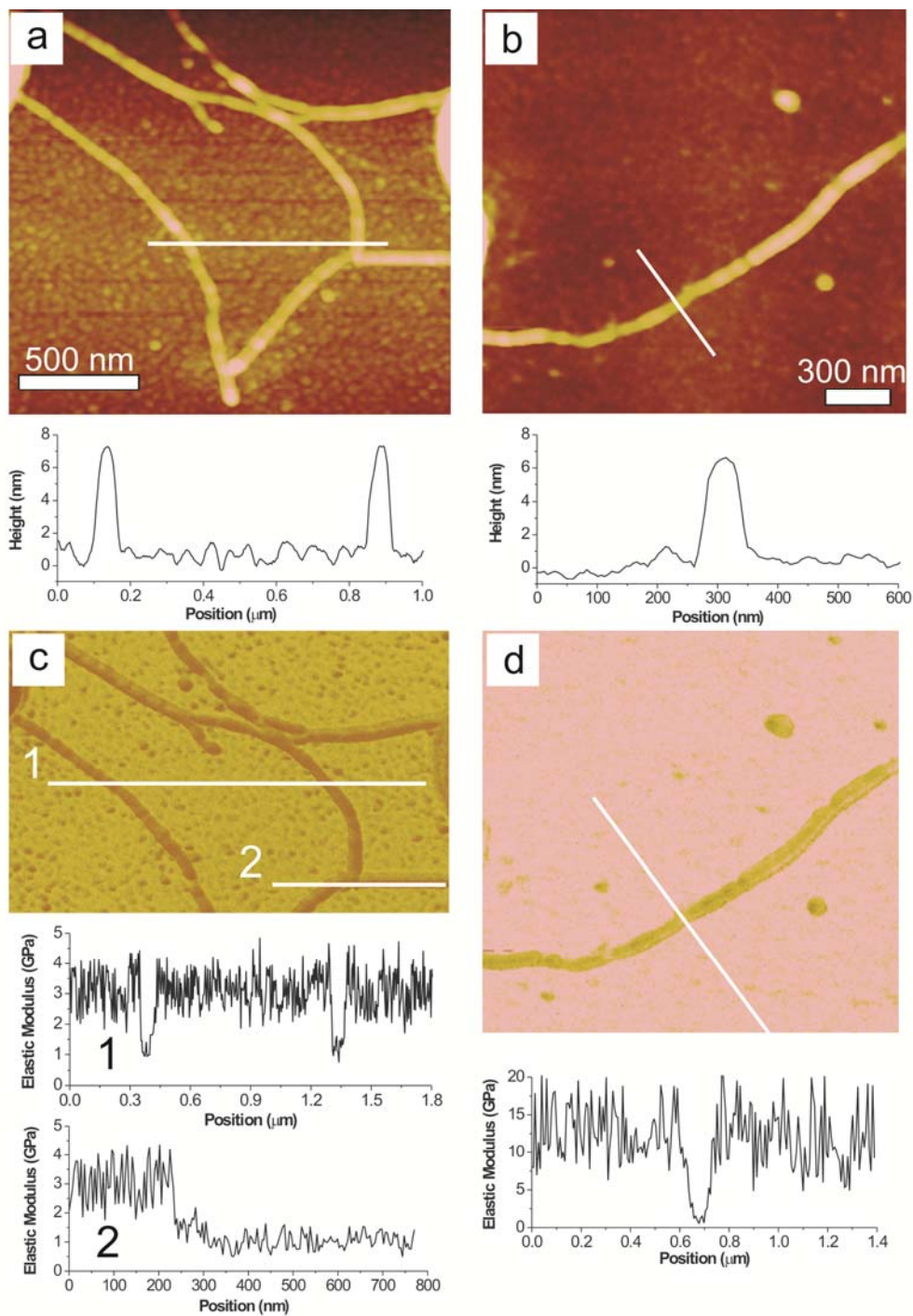


**Figure 6.4: Topographic (a and b) and corresponding elastic modulus (c and d) micrographs of bacterial nanowires supported on PMMA and borosilicate glass substrates, respectively. Numerical values across the sections indicated by the white lines are plotted below the images.**

Figure 6.4(a, c) and 6.4(b, d) show the topography and the corresponding elastic modulus map of bacterial nanowires supported on PMMA and borosilicate glass, respectively. The measured heights of the nanowires are both  $\sim 7$  nm, consistent with the measurements on HOPG. The modulus profile across two nanowires (section 1 of Figure 6.4(c)) displays two troughs, both with values of  $\sim 1$  GPa. Another profile (section 2) shows more elastic modulus data points along a straight portion of the nanowire. Averaging the modulus values over 120 data points along this segment yields a modulus value of 1.03 GPa with a standard deviation of 0.27 GPa. The measured modulus of nanowires supported on PMMA is in good agreement with that measured on HOPG, verifying that a more compliant substrate would not affect the measurements. The measured elastic modulus of PMMA mainly fluctuates between 2 and 4 GPa with a mean value of 3.16 GPa, which is close to the reported modulus of thick ( $>100$  nm) PMMA films [99]. A similar trend can be seen from the modulus profile shown in Figure 6.4(d) when a nanowire was supported on borosilicate glass, again showing a trough ( $\sim 1$  GPa) at the nanowire. However, the measured modulus of borosilicate glass is much lower than the actual value ( $\sim 70$  GPa). This phenomenon has been explained by the saturation mechanism of torsional vibrations in HarmoniX mode AFM as the tip-sample contact durations are too short on stiff samples such that the time-varying tip-sample forces cannot be accurately followed [96]. Nevertheless, all of these separate experiments measured on different substrates showed consistently that the elastic modulus of bacterial nanowires was on the order of 1 GPa. According to the data obtained from nanomechanical mapping, there were no significant variations in local elasticity along individual nanowires observed, neither along the transverse or longitudinal direction nor at bifurcated sites for branched nanowires. These

findings seemed to imply homogeneity in structural properties along these bio-nanostructures, however, further investigations are necessary to draw a definite conclusion.

## 6.4 Conventional AFM Nanoindentation on *Shewanella* Nanowires

Conventional AFM nanoindentation was performed on bacterial nanowires supported on HOPG. Figure 6.5(b) displays the F–S curves obtained by indenting at three different locations on a bacterial nanowire as indicated in Figure 6.5(a). Note the difference in measured height of the nanowire under typical tapping mode (inset of Figure 6.5(a)) which is  $\sim 10$  nm compared to  $\sim 7$  nm under HarmoniX mode. The elastic modulus of the nanowire was deduced by fitting over 30 force curves collected at different locations on the nanowire according to the classical Hertzian model. Force curves obtained from indentations on the edges of the nanowire, which can be distinguished by their instabilities as a result of tip sliding toward the substrate (an example shown in inset of Figure 6.5(b)), were not used for curve fitting. By assuming Poisson's ratios between 0.33 and 0.40 [100], the Young's modulus of the bacterial nanowires is deduced to be  $1.36 \pm 0.64$  GPa. The modulus value obtained from this method is slight larger than that obtained from HarmoniX measurements. One of the possible explanations is that in Hertz model adhesion forces are neglected, thus resulting in such deviations. Nevertheless, both AFM techniques employed in this study mutually agreed with each other and demonstrated elastic modulus of individual bacterial nanowires to be on the order of 1 GPa, which is very close to that of peptide  $\alpha$ -helix structures [101] and slightly higher

than that of organic nanofibers from *para*-hexaphenylene [102]. Table 6.1 summarizes the averaged elastic modulus of bacterial nanowires supported on different substrates measured in this study.

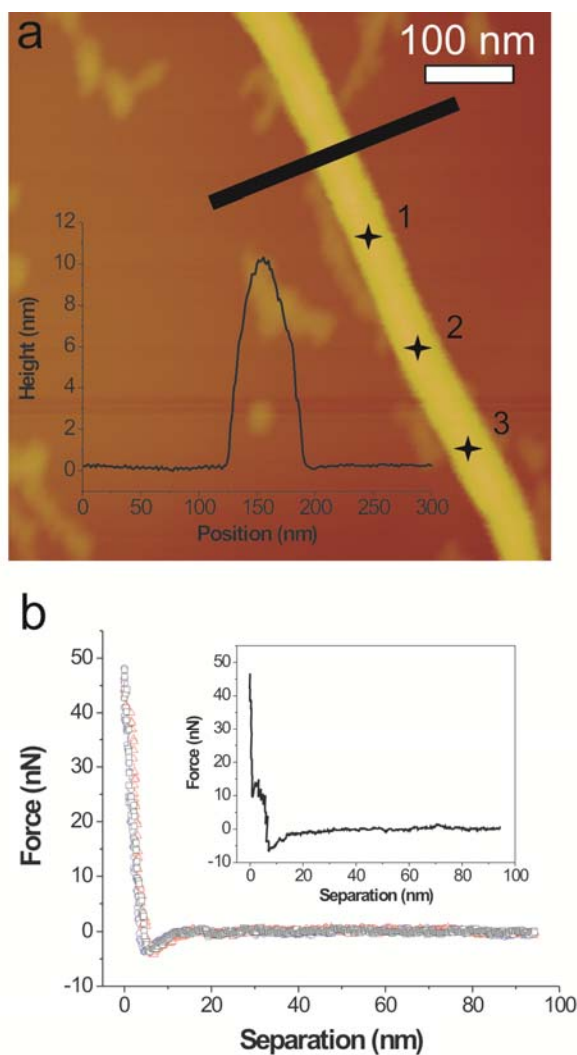


**Figure 6.5: (a) Tapping-mode topography image of a bacterial nanowire supported on HOPG. Inset of (a) shows the height profile across the section indicated by the black line. (b) Force-separation curves collected by indentation on three different points (indicated by asterisks; 1–square, 2–circle, and 3–triangle) on the nanowire. Inset of (b) shows an example of a force curve obtained by indentation on the edge of the nanowire.**



**Table 6.1**


---

Measured elastic modulus of bacterial nanowires supported on different substrates.

---

Substrate	Elastic modulus (GPa)
HOPG	$1.12 \pm 0.29^{\#}$
	$1.36 \pm 0.64^*$
PMMA	$1.08 \pm 0.30^{\#}$
Borosilicate glass	$1.09 \pm 0.41^{\#}$

<sup>#</sup>Obtained from elastic modulus mapping by HarmoniX . <sup>\*</sup>Obtained from nanoindentation and fitting by the Hertz model.

---

## 6.5 Discussion

It has been suggested that bacterial nanowires from *S. oneidensis* MR-1 comprise closely packed electron-transfer proteins (cytochromes) along the filamentous structures [45]. To the best of our knowledge, there are no mechanical data available on cytochromes in the literature, thus it is unable to correlate the findings in this work with any previous work. Reported elasticities of other proteins range from tens of MPa to several GPa, depending on the type of proteins and methods of measurement used [100, 103]. The modulus value of  $\sim 1$  GPa obtained in this work suggests that bacterial nanowires are associated with relatively rigid protein molecules in order to maintain mechanical strength under physiological conditions. This characteristic is an added advantage for the possible use of bacterial nanowires for device applications where they are required to be manipulated or

subjected to external forces. As the elasticity of bacterial nanowires studied in this work was measured in their dry or partially dry state, it would be interesting to compare the results to the elasticity of fully hydrated bacterial nanowires, for instance, in culture media or buffer solutions. Furthermore, if the protein molecules are packed and aligned along the nanowires in an ordered structure, anisotropic mechanical behaviour will be possible. Therefore, further experiments are required in order to answer these fundamental questions. With electronic and electrical properties (resistivity on the order of  $1 \text{ } \Omega \cdot \text{cm}$ ) [92] comparable to that of lightly doped semiconductors such as silicon nanowires [91] and elastic modulus similar to most polymeric materials, *Shewanella* bacterial nanowires might serve as potential candidates in applications such as bionanoelectronics and flexible nanodevices.

## 6.6 Concluding Remarks

In summary, the elasticity of bacterial nanowires from *Shewanella oneidensis* MR-1 cultured under electron-acceptor limiting conditions was primarily studied using two separate AFM techniques: (i) real-time elastic modulus mapping using torsional harmonic cantilevers with a T-shaped geometry and an offset tip, and (ii) conventional AFM nanoindentation with subsequent curve fitting based on the classical Hertz model. The two AFM techniques revealed consistently that the elastic modulus of bacterial nanowires was on the order of 1 GPa. Nanomechanical mapping did not show significant variations in local elasticity along individual nanowires, suggesting their homogeneity in structural properties. In addition, electrically conductive *Shewanella* bacterial nanowires comprise relatively rigid protein molecules that might be helpful to maintain their mechanical

robustness under physiological conditions. Finally, this work inspires us with new applications of bacterial nanowires: with electrical conductivity comparable to that of moderately doped inorganic semiconductors and elasticity similar to polymeric materials, bacterial nanowires may function as building blocks for bionanoelectronics and flexible nanoelectronics.

## Chapter 7

### 7 Thesis Summary and Future Work

#### 7.1 Summary

The recent discovery of electrically conductive bacterial nanowires from a variety of microbes has significant physiological, ecological, and biotechnological implications, and has motivated this thesis work on studying bacterial nanowires from one of the dissimilatory metal-reducing bacteria, *Shewanella oneidensis* MR-1, in order to explore their properties, identify their functions, and investigate for potential applications.

A number of microbial strategies for electron transfer to extracellular electron acceptors and related applications in environmental biotechnology as well as in bio-energy production are reviewed and discussed in Chapter 2. In addition to some previously recognized extracellular electron transfer pathways such as through outer-membrane cytochromes and biosynthesized organic molecules, bacterial nanowires appear to be a more general, but previously unknown, microbial strategy for effective electron transfer to distantly located electron acceptors, including solid-phase metal-oxide minerals, electrodes and possibly neighboring cells.

Chapter 3 describes the detailed cultivation procedures and the optimal growth conditions (i.e. electron-acceptor limited conditions) to induce bacterial nanowire production by *Shewanella oneidensis* strain MR-1 (wild-type). Cell cultivation in continuous flow

bioreactors is preferred over batch cultures in order to minimize the presence of EPS in the media that could challenge microscopic analyses and electrical measurements of bacterial nanowires. Bacterial nanowires range from tens of nanometer to tens of micrometers long, with a lateral dimension of  $\sim 10$  nm for single, non-bundled nanowires as characterized by a variety of microscopy techniques including SEM, TEM, AFM and STM. Fluorescence microscopy reveals that the nature of bacterial nanowires is protein. Moreover, CP-AFM and STM confirms that bacterial nanowires are efficient electrical conductors. Hence, *Shewanella* nanowires are proposed to be composed of closely packed conductive proteins that can facilitate long-range transport of electrons along the nanowires.

Studies presented in Chapter 4 demonstrate direct electrical transport measurements along bacterial nanowires from *S. oneidensis* MR-1 using nanofabricated electrodes and CP-AFM. With a measured resistivity on the order of  $1 \Omega \cdot \text{cm}$  and electron transport rates up to  $10^9/\text{s}$  at 100 mV of applied voltage (which is close to typical physiological potentials), bacterial nanowires can serve as a viable microbial strategy for efficient extracellular electron transport. The measurements reported in this study motivate further investigations into the molecular structure and physical transport mechanism of bacterial nanowires, both to understand and realize the broad implications for natural microbial systems and biotechnological applications such as microbial fuel cells.

CP-AFM electrical measurements and conductance modulation under NW-FET device structures, as presented in Chapter 5, reveal that bacterial nanowires produced by *Shewanella oneidensis* MR-1 behave as a gateable p-type semiconductor with a Fermi level close to 5.3 eV. This study suggests that *Shewanella* nanowires may not only serve

as conduits to transfer electrons throughout the extracellular matrix, but also as cables for efficient energy distribution and electronic information exchange (e.g. cell-cell communication) within microbial communities. This study will inspire further investigations into the molecular and electronic structures of nanowires from a variety of microbes, both to reveal their role(s) in diverse natural environments and for accelerating a wealth of potential applications, from enhanced power output from microbial fuel cells to the novel treatment of opportunistic pathogens. On the other hand, semiconducting bacterial nanowires might potentially be a new class of functional, one-dimensional bio-nanomaterials for applications such as nanoelectronics and nanosensors, which deserve further investigations.

Chapter 6 presents studies on the mechanical properties of *Shewanella* bacterial nanowires using two separate AFM techniques: (i) real-time elastic modulus mapping using torsional harmonic cantilevers with a T-shaped geometry and an offset tip, and (ii) conventional AFM nanoindentation with subsequent curve fitting based on the classical Hertz model. Both techniques consistently confirm that the elastic modulus of *Shewanella* nanowires is on the order of 1 GPa. Nanomechanical mapping reveals no significant variations in local elasticity along individual nanowires, suggesting their homogeneity in structural properties. In addition, *Shewanella* bacterial nanowires comprise relatively rigid protein molecules that may be helpful to maintain their mechanical robustness under physiological conditions. This work also inspires us with new applications of bacterial nanowires: with their electronic properties comparable to those of moderately doped inorganic semiconductors and elasticity close to polymeric

materials, bacterial nanowires may function as building blocks for bionanoelectronics and flexible nanoelectronics.

## 7.2 Thesis Contributions

The contributions of this thesis are summarized below:

- The first measurement of electrical transport along bacterial nanowires produced by *Shewanella oneidensis* MR-1 was performed. It was established that a single bacterial nanowire could discharge an entire supply of respiratory electrons. The measurements reported in this thesis allow for bacterial nanowires to serve as a viable microbial strategy for extracellular electron transport.
- The semiconducting behavior observed in *Shewanella* bacterial nanowires suggests that the nanowires may serve as bioelectronic conduits to transfer electrons throughout the extracellular matrix. This finding also suggests that microbial colonies may survive, communicate, and share energy through bacterial nanowires.
- By exploring the electronic and mechanical properties of bacterial nanowires, this thesis work opens up future opportunities of utilizing bacterial nanowires as functional nanobiomaterials for applications such as nanobioelectronics, flexible nanoelectronics, and biosensors, which should be explored in depth.
- This thesis work inspires further investigations into the molecular and electronic structures of nanowires from a variety of microbes, both to reveal their role(s) in diverse natural environments and for accelerating a wide range of potential applications, from enhanced power output from microbial fuel cells to the novel treatment of opportunistic pathogens.

### 7.3 Future Work

The achievement of this research work can be continued by using microfluidic or nanofluidic techniques to study fully hydrated or living bacterial nanowires. Microfluidic devices can be employed to coax bacteria into producing nanowires through well-defined nanochannels, separating the bacteria and available electron acceptors. This experiment would allow for real-time monitoring of bacterial nanowire growth and measurements of nanowires under physiological conditions by installing probes in the nanochannels. Moreover, investigating methods to isolate and purify bacterial nanowires would allow for mass production of these naturally-occurring, conductive nanobiomaterials at very low cost.



## References

- [1] Gralnick J A and Newman D K 2007 Extracellular respiration *Molecular Microbiology* **65** 1-11
- [2] Myers C R and Nealson K H 1988 Bacterial Manganese Reduction and Growth with Manganese Oxide as the Sole Electron-Acceptor *Science* **240** 1319-21
- [3] Shi L, Squier T C, Zachara J M and Fredrickson J K 2007 Respiration of metal (hydr)oxides by *Shewanella* and *Geobacter*: a key role for multihaem c-type cytochromes *Molecular Microbiology* **65** 12-20
- [4] Lovley D R and Phillips E J P 1988 Novel Mode of Microbial Energy-Metabolism - Organic-Carbon Oxidation Coupled to Dissimilatory Reduction of Iron or Manganese *Applied and Environmental Microbiology* **54** 1472-80
- [5] Lovley D R, Phillips E J P, Lonergan D J and Widman P K 1995 Fe(III) and S<sup>0</sup> Reduction by *Pelobacter-Carbinolicus* *Applied and Environmental Microbiology* **61** 2132-8
- [6] Caccavo F, Coates J D, RosselloMora R A, Ludwig W, Schleifer K H, Lovley D R and McInerney M J 1996 *Geovibrio ferrireducens*, a phylogenetically distinct dissimilatory Fe(III)-reducing bacterium *Archives of Microbiology* **165** 370-6
- [7] Rossellomora R A, Ludwig W, Kampfer P, Amann R and Schleifer K H 1995 *Ferrimonas-Balearica* Gen-Nov, Spec-Nov, a New Marine Facultative Fe(III)-Reducing Bacterium *Systematic and Applied Microbiology* **18** 196-202
- [8] Liesack W and Finster K 1994 Phylogenetic Analysis of 5 Strains of Gram-Negative, Obligately Anaerobic, Sulfur-Reducing Bacteria and Description of *Desulfuromusa* Gen-Nov, Including *Desulfuromusa-Kysingii* Sp-Nov, *Desulfuromusa-Bakii* Sp-Nov, and *Desulfuromusa-Succinoxidans* Sp-Nov *International Journal of Systematic Bacteriology* **44** 753-8

- [9] Roden E E and Lovley D R 1993 Dissimilatory Fe(III) Reduction by the Marine Microorganism *Desulfuromonas-Acetoxidans* *Applied and Environmental Microbiology* **59** 734-42
- [10] Lower S K, Hochella M F and Beveridge T J 2001 Bacterial recognition of mineral surfaces: Nanoscale interactions between *Shewanella* and alpha-FeOOH *Science* **292** 1360-3
- [11] Xiong Y J, Shi L, Chen B W, Mayer M U, Lower B H, Londer Y, Bose S, Hochella M F, Fredrickson J K and Squier T C 2006 High-affinity binding and direct electron transfer to solid metals by the *Shewanella oneidensis* MR-1 outer membrane c-type cytochrome OmcA *Journal of the American Chemical Society* **128** 13978-9
- [12] Parikh S J and Chorover J 2006 ATR-FTIR spectroscopy reveals bond formation during bacterial adhesion to iron oxide *Langmuir* **22** 8492-500
- [13] Lall R and Mitchell J 2007 Metal reduction kinetics in *Shewanella* *Bioinformatics* **23** 2754-9
- [14] Hernandez M E and Newman D K 2001 Extracellular electron transfer *Cellular and Molecular Life Sciences* **58** 1562-71
- [15] Nevin K P and Lovley D R 2002 Mechanisms for Fe(III) oxide reduction in sedimentary environments *Geomicrobiology Journal* **19** 141-59
- [16] Lovley D R 2003 Cleaning up with genomics: Applying molecular biology to bioremediation *Nature Reviews Microbiology* **1** 35-44
- [17] Anderson R T and Lovley D R 1997 Ecology and biogeochemistry of in situ groundwater bioremediation *Advances in Microbial Ecology, Vol 15* **15** 289-350
- [18] Lovley D R, Baedeker M J, Lonergan D J, Cozzarelli I M, Phillips E J P and Siegel D I 1989 Oxidation of Aromatic Contaminants Coupled to Microbial Iron Reduction *Nature* **339** 297-300

- [19] Lovley D R 1991 Dissimilatory Fe(III) and Mn(IV) Reduction *Microbiological Reviews* **55** 259-87
- [20] Lovley D R, Woodward J C and Chapelle F H 1994 Stimulated Anoxic Biodegradation of Aromatic-Hydrocarbons Using Fe(III) Ligands *Nature* **370** 128-31
- [21] Spormann A M and Widdel F 2000 Metabolism of alkylbenzenes, alkanes, and other hydrocarbons in anaerobic bacteria *Biodegradation* **11** 85-105
- [22] Smidt H and de Vos W M 2004 Anaerobic microbial dehalogenation *Annual Review of Microbiology* **58** 43-73
- [23] Mohn W W and Tiedje J M 1992 Microbial Reductive Dehalogenation *Microbiological Reviews* **56** 482-507
- [24] Liu C X, Gorby Y A, Zachara J M, Fredrickson J K and Brown C F 2002 Reduction kinetics of Fe(III), Co(III), U(VI) Cr(VI) and Tc(VII) in cultures of dissimilatory metal-reducing bacteria *Biotechnology and Bioengineering* **80** 637-49
- [25] Lovley D R, Phillips E J P, Gorby Y A and Landa E R 1991 Microbial Reduction of Uranium *Nature* **350** 413-6
- [26] Wall J D and Krumholz L R 2006 Uranium reduction *Annual Review of Microbiology* **60** 149-66
- [27] Bencheikh-Latmani R, Williams S M, Haucke L, Criddle C S, Wu L Y, Zhou J Z and Tebo B M 2005 Global transcriptional profiling of *Shewanella oneidensis* MR-1 during Cr(VI) and U(VI) reduction *Applied and Environmental Microbiology* **71** 7453-60
- [28] Truex M J, Peyton B M, Valentine N B and Gorby Y A 1997 Kinetics of U(VI) reduction by a dissimilatory Fe(III)-reducing bacterium under non-growth conditions *Biotechnology and Bioengineering* **55** 490-6

- [29] Anderson R T, Vrionis H A, Ortiz-Bernad I, Resch C T, Long P E, Dayvault R, Karp K, Marutzky S, Metzler D R, Peacock A, White D C, Lowe M and Lovley D R 2003 Stimulating the in situ activity of *Geobacter* species to remove uranium from the groundwater of a uranium-contaminated aquifer *Applied and Environmental Microbiology* **69** 5884-91
- [30] Suzuki Y, Kelly S D, Kemner K M and Banfield J F 2004 Enzymatic U(VI) reduction by *Desulfosporosinus* species *Radiochimica Acta* **92** 11-6
- [31] Lovley D R and Phillips E J P 1992 Reduction of Uranium by *Desulfovibrio-Desulfuricans* *Applied and Environmental Microbiology* **58** 850-6
- [32] Marsili E, Beyenal H, Di Palma L, Merli C, Dohnalkova A, Amonette J E and Lewandowski Z 2005 Uranium removal by sulfate reducing biofilms in the presence of carbonates *Water Science and Technology* **52** 49-55
- [33] Francis A J, Dodge C J, Lu F L, Halada G P and Clayton C R 1994 Xps and Xanes Studies of Uranium Reduction by *Clostridium* Sp *Environmental Science & Technology* **28** 636-9
- [34] Marshall M J, Beliaev A S, Dohnalkova A C, Kennedy D W, Shi L, Wang Z M, Boyanov M I, Lai B, Kemner K M, McLean J S, Reed S B, Culley D E, Bailey V L, Simonson C J, Saffarini D A, Romine M F, Zachara J M and Fredrickson J K 2006 c-Type cytochrome-dependent formation of U(IV) nanoparticles by *Shewanella oneidensis* *Plos Biology* **4** 1324-33
- [35] Suzuki Y, Kelly S D, Kemner K M and Banfield J F 2002 Radionuclide contamination - Nanometre-size products of uranium bioreduction *Nature* **419** 134-
- [36] Bretschger O, Obraztsova A, Sturm C A, Chang I S, Gorby Y A, Reed S B, Culley D E, Reardon C L, Barua S, Romine M F, Zhou J, Beliaev A S, Bouhenni R, Saffarini D, Mansfeld F, Kim B H, Fredrickson J K and Nealson K H 2007

- Current production and metal oxide reduction by *Shewanella oneidensis* MR-1 wild type and mutants *Applied and Environmental Microbiology* **73** 7003-12
- [37] Bond D R and Lovley D R 2003 Electricity production by *Geobacter sulfurreducens* attached to electrodes *Applied and Environmental Microbiology* **69** 1548-55
- [38] Holmes D E, Chaudhuri S K, Nevin K P, Mehta T, Methe B A, Liu A, Ward J E, Woodard T L, Webster J and Lovley D R 2006 Microarray and genetic analysis of electron transfer to electrodes in *Geobacter sulfurreducens* *Environmental Microbiology* **8** 1805-15
- [39] Logan B E and Regan J M 2006 Electricity-producing bacterial communities in microbial fuel cells *Trends in Microbiology* **14** 512-8
- [40] Berger D J 1999 Fuel cells and precious-metal catalysts *Science* **286** 49-
- [41] Zhan Z L and Barnett S A 2005 An octane-fueled solid oxide fuel cell *Science* **308** 844-7
- [42] Lovley D R 2006 Bug juice: harvesting electricity with microorganisms *Nature Reviews Microbiology* **4** 497-508
- [43] Rabaey K, Rodriguez J, Blackall L L, Keller J, Gross P, Batstone D, Verstraete W and Nealon K H 2007 Microbial ecology meets electrochemistry: electricity-driven and driving communities *Isme Journal* **1** 9-18
- [44] Reguera G, McCarthy K D, Mehta T, Nicoll J S, Tuominen M T and Lovley D R 2005 Extracellular electron transfer via microbial nanowires *Nature* **435** 1098-101
- [45] Gorby Y A, Yanina S, McLean J S, Rosso K M, Moyles D, Dohnalkova A, Beveridge T J, Chang I S, Kim B H, Kim K S, Culley D E, Reed S B, Romine M F, Saffarini D A, Hill E A, Shi L, Elias D A, Kennedy D W, Pinchuk G, Watanabe K, Ishii S, Logan B, Nealon K H and Fredrickson J K 2006 Electrically conductive bacterial nanowires produced by *Shewanella oneidensis*

strain MR-1 and other microorganisms *Proceedings of the National Academy of Sciences of the United States of America* **103** 11358-63

- [46] Klimes A, Franks A E, Glaven R H, Tran H, Barrett C L, Qiu Y, Zengler K and Lovley D R 2010 Production of pilus-like filaments in *Geobacter sulfurreducens* in the absence of the type IV pilin protein PilA *Fems Microbiology Letters* **310** 62-8
- [47] Reguera G, Nevin K P, Nicoll J S, Covalla S F, Woodard T L and Lovley D R 2006 Biofilm and nanowire production leads to increased current in *Geobacter sulfurreducens* fuel cells *Applied and Environmental Microbiology* **72** 7345-8
- [48] Mehta T, Coppi M V, Childers S E and Lovley D R 2005 Outer membrane c-type cytochromes required for Fe(III) and Mn(IV) oxide reduction in *Geobacter sulfurreducens* *Applied and Environmental Microbiology* **71** 8634-41
- [49] Inoue K, Qian X L, Morgado L, Kim B C, Mester T, Izallalen M, Salgueiro C A and Lovley D R 2010 Purification and Characterization of OmcZ, an Outer-Surface, Octaheme c-Type Cytochrome Essential for Optimal Current Production by *Geobacter sulfurreducens* *Applied and Environmental Microbiology* **76** 3999-4007
- [50] Leang C, Qian X L, Mester T and Lovley D R 2010 Alignment of the c-Type Cytochrome OmcS along Pili of *Geobacter sulfurreducens* *Applied and Environmental Microbiology* **76** 4080-4
- [51] Ntarlagiannis D, Atekwana E A, Hill E A and Gorby Y 2007 Microbial nanowires: Is the subsurface "hardwired"? *Geophys. Res. Lett.* **34** 5
- [52] El-Naggar M Y, Gorby Y A, Xia W and Nealson K H 2008 The molecular density of states in bacterial nanowires *Biophysical Journal* **95** L10-L2
- [53] Craig L, Pique M E and Tainer J A 2004 Type IV pilus structure and bacterial pathogenicity *Nature Reviews Microbiology* **2** 363-78

- [54] Van Houdt R and Michiels C W 2005 Role of bacterial cell surface structures in Escherichia coli biofilm formation *Research in Microbiology* **156** 626-33
- [55] Shime-Hattori A, Iida T, Arita M, Park K S, Kodama T and Honda T 2006 Two type IV pili of Vibrio parahaemolyticus play different roles in biofilm formation *Fems Microbiology Letters* **264** 89-97
- [56] Varga J J, Therit B and Melville S B 2008 Type IV Pili and the CcpA Protein Are Needed for Maximal Biofilm Formation by the Gram-Positive Anaerobic Pathogen Clostridium perfringens *Infection and Immunity* **76** 4944-51
- [57] Harrington L C and Rogerson A C 1990 The F-Pilus of Escherichia-Coli Appears to Support Stable DNA Transfer in the Absence of Wall-to-Wall Contact between Cells *Journal of Bacteriology* **172** 7263-4
- [58] Marsh J W and Taylor R K 1999 Genetic and transcriptional analyses of the Vibrio cholerae mannose-sensitive hemagglutinin type 4 pilus gene locus *Journal of Bacteriology* **181** 1110-7
- [59] Shu A C, Wu C C, Chen Y Y, Peng H L, Chang H Y and Yew T R 2008 Evidence of DNA transfer through F-pilus channels during Escherichia coli conjugation *Langmuir* **24** 6796-802
- [60] Ray R, Lizewski S, Fitzgerald L A, Little B and Ringeisen B R Methods for imaging Shewanella oneidensis MR-1 nanofilaments *Journal of Microbiological Methods* **82** 187-91
- [61] Chandler F W, Roth I L, Callaway C S, Bump J L, Thomason B M and Weaver R E 1980 Flagella on Legionnaires-Disease Bacteria - Ultrastructural Observations *Annals of Internal Medicine* **93** 711-4
- [62] Bieber D, Ramer S W, Wu C Y, Murray W J, Tobe T, Fernandez R and Schoolnik G K 1998 Type IV pili, transient bacterial aggregates, and virulence of enteropathogenic Escherichia coli *Science* **280** 2114-8

- [63] Wolfgang M, van Putten J P M, Hayes S F, Dorward D and Koomey M 2000 Components and dynamics of fiber formation define a ubiquitous biogenesis pathway for bacterial pili *Embo Journal* **19** 6408-18
- [64] Elliott S J, Nandapalan N and Chang B J 1991 Production of Type-1 Fimbriae by Escherichia-Coli Hb101 *Microbial Pathogenesis* **10** 481-6
- [65] Konnov N P, Baibyrin V B, Zadnova S P and Volkov U P 1999 Comparative microscopy study of Vibrio cholerae flagella *Scanning and Force Microscopies for Biomedical Applications, Proceedings Of* **3607** 123-5
- [66] Kirn T J, Lafferty M J, Sandoe C M P and Taylor R K 2000 Delineation of pilin domains required for bacterial association into microcolonies and intestinal colonization by Vibrio cholerae *Molecular Microbiology* **35** 896-910
- [67] Collins R F, Frye S A, Balasingham S, Ford R C, Tonjum T and Derrick J P 2005 Interaction with type IV pili induces structural changes in the bacterial outer membrane secretin PilQ *Journal of Biological Chemistry* **280** 18923-30
- [68] Jalili N and Laxminarayana K 2004 A review of atomic force microscopy imaging systems: application to molecular metrology and biological sciences *Mechatronics* **14** 907-45
- [69] Chang I S, Moon H, Bretschger O, Jang J K, Park H I, Nealson K H and Kim B H 2006 Electrochemically active bacteria (EAB) and mediator-less microbial fuel cells *J. Microbiol. Biotechnol.* **16** 163-77
- [70] Yu J Y, Chung S W and Heath J R 2000 Silicon nanowires: Preparation, device fabrication, and transport properties *Journal of Physical Chemistry B* **104** 11864-70
- [71] Cohen H, Nogues C, Naaman R and Porath D 2005 Direct measurement of electrical transport through single DNA molecules of complex sequence *Proceedings of the National Academy of Sciences of the United States of America* **102** 11589-93



- [72] Andolfi L and Cannistraro S 2005 Conductive atomic force microscopy study of plastocyanin molecules adsorbed on gold electrode *Surface Science* **598** 68-77
- [73] Cai L T, Tabata H and Kawai T 2001 Probing electrical properties of oriented DNA by conducting atomic force microscopy *Nanotechnology* **12** 211-6
- [74] McLean J S, Wanger G, Gorby Y A, Wainstein M, McQuaid J, Ishii S I, Bretschger O, Beyenal H and Nealson K H 2010 Quantification of Electron Transfer Rates to a Solid Phase Electron Acceptor through the Stages of Biofilm Formation from Single Cells to Multicellular Communities *Environmental Science & Technology* **44** 2721-7
- [75] Szent-Gyorgyi A 1941 Towards a new biochemistry? *Science* **93** 609-11
- [76] Evans M G and Gergely J 1949 A Discussion of the Possibility of Bands of Energy Levels in Proteins - Electronic Interaction in Non Bonded Systems *Biochimica Et Biophysica Acta* **3** 188-97
- [77] Rosenberg B 1962 Electrical Conductivity of Proteins *Nature* **193** 364-5
- [78] Gray H B and Winkler J R 1996 Electron transfer in proteins *Annual Review of Biochemistry* **65** 537-61
- [79] Gray H B and Winkler J R 2005 Long-range electron transfer *Proceedings of the National Academy of Sciences of the United States of America* **102** 3534-9
- [80] Ron I, Pecht I, Sheves M and Cahen D 2010 Proteins as Solid-State Electronic Conductors *Accounts of Chemical Research* **43** 945-53
- [81] del Mercato L L, Pompa P P, Maruccio G, Della Torre A, Sabella S, Tamburro A M, Cingolani R and Rinaldi R 2007 Charge transport and intrinsic fluorescence in amyloid-like fibrils *Proceedings of the National Academy of Sciences of the United States of America* **104** 18019-24

- [82] Xu D G, Watt G D, Harb J N and Davis R C 2005 Electrical conductivity of ferritin proteins by conductive AFM *Nano Letters* **5** 571-7
- [83] Rinaldi R, Biasco A, Maruccio G, Arima V, Visconti P, Cingolani R, Facci P, De Rienzo F, Di Felice R, Molinari E, Verbeet M P and Canters G W 2003 Electronic rectification in protein devices *Applied Physics Letters* **82** 472-4
- [84] Zhao J W, Davis J J, Sansom M S P and Hung A 2004 Exploring the electronic and mechanical properties of protein using conducting atomic force microscopy *Journal of the American Chemical Society* **126** 5601-9
- [85] Ron I, Sepunaru L, Itzhakov S, Belenkova T, Friedman N, Pecht I, Sheves M and Cahen D 2010 Proteins as Electronic Materials: Electron Transport through Solid-State Protein Monolayer Junctions *Journal of the American Chemical Society* **132** 4131-40
- [86] Zhang Z Y, Yao K, Liu Y, Jin C H, Liang X L, Chen Q and Peng L M 2007 Quantitative analysis of current-voltage characteristics of semiconducting nanowires: Decoupling of contact effects *Advanced Functional Materials* **17** 2478-89
- [87] Briseno A L, Mannsfeld S C B, Jenekhe S A, Bao Z and Xia Y 2008 Introducing organic nanowire transistors *Materials Today* **11** 38-47
- [88] Nokhrin S, Baru M and Lee J S 2007 A field-effect transistor from m-DNA *Nanotechnology* **18** 095205
- [89] Maruccio G, Biasco A, Visconti P, Bramanti A, Pompa P P, Calabi F, Cingolani R, Rinaldi R, Corni S, Di Felice R, Molinari E, Verbeet M R and Canters G W 2005 Towards protein field-effect transistors: Report and model of prototype *Advanced Materials* **17** 816-22
- [90] Shi L, Chen B W, Wang Z M, Elias D A, Mayer M U, Gorby Y A, Ni S, Lower B H, Kennedy D W, Wunschel D S, Mottaz H M, Marshall M J, Hill E A, Beliaev A S, Zachara J M, Fredrickson J K and Squier T C 2006 Isolation of a high-affinity

- functional protein complex between OmcA and MtrC: Two outer membrane decaheme c-type cytochromes of *Shewanella oneidensis* MR-1 *Journal of Bacteriology* **188** 4705-14
- [91] Eichfeld S M, Ho T T, Eichfeld C M, Cranmer A, Mohny S E, Mayer T S and Redwing J M 2007 Resistivity measurements of intentionally and unintentionally template-grown doped silicon nanowire arrays *Nanotechnology* **18** 315201
- [92] El-Naggar M Y, Wanger G, Leung K M, Yuzvinsky T D, Southam G, Yang J, Lau W M, Nealon K H and Gorby Y A 2010 Electrical transport along bacterial nanowires from *Shewanella oneidensis* MR-1 *Proceedings of the National Academy of Sciences of the United States of America* **107** 18127-31
- [93] Wu B, Heidelberg A and Boland J J 2005 Mechanical properties of ultrahigh-strength gold nanowires *Nature Materials* **4** 525-9
- [94] Barth S, Harnagea C, Mathur S and Rosei F 2009 The elastic moduli of oriented tin oxide nanowires *Nanotechnology* **20** 115705
- [95] Sahin O, Magonov S, Su C, Quate C F and Solgaard O 2007 An atomic force microscope tip designed to measure time-varying nanomechanical forces *Nature Nanotechnology* **2** 507-14
- [96] Sahin O and Erina N 2008 High-resolution and large dynamic range nanomechanical mapping in tapping-mode atomic force microscopy *Nanotechnology* **19** 445717
- [97] Hutter J L and Bechhoefer J 1993 Calibration of Atomic-Force Microscope Tips *Rev. Sci. Instrum.* **64** 1868-73
- [98] Longtin R, Fauteux C, Coronel E, Wiklund U, Pegna J and Boman M 2004 Nanoindentation of carbon microfibers deposited by laser-assisted chemical vapor deposition *Applied Physics a-Materials Science & Processing* **79** 573-7

- [99] Torres J M, Stafford C M and Vogt B D 2009 Elastic Modulus of Amorphous Polymer Thin Films: Relationship to the Glass Transition Temperature *Acs Nano* **3** 2677-85
- [100] Ikai A, Afrin R and Sekiguchi H 2007 Pulling and pushing protein molecules by AFM *Current Nanoscience* **3** 17-29
- [101] Ptak A, Takeda S, Nakamura C, Miyake J, Kageshima M, Jarvis S P and Tokumoto H 2001 Modified atomic force microscope applied to the measurement of elastic modulus for a single peptide molecule *Journal of Applied Physics* **90** 3095-9
- [102] Kjelstrup-Hansen J, Hansen O, Rubahn H G and Boggild P 2006 Mechanical properties of organic nanofibers *Small* **2** 660-6
- [103] Ikai A 2005 Local rigidity of a protein molecule *Biophysical Chemistry* **116** 187-91

## Curriculum Vitae

**Name:** Kar Man Leung

**Post-secondary Education and Degrees:** The University of Western Ontario  
London, Ontario, Canada  
2006-2011 Ph.D.

City University of Hong Kong  
Hong Kong SAR  
2004-2006 M.Phil.

City University of Hong Kong  
Hong Kong SAR  
2001-2004 B.Eng.

**Honours and Awards:** Western Graduate Research Scholarship  
2006-2011

Outstanding Research Thesis Award  
2006

Postgraduate Tuition Scholarship  
2005-2006

**Related Work Experience** Teaching Assistant  
The University of Western Ontario  
2006-2011

Research Assistant  
The University of Western Ontario  
2006-2011

Postgraduate Assistant  
City University of Hong Kong  
2004-2006

### Publications:

1. K. M. Leung, G. Wanger, Q. Guo, Y. Gorby, G. Southam, W. M. Lau and Jun Yang, "Bacterial nanowires: conductive as silicon, soft as polymer", *Soft Matter* 7, 6617 (2011).

2. B. Yu, K. M. Leung, Q. Guo, W. M. Lau and J. Yang, "Synthesis of Ag-TiO<sub>2</sub> composite nano-thin film for antimicrobial application", *Nanotechnology* 22, 115603 (2011).
3. Y. Liu, K. M. Leung, H. -Y. Nie, W. M. Lau and J. Yang, "A new AFM nanotribology method using a T-shaped cantilever with an off-axis tip for friction coefficient measurement with minimized Abbe' error", *Tribology Letters* 41, 313 (2011).
4. M. Y. El-Naggar, G. Wanger, K. M. Leung, T. D. Yuzvinsky, G. Southam, J. Yang, W. M. Lau, K. H. Neilson and Y. Gorby, "Electrical transport along bacterial nanowires from *Shewanella oneidensis* MR-1", *Proceedings of the National Academy of Sciences of the United States of America* 107, 18127 (2010).
5. T. Li, L. Zhang, K. M. Leung and J. Yang, "Out-of-plane microvalves for whole blood separation on lab-on-a-CD", *Journal of Micromechanics and Microengineering* 20, 105024 (2010).
6. H. Q. Li, K. M. Leung, K. L. Ma, Q. Ye, Y. M. Chong, Y. S. Zou, W. J. Zhang, S. T. Lee and I. Bello, "Nanocubic boron nitride/nanodiamond multilayer structures", *Applied Physics Letters* 91, 201918 (2007).
7. A. Spiesser, Y. M. Chong, K. M. Leung, G. Abel, G. G. Ross, M. J. Walzak, R. Jacklin, W. M. Lau, W. J. Zhang and I. Bello, "Surface free energy of cubic boron nitride films deposited on nanodiamond", *Journal of Physical Chemistry C* 111, 12768 (2007).
8. K. M. Leung, H. Q. Li, Y. S. Zou, K. L. Ma, Y. M. Chong, Q. Ye, W. J. Zhang, S. T. Lee and I. Bello, "Structural analysis of cubic boron nitride films by ultraviolet Raman spectroscopy", *Applied Physics Letters* 88, 241922 (2006).
9. Y. M. Chong, K. L. Ma, K. M. Leung, C. Y. Chan, Q. Ye, I. Bello, W. J. Zhang and S. T. Lee, "Synthesis and mechanical properties of cubic boron nitride/nanodiamond composite films", *Chemical Vapor Deposition* 12, 33 (2006).
10. Y. M. Chong, K. M. Leung, K. L. Ma, W. J. Zhang, I. Bello and S. T. Lee, "Growing cubic boron nitride films at different temperatures", *Diamond and Related Materials* 15, 1155 (2006).
11. K. L. Ma, W. J. Zhang, Y. S. Zou, Y. M. Chong, K. M. Leung, I. Bello and S. T.

- Lee, "Electrical properties of nitrogen incorporated nanocrystalline diamond films", *Diamond and Related Materials* 15, 626 (2006).
12. K. M. Leung, C. Y. Chan, Y. M. Chong, Y. Yao, K. L. Ma, I. Bello, W. J. Zhang and S. T. Lee, "Studying the growth of cubic boron nitride on amorphous tetrahedral carbon interlayers", *Journal of Physical Chemistry B* 109, 16272 (2005).
  13. I. Bello, Y. M. Chong, K. M. Leung, C. Y. Chan, K. L. Ma, W. J. Zhang, S. T. Lee and A. Layyous, "Cubic boron nitride films for industrial applications", *Diamond and Related Materials* 14, 1784 (2005).
  14. I. Bello, C. Y. Chan, W. J. Zhang, Y. M. Chong, K. M. Leung, S. T. Lee and Y. Lifshitz, "Deposition of thick cubic boron nitride films: The route to practical applications", *Diamond and Related Materials* 14, 1154 (2005).

**Patents:**

1. W. J. Zhang, S. T. Lee, I. Bello, K. M. Leung, H. Q. Li, Y. S. Zou, Y. M. Zhong and K. L. Ma, "Ultrahard multilayer coating comprising nanocrystalline diamond and nanocrystalline cubic boron nitride", **United States Patent No. US 2009022969**.
2. S. T. Lee, W. J. Zhang, Y. S. Zou, I. Bello, K. L. Ma, K. M. Leung and Y. M. Chong, "Surface acoustic wave (SAW) devices based on cubic boron nitride/diamond composite structures", **United States Patent No. US 7,579,759 B2**, Aug. 25, 2009.